Technische Universität München
Fakultät für Physik
Lehrstuhl für theoretische Physik IV (T31)

Supersymmetry, the Flavour Puzzle and Rare B Decays

David Michael Straub

Vollständiger Abdruck der von der Fakultät für Physik der Technischen Universität München zur Erlangung des akademischen Grades eines

Doktors der Naturwissenschaften

genehmigten Dissertation.

Vorsitzender:	Univ.-Prof. Dr. Lothar Oberauer
Prüfer der Dissertation:	1. Univ.-Prof. Dr. Andrzej J. Buras
	2. Hon.-Prof. Dr. Wolfgang F. L. Hollik

Die Dissertation wurde am 28. Juni 2010 bei der Technischen Universität München eingereicht und durch die Fakultät für Physik am 14. Juli 2010 angenommen.

Zusammenfassung

Das Eichhierarchie-Problem und das Flavour-Rätsel gehören zu den drängendsten offenen Fragen des Standardmodells der Teilchenphysik. Supersymmetrie ist das wohl beliebteste Konzept für Physik jenseits des Standardmodells und bietet eine elegante Lösung des Eichhierarchie-Problems; allerdings verschärft sie das Flavour-Rätsel noch. Im ersten Teil dieser Dissertation behandle ich mehrere Ansätze, um das Flavour-Rätsel im Rahmen der minimalen supersymmetrischen Erweiterung des Standardmodells anzugehen sowie deren experimentelle Überprüfung: supersymmetrische große vereinheitlichte Theorien mit einer Vereinigung der Yukawa-Kopplungen bei hohen Energien, Theorien mit minimaler Flavour-Verletzung und zusätzlichen Quellen der CP-Verletzung sowie Theorien mit Eichvermittlung der Supersymmetrie-Brechung und einem großen Verhältnis der Higgs-Vakuumerwartungswerte. Im zweiten Teil der Dissertation diskutiere ich die Phänomenologie zweier seltener B-Meson-Zerfallskanäle, die viel versprechende Messsonden für Physik jenseits des Standardmodells darstellen: Den exklusiven Zerfall $B \to K^* \ell^+ \ell^-$, dessen Zerfallswinkelverteilung am LHC studiert werden wird und die Messung einer großen Anzahl von Observablen erlaubt sowie die Zerfälle $b \to s\nu\bar{\nu}$, denen das Interesse geplanter Super-B-Fabriken mit hoher Luminosität gilt. Ich bespreche die Vorhersagen des Standardmodells für diese Observablen sowie deren Empfindlichkeit auf neue Physik.

Abstract

The gauge hierarchy problem and the flavour puzzle belong to the most pressing open questions in the Standard Model of particle physics. Supersymmetry is arguably the most popular framework of physics beyond the Standard Model and provides an elegant solution to the gauge hierarchy problem; however, it aggravates the flavour puzzle. In the first part of this thesis, I discuss several approaches to address the flavour puzzle in the minimal supersymmetric extension of the Standard Model and experimental tests thereof: supersymmetric grand unified theories with a unification of Yukawa couplings at high energies, theories with minimal flavour violation and additional sources of CP violation and theories with gauge mediation of supersymmetry breaking and a large ratio of Higgs vacuum expectation values. In the second part of the thesis, I discuss the phenomenology of two rare B meson decay modes which are promising probes of physics beyond the Standard Model: The exclusive $B \to K^* \ell^+ \ell^-$ decay, whose angular decay distribution will be studied at LHC and gives access to a large number of observables and the $b \to s\nu\bar{\nu}$ decays, which are in the focus of planned high-luminosity Super B factories. I discuss the predictions for these observables in the Standard Model and their sensitivity to New Physics.

Contents

Introduction

The first high-energy proton-proton collisions in the Large Hadron Collider (LHC) at CERN in March 2010 might mark the beginning of a new era in particle physics. There are strong reasons to expect that the unprecedented collision energy at the LHC will allow to shed light on the puzzling questions the "Standard Model" – an extremely modest name for a precisely tested theory describing the strong, weak and electromagnetic interactions – has left open. One of the most pressing questions is how the electroweak (EW) symmetry is broken. The solution implemented in the Standard Model (SM) is that of a fundamental scalar Higgs field obtaining a vacuum expectation value (VEV) v breaking the EW symmetry. While this solution is the arguably simplest and most straightforward one, it has not been confirmed experimentally yet and it is plagued by a fundamental naturalness problem. Not least due to the unresolved incorporation of gravity, the SM has to be viewed as a low-energy effective theory of a more fundamental theory. In such an effective theory, however, fundamental scalar particles like the Higgs boson receive quantum corrections to their mass which are quadratically sensitive to any new mass scale in the theory. While it is formally possible to *assume* that the renormalized, physical Higgs mass is of the order of the EW scale $v \simeq 246$ GeV, this implies an enormous cancellation between a huge bare mass and equally huge quantum corrections. Stated differently, the huge hierarchy between the EW scale and the Planck scale $M_{\rm Pl} \simeq 10^{19}$ GeV is unstable under quantum corrections in the SM and its existence seems very unnatural. If this *gauge hierarchy problem* is taken seriously, it implies that the limitied domain of validity of the SM – as a limiting case of a more fundamental theory – is already to be reached at scales not too far above the EW scale.

On the other hand, the SM Higgs mechanism is very economical in the Occamian sense: It does not only provide for the breaking of the EW symmetry, but also for the masses of quarks and charged leptons. This comes about because the Yukawa couplings give rise to mass terms when the Higgs field obtains a VEV. Since quarks and leptons come in three generations, these Yukawa couplings are 3×3 complex matrices; Since they cannot be simultaneously diagonalized, they leave as their observable remnant the Cabibbo-Kobayashi-Maskawa (CKM) matrix parametrizing flavour violation in weak charged currents. The CKM mechanism has been tested to a remarkable precision in recent years and has been found to give an excellent description of flavour violation as well as CP violation induced by the CKM matrix's complex phase.

In spite of this success, the SM Yukawa sector itself raises many questions, col-

lectively referred to as the *flavour puzzle*. The Yukawa matrices contain, exploiting all possible field redefinitions, 13 free parameters: 9 masses, 3 CKM angles and the CKM phase. Not only is this large number of free parameters unsatisfactory (the SM with massless neutrinos only contains 19 free parameters in total), but the actual numerical values of these 13 parameters are disturbing without a more fundamental explanation of their origin. The quark and lepton masses span over more than five orders of magnitude, from the electron mass at 511 keV to the top quark mass at 173 GeV; and also the CKM angles are hierarchical, being roughly 13°, 2° and 0.5°, respectively.

These two puzzles, the gauge hierarchy problem and the flavour puzzle, seem to be quite different conceptually and indeed it is not known at present whether they are related. However, it is interesting to note that most models of New Phyics (NP), i.e. physics beyond the SM, competing as candidate solutions to the gauge hierarchy problem, aggravate the flavour puzzle instead of solving it. The reason is that any NP involves new heavy particles couplings to SM fields and potentially contributing to precision observables in the flavour sector. The fact that no significant deviations from the SM expectations have been found in the flavour sector then turns into the question why the flavour structure of the NP theory is so similar to the SM one.

This interplay highlights the necessity of experimental searches for NP complementary to the high-energy frontier pursued at LHC and probing the scale of the NP. High-precision and high-luminosity experiments searching for non-standard flavour structures or CP violation in flavour-changing neutral current (FCNC) decays of mesons or leptons or searches for non-standard effects in electric or magnetic dipole moments are indispensable tools to test the SM and to distinguish NP theories, given future input from LHC. Rare decays of B mesons are particularly promising in this respect, being an important part of the LHC flavour physics programme and in the focus of planned dedicated asymmetric e^+-e^- colliders (the Super B factories).

Among the extensions of the SM, supersymmetry (SUSY) has arguably been the most popular framework from the 1980s till today. SUSY is an extension of the Poincaré group, i.e. an extension of the symmetries of spacetime, transforming fermionic and bosonic states into each other. In addition to being interesting from a purely conceptual point of view, SUSY has the remarkable property that the quadratic sensivity of fundamental scalar masses to higher energy scales is lifted because the fermionic and bosonic contributions to the quantum corrections cancel each other. As a consquence, the vast hierarchy between the EW and the Planck scale is stabilized in a SUSY extension of the SM and the gauge hierarchy problem is solved.

The flavour puzzle, on the other hand, persists almost unchanged compared to the SM since SUSY by itself does not provide any explanation for the origin of Yukawa couplings. In addition, SUSY is obviously not an exact symmetry of our vacuum, but whatever interaction breaks supersymmetry should also be expected, on general grounds, to violate flavour and CP. Thus, if SUSY is among the symmetries of

our universe, both new theoretical ideas explaining the peculiar flavour structure of Yukawa couplings and SUSY breaking interactions and high-sensitivity experimental searches for flavour and CP violation are mandatory.

In the first part of this thesis, I will discuss several theoretical aspects of the SUSY flavour puzzle and confront them with phenomenology. After a review of the minimal supersymmetric extension of the SM (MSSM) in chapter 1, chapter 2 contains an extensive discussion of the unification of Yukawa couplings at high energies which can occur if the three gauge interactions of the SM have a common, "grand unified" origin and quarks and leptons are just two sides of the same coin. To explain the excellent agreement of flavour physics experiments with the SM expectations, the strongest assumption one can make on the terms breaking supersymmetry is that they have the same flavour structure as the Yukawa couplings. Even with this hypothesis of minimal flavour violation (MFV), CP can still be violated at observable levels as will be discussed in section 3.1. Large effects in flavour physics are also expected if $\tan\beta$, the ratio of vacuum expectation values of the two Higgs doublets present in the MSSM, is large. The phenomenological limits on its size are the topic of section 3.2.

The second part of the thesis deals with the phenomenology of rare semi-leptonic B decays. A particularly promising decay mode to discover or constrain NP is $B \to K^* \ell^+ \ell^-$, which offers several observables sensitive to flavour and CP violation. Chapter 4 is devoted to a phenomenological analysis of this decay mode, concentrating on the identification of theoretically clean and NP-sensitive observables. Related decay modes, which however require the clean environment of an e^+-e^- machine like the planned Super B factories, are the $b \to s\nu\bar{\nu}$ decays. Their sensitivity to NP, and the possible pollution of experimental studies by even more exotic NP, is studied in chapter 5.

Part I

The SUSY flavour puzzle

1 The Minimal Supersymmetric Standard Model

Among the theories which have been suggested as solutions of one or the other problem of the SM, the interest in supersymmetry, even in absence of a strong experimental hint in its favour, can be traced back to numerous virtues a supersymmetric extension of the SM would have.

First, there is theoretical motivation. SUSY is the only meaningful extension of the symmetries of four-dimensional spacetime [1] and is the only way to relate fermions and bosons to a common origin.

Second, there is phenomenological motivation. In addition to curing the Standard Model's gauge hierarchy problem, SUSY indicates that gauge couplings unify at high energies [2], pointing to a "grand" unification of gauge interactions; It predicts particles that may act as the dark matter of the universe; And it can accomodate the apparent deviation of the anomalous magnetic moment of the muon from its SM expectation.

Third, there is practical motivation. Being perturbative up to very high energies, the minimal supersymmetric extension of the SM, or MSSM in short, has the mundane advantage that its effects are *calculable*.

The SUSY formalism will not be repeated here – see [3–8] for a collection of excellent text books and reviews. Rather, this chapter will concentrate on the construction of the MSSM, stressing right away that the "M" as in "minimal" does *not* refer to the number of parameters, but to the required field content. On the contrary, the number of paramers in the general, broken MSSM is understandably one of the main criticisms of this framework. Still, it should be emphasized that a deeper understanding of the mechanism of SUSY breaking (requiring experimental input of course) could allow to drastically reduce the number of unknowns related to this breaking.

1.1 MSSM fields and couplings

When constructing a supersymmetric extension of the SM, the first observation is that none of the SM bosons can share a SUSY multiplet with any of the SM fermions. This is simply because their gauge quantum numbers do not match, with the exception of the the left-handed lepton doublet ℓ_L, which has the same gauge quantum numbers as the SM Higgs doublet H. However, identifying the components

Superfields	Scalars	Fermions	G_{SM} rep.	$U(1)_{\text{PQ}}$	$U(1)_R$ (f,b)
Q_i	$\tilde{q}_{Li} = \begin{pmatrix} \tilde{u}_{Li} \\ \tilde{d}_{Li} \end{pmatrix}$	$q_{Li} = \begin{pmatrix} u_{Li} \\ d_{Li} \end{pmatrix}$	$(3,2)_{1/6}$	$-\frac{1}{2}$	$(\frac{1}{2}, -\frac{1}{2})$
U_i	$(\tilde{u}_{Ri})^*$	$(u_{Ri})^c$	$(\bar{3},1)_{-2/3}$	$-\frac{1}{2}$	$(\frac{1}{2}, -\frac{1}{2})$
D_i	$(\tilde{d}_{Ri})^*$	$(d_{Ri})^c$	$(\bar{3},1)_{1/3}$	$-\frac{1}{2}$	$(\frac{1}{2}, -\frac{1}{2})$
L_i	$\tilde{\ell}_{Li} = \begin{pmatrix} \tilde{\nu}_{Li} \\ \tilde{e}_{Li} \end{pmatrix}$	$\ell_{Li} = \begin{pmatrix} \nu_{Li} \\ e_{Li} \end{pmatrix}$	$(1,2)_{-1/2}$	$-\frac{1}{2}$	$(\frac{1}{2}, -\frac{1}{2})$
E_i	$(\tilde{e}_{Ri})^*$	$(e_{Ri})^c$	$(1,1)_1$	$-\frac{1}{2}$	$(\frac{1}{2}, -\frac{1}{2})$
H_d	H_d	$\tilde{H}_u$	$(1,2)_{-1/2}$	1	$(1,0)$
H_u	H_u	$\tilde{H}_d$	$(1,2)_{1/2}$	1	$(1,0)$

Table 1.1: MSSM supermultiplets and their quantum numbers under the SM gauge group $G_{\text{SM}} = SU(3)_c \times SU(2)_L \times U(1)_Y$. For (s)fermions, i is the generation index. (Note that the Higgs superfield and scalar doublets are denoted by the same symbol here, it should however always be clear from context which one is meant.)

of H with a slepton and a sneutrino would explicitly and strongly violate lepton number and is not phenomenologically viable. Therefore, the particle spectrum of the MSSM has to at least contain one as yet unobserved superpartner for each SM particle.

Doubling the particle spectrum of the SM still does not give rise to a phenomenologically viable theory. First, it is impossible to generate Yukawa couplings of both up- and down-type quarks to the same Higgs doublet, as in the SM where

$$\mathcal{L}_{\text{SM}} \supset -\epsilon_{ab}(Y_U)_{ij} H^{\dagger\, a} \bar{q}^b_{Li} u_{Rj} - (Y_D)_{ij} H_a \bar{q}^a_{Li} d_{Rj} - (Y_E)_{ij} H_a \bar{\ell}^a_{Li} e_{Rj} + \text{ h.c.}\,, \tag{1.1}$$

since the superpotential has to be an analytic function of superfields and cannot contain $H^\dagger$. Second, the additional contributions to the chiral anomaly from Higgsinos and gauginos do not cancel. Both problems can be solved simultaneously if one introduces a second Higgs doublet with opposite hypercharge. The final superfield content of the MSSM is given in table 1.1.

1.1.1 MSSM superpotential

The most general superpotential for this field content contains baryon and lepton number violating terms which are very problematic phenomenologically. A simple possibility to get rid of them is to postulate the conservation of R-parity defined as

$$R_p = (-1)^{3(B-L)+2s}\,, \tag{1.2}$$

where B and L are the baryon and lepton number and s the spin of a given particle.

The resulting, most general renormalizable superpotential of the R-parity conserving MSSM is given by

$$W_{\text{MSSM}} = \epsilon_{ab}\left[(Y_U)_{ij}H_u^a Q_i^b U_j - (Y_D)_{ij}H_d^a Q_i^b D_j - (Y_E)_{ij}H_d^a L_i^b E_j + \mu H_d^a H_u^b\right] . \quad (1.3)$$

1.1.2 Soft SUSY breaking

Accounting for the fact that our vacuum is not supersymmetric, but assuming that supersymmetry is responsible for the solution of the gauge hierarchy problem, SUSY breaking terms have to be introduced to the Lagrangian which are *soft* in the sense that they do not introduce quadratic divergencies to scalar masses, which are absent in the SUSY limit. If SUSY is spontaneously broken, this requirement is automatically fulfilled. However, coupling the MSSM fields directly, i.e. via tree-level renormalizable terms, to the SUSY breaking sector is not phenomenologically viable. The reason is that it would imply conditions on the SUSY spectrum, the supertrace conditions, forcing some of the superpartners to be unacceptably light. Consequently, SUSY breaking is usually assumed to occur in a separate *hidden sector* communicating with the MSSM only via suppressed interactions. Mechanisms for mediating this breaking will be discussed in section 1.4.1.

Regardless of the mediation mechanism, one can parametrize the most general SUSY breaking terms compatible with the field content in table 1.1, the conservation of R-parity and the requirement that these terms break SUSY softly. The soft SUSY breaking Lagrangian of the MSSM then reads

$$\begin{aligned}
\mathcal{L}_{\text{soft}} = &\frac{1}{2}\left(M_1\tilde{B}\tilde{B} + M_2\tilde{W}^i\tilde{W}_i + M_3\tilde{g}^a\tilde{g}_a + \text{ h.c.}\right) \\
&- \epsilon_{ab}\left[(T_U)_{ij}H_u^a\tilde{Q}_{Li}^b\tilde{u}_{Rj}^* - (T_D)_{ij}H_d^a\tilde{Q}_{Li}^b\tilde{d}_{Rj}^* - (T_E)_{ij}H_d^a\tilde{L}_{Li}^b\tilde{e}_{Rj}^*\right] + \text{ h.c.} \\
&- \tilde{Q}_{La}^{*i}(m_Q^2)^{ij}\tilde{Q}_L^{aj} - \tilde{u}_R^{*i}(m_U^2)^{ij}\tilde{u}_R^j - \tilde{d}_R^{*i}(m_D^2)^{ij}\tilde{d}_R^j \\
&- \tilde{L}_{La}^{*i}(m_L^2)^{ij}\tilde{L}_L^{aj} - \tilde{e}_R^{*i}(m_E^2)^{ij}\tilde{e}_R^j \\
&- m_{H_d}^2 H_{d\,a}^* H_d^a - m_{H_u}^2 H_{u\,a}^* H_u^a - (b\,\epsilon_{ab}H_d^a H_u^b + \text{ h.c.}) ,
\end{aligned} \quad (1.4)$$

containing, from top to bottom, gaugino masses, trilinear couplings, squark masses, slepton masses and Higgs bilinears.

For the diagonal elements of the trilinear couplings $T_{U,D,E}$, it is sometimes useful to write them as a product of the corresponding Yukawa coupling and an A *term* as

$$(T_{U,D,E})_{ij} = (A_{U,D,E})_{ij}(Y_{U,D,E})_{ij} . \quad (1.5)$$

Although this notation will be used occasionally in the remainder of this thesis, it should be stressed that the $T_{U,D,E}$ are the fundamental parameters and can be nonzero even if the corresponding Yukawa matrix elements vanish.

As a side remark, it is often a tedious task to translate the different notations for SUSY and SUSY breaking parameters in use into each other. The dictionary in appendix A takes care of this issue for the notation used in this thesis and the most popular ones present in the literature.

1.2 Symmetries of the MSSM Lagrangian

1.2.1 Parameter counting

It is instructive to count the total number of physical parameters in the MSSM, given the superpotential (1.3) and the soft SUSY breaking Lagrangian (1.4). The 5 sfermion mass matrices are hermitian 3×3 matrices and each have 6 angles and 3 phases. The 3 Yukawa coupling matrices and 3 trilinear matrices are complex 3×3 matrices with 9 angles and 9 phases each. The 3 gaugino masses, the μ and b terms are complex, while the 2 Higgs soft masses are real. Finally, there are the three real gauge couplings and the QCD vacuum angle. The total number of real parameters and phases is then $(94, 75)$, respectively.

However, not all of these parameters are physical as some can be removed by field redefinitions. In the absence of soft SUSY breaking terms, Yukawa couplings and the μ term, the MSSM is invariant under the large chiral symmetry group

$$G = U(3)_Q \times U(3)_U \times U(3)_D \times U(3)_L \times U(3)_E \times U(1)_R \times U(1)_{\mathrm{PQ}} \times U(1)_Y \,, \quad (1.6)$$

where the sfermion fields transform as triplets under "their" $U(3)$ and singlets under the remaining $U(3)$s. Under the $U(1)_R$ and $U(1)_{\mathrm{PQ}}$ symmetries, both (s)fermion and Higgs(ino) fields are charged. $U(1)_{\mathrm{PQ}}$ commutes with supersymmetry, while $U(1)_R$ acts differently on the components of a supermultiplet. A possible choice of charge assignments is shown in table 1.1. $U(1)_Y$ is the usual hypercharge. Since the $U(3)$ rotation matrices are unitary and have 3 angles and 6 phases each, while the 3 extra $U(1)$s correspond to 3 phases, the total number of parameters in G is $(15, 33)$.

To determine the number of *physical* parameters, it is important to notice that a subgroup H of G,

$$H = U(1)_B \times U(1)_L \times U(1)_Y \,, \quad (1.7)$$

containing baryon number, lepton number and hypercharge, is conserved even in presence of the MSSM superpotential and $\mathcal{L}_{\mathrm{soft}}$. One can now consider chiral transformations of the MSSM superfields under the group G/H, which is completely broken by the superpotential and soft SUSY breaking parameters. The Lagrangian can then be made formally invariant under these transformations if the couplings are viewed as spurion fields with appropriate transformation properties under G/H. For example, the $U(1)_{\mathrm{PQ}}$ and $U(1)_R$ charge assignments of the relevant couplings are shown in table 1.2. Couplings related in this way via a G/H transformation

	$M_{1,2,3}$	$T_{U,D,E}$	b	μ
$U(1)_{\mathrm{PQ}}$	0	0	-2	-2
$U(1)_R$	-2	-2	-2	0

Table 1.2: $U(1)_{\mathrm{PQ}}$ and $U(1)_R$ charges of MSSM spurions. All the remaining superpotential and soft SUSY breaking parameters are uncharged under both symmetries.

form an equivalence class since they correspond to physically equivalent theories. The number of *unphysical* parameters is thus precisely the number of parameters in G/H.

The total number of physical parameters in the MSSM is then

$$N_{\mathrm{phys}} = N_{\mathrm{tot}} - (N_G - N_H) = (94, 75) - (15, 33) + (0, 3) = (79, 45)\,. \tag{1.8}$$

The general MSSM thus has 124 parameters (including the SM ones), 45 of which violate CP.

1.2.2 Minimal Flavour Violation

Leaving aside the $U(1)_{\mathrm{PQ}}$ and $U(1)_R$ symmetries, which are only broken by the soft SUSY breaking parameters and the μ term (cf. tab. 1.2), the global flavour symmetry

$$G_f = U(3)^5 \times U(1)_Y \tag{1.9}$$

is broken down to H (1.7) by the Yukawa couplings just as in the SM[1]. Also the sfermion masses and trilinear couplings break G_f; however, this breaking is very strongly constrained from the excellent agreement of flavour physics experiments with the SM predicitions. One can postulate G_f conservation in the soft SUSY breaking sector, i.e. *flavour blindness* of SUSY breaking, however this statement is not even renormalization group invariant, since contributions from the G_f breaking Yukawa couplings are always present.

The minimal amount of flavour breaking is thus obtained by assuming that the Yukawa couplings are the only non-trivial spurions of G_f in the MSSM. Under this assumption of Minimal Flavour Violation (MFV) [9, 10], the sfermion mass matrices and trilinear coupling matrices can be written as expansions in terms of Yukawa coupling matrices. Making use of hierarchies present in the Yukawa couplings to simplify some terms, these expansions can be written for squarks as [11]

$$\left(m_Q^2\right)^T = \tilde{m}^2 \left[a_1 \mathbb{1} + b_1 Y_U Y_U^\dagger + b_2 Y_D Y_D^\dagger + \left(b_3 Y_U Y_U^\dagger Y_D Y_D^\dagger + \text{ h.c.}\right)\right], \tag{1.10}$$

[1] In the SM as well as in the MSSM in the limit $\mathcal{L}_{\mathrm{soft}} \to 0$, the conserved global symmetry is actually $U(1)_B \times U(1)_{L_e} \times U(1)_{L_\mu} \times U(1)_{L_\tau} \times U(1)_Y$. In the MSSM, the individual lepton family numbers are broken down to $U(1)_L$ by the slepton masses and trilinear couplings.

$$\left(m_U^2\right)^T = \tilde{m}^2 \left[a_2 \mathbb{1} + Y_U^\dagger \left(b_5 \mathbb{1} + c_1 Y_U Y_U^\dagger + c_2 Y_D Y_D^\dagger + \left(c_3 Y_U Y_U^\dagger Y_D Y_D^\dagger + \text{ h.c.}\right)\right) Y_U\right] , \tag{1.11}$$

$$\left(m_D^2\right)^T = \tilde{m}^2 \left[a_3 \mathbb{1} + Y_D^\dagger \left(b_6 \mathbb{1} + c_4 Y_U Y_U^\dagger + c_5 Y_D Y_D^\dagger + \left(c_6 Y_U Y_U^\dagger Y_D Y_D^\dagger + \text{ h.c.}\right)\right) Y_D\right] , \tag{1.12}$$

$$T_U = A \left(a_4 \mathbb{1} + b_7 Y_D Y_D^\dagger + c_7 Y_U Y_U^\dagger + c_8 Y_U Y_U^\dagger Y_D Y_D^\dagger + c_9 Y_D Y_D^\dagger Y_U Y_U^\dagger\right) Y_U , \tag{1.13}$$

$$T_D = A \left(a_5 \mathbb{1} + b_8 Y_U Y_U^\dagger + c_{10} Y_D Y_D^\dagger + c_{11} Y_U Y_U^\dagger Y_D Y_D^\dagger + c_{12} Y_D Y_D^\dagger Y_U Y_U^\dagger\right) Y_D , \tag{1.14}$$

and for sleptons

$$\left(m_L^2\right)^T = \tilde{m}^2 \left[a_6 \mathbb{1} + b_{13} Y_E Y_E^\dagger\right] , \tag{1.15}$$

$$\left(m_E^2\right)^T = \tilde{m}^2 \left[a_7 \mathbb{1} + b_{14} Y_E^\dagger Y_E\right] , \tag{1.16}$$

$$T_E = A \left(a_8 \mathbb{1} + b_{15} Y_E Y_E^\dagger\right) Y_E . \tag{1.17}$$

In the absence of neutrino masses, one can choose a basis where both Y_D and Y_E are diagonal. In this basis, one has $Y_U = V_{\text{CKM}}^T \, Y_U^{\text{diag}}$ and the only non-diagonal structure in the above equations is

$$Y_U Y_U^\dagger = V_{\text{CKM}}^T \begin{pmatrix} y_u & 0 & 0 \\ 0 & y_c & 0 \\ 0 & 0 & y_t \end{pmatrix} V_{\text{CKM}}^* . \tag{1.18}$$

It is important to note that, since the sfermion mass matrices are hermitian, the MFV coefficients in their expansions have to be real, with the exception of the coefficients b_3, c_3 and c_6, which are however suppressed by at least four powers of Yukawa couplings. The coefficients in the MFV expansion of trilinear couplings, on the other hand, can be complex in general. The consequences of nonzero phases in these coefficients will be discussed in section 3.1.

An interesting alternative formulation of MFV is by means of a nonlinear realization which makes the special role of the top Yukawa (and the bottom Yukawa if $\tan\beta$ is large) apparent [12, 13]. It leads to the same physical results (see also [14]) unless interpreted in a dynamical way as a sequential breaking of the MFV symmetry at different intermediate scales [15].

1.2.3 CP violation

As mentioned above, 45 out of the 124 parameters in the general MSSM are CP-violating phases. Since they can in principle lead to large particle electric dipole

moments (EDMs) or deviations from the SM predictions for CP violation in the K, $B_{d,s}$ or D meson systems, none of which has been established experimentally, many of these phases are strongly constrained.

Let us have a look at where these 45 phases reside. Two of them are also present in the SM: the CKM phase δ, which is measured to be sizable, around 80°, and the QCD vacuum angle θ, which has to be extremely small, giving rise to the strong CP problem, a problem which is not mitigated in the MSSM and will not be considered in the following.

Many of the phases also require non-zero flavour violation: 21 phases belong to the off-diagonal elements of the squark mass matrices and trilinear couplings, 10 to the slepton mass matrices and trilinear couplings[2]. In the case of MFV, the off-diagonal phases in the slepton sector are absent and the ones in the squark sector highly suppressed.

The remaing 12 *flavour blind* phases belong to the 9 diagonal trilinear couplings, 3 gaugino masses, the μ and the b term. Two of these parameters – or combinations thereof – can thus be chosen to be real by making use of the $U(1)_{\mathrm{PQ}}$ and $U(1)_R$ phase rotations, according to their spurion transformation properties given in table 1.2. Usually, a combined $U(1)_{\mathrm{PQ}}$ and $U(1)_R$ transformation is performed to make the b term real at the EWSB scale, since otherwise the Higgs VEVs would not be real. Then, one can use the remaining freedom to remove e.g. the phase of the μ term, the overall phase of the trilinear couplings or one of the gaugino mass phases.

1.3 Renormalization of the MSSM

Once all the parameters in the superpotential (1.3) and the soft SUSY breaking Lagrangian (1.4) have been specified, it is straightforward to construct the mass spectrum of the MSSM at tree level (see e.g. [16]). However, to relate the SUSY parameters to physical observables, and in particular to precision observables, it is worth to have a closer look at the renormalization of the MSSM at the one loop level.

This issue is particularly relevant for the determination of the parameters required to obtain correct electroweak symmetry breaking (EWSB) (section 1.3.2), the modification of relations between Yukawa couplings and fermion masses (section 1.3.3) and the renormalization group (RG) evolution of MSSM parameters to low energies (section 1.3.4), given some input at a high energy scale such as the scale of grand unification.

Since many aspects have already been discussed in [17] (cf. also [18]), the aim of this section is not an exhaustive (and exhausting) discussion, but to stress the

[2]Two of the 12 phases in the slepton mass matrices and trilinear couplings can be removed by performing individual rotations on the slepton fields of different generations, if neutrinos are massless.

issues which will be most relevant for the remainder of this thesis and to present some approximate expressions useful to get an analytical understanding of important effects.

1.3.1 The mass insertion approximation

In the general MSSM, the off-diagonal elements of the soft SUSY breaking sfermion mass matrix elements lead to effective flavour violating couplings of sfermions to neutralinos and gluinos in the mass eigenbasis [19]. These couplings can be obtained by diagonalizing the sfermion mass matrices; however, this can only be done numerically. To get an analytical understanding of flavour violating effects in the MSSM stemming from these off-diagonal elements, it is often useful to work in the mass insertion approximation (MIA). In the MIA, one assumes that the off-diagonal elements are small with respect to the diagonal ones and expands the 6×6 sfermion mass matrices as

$$\mathcal{M}^2 = \widetilde{m}^2 \mathbb{1} + \widetilde{m}^2 \begin{pmatrix} \delta^{LL} & \delta^{LR} \\ \delta^{LR\dagger} & \delta^{RR} \end{pmatrix}, \tag{1.19}$$

where $\tilde{m}$ is an average mass. Accordingly, one can expand all loop functions depending on the mass eigenvalues m_i^2 of $\mathcal{M}^2$ as a multivariate expansion in the quantities $(m_i^2 - \widetilde{m}^2)/\widetilde{m}^2$.

1.3.2 Higgs tadpoles

In order for the electroweak symmetry to be broken correctly in the MSSM, with the two Higgs doublets acquiring the VEVs

$$\langle H_u \rangle = \frac{1}{\sqrt{2}} \begin{pmatrix} v_u \\ 0 \end{pmatrix}, \qquad \langle H_d \rangle = \frac{1}{\sqrt{2}} \begin{pmatrix} 0 \\ v_d \end{pmatrix}, \tag{1.20}$$

two conditions have to be fulfilled by the parameters entering the scalar Higgs potential, which read at the tree level

$$\frac{g^2 + g'^2}{8} v^2 \cos(2\beta) + m_{H_d}^2 + |\mu|^2 = b \tan\beta \ , \tag{1.21}$$

$$-\frac{g^2 + g'^2}{8} v^2 \cos(2\beta) + m_{H_u}^2 + |\mu|^2 = b \cot\beta \ , \tag{1.22}$$

where $v^2 = v_u^2 + v_d^2$, $\tan\beta = v_u/v_d$ and

$$\frac{g^2 + g'^2}{8} v^2 = \frac{m_Z^2}{2} \ . \tag{1.23}$$

Beyond the tree level, one has to add the contributions from the Higgs tadpoles $T_{u,d}$, i.e. loop corrections to the terms in the effective Higgs potential linear in the

fields, which can be taken into account by replacing

$$m^2_{H_{u,d}} \to m^2_{H_{u,d}} + \frac{T_{u,d}}{v_{u,d}} \tag{1.24}$$

in the above conditions.

The tadpoles can be calculated from one-particle irreducible (1PI) one-point diagrams with the external propagator removed as shown in figure 1.1. The dominant contribution typically comes from stop loops due to the large top Yukawa coupling. Therefore, one usually imposes the EWSB conditions at a scale $m_{\text{EWSB}} = \sqrt{m_{\tilde{t}_1} m_{\tilde{t}_2}}$, where the logarithmic part of the stop contributions are minimized. Still, even at that scale, it is important to include the tadpoles since contributions e.g. from sbottoms or charginos can still be sizable.

In the mass insertion approximation, neglecting 1st and 2nd generation Yukawas and trilinears, dropping terms suppressed by $1/\tan\beta$ and using $m_{\tilde{u}^i_L} = m_{\tilde{d}^i_L} \equiv m_{\tilde{q}^i_L}$, one can write the contributions from sfermions as

$$\begin{aligned} -16\pi^2 \, \frac{T_u^{\tilde{f}}}{v_u} = {} & 3A_t^2 B_0(m_{\tilde{t}_L}, m_{\tilde{t}_R}) + 3\mu^2 Y_b^2 B_0(m_{\tilde{b}_L}, m_{\tilde{b}_R}) + \mu^2 Y_\tau^2 B_0(m_{\tilde{\tau}_L}, m_{\tilde{\tau}_R}) \\ & + 3Y_t^2 \left[A_0(m_{\tilde{t}_L}) + A_0(m_{\tilde{t}_R})\right] + \frac{(g')^2}{2} \sum_{i=1}^{3} \Bigg[A_0(m_{\tilde{q}^i_L}) - 2A_0(m_{\tilde{u}^i_R}) \\ & + A_0(m_{\tilde{d}^i_R}) + \left(\frac{1 - 2s_w^2}{2s_w^2}\right) A_0(m_{\tilde{l}^i_L}) + A_0(m_{\tilde{l}^i_R}) \Bigg] \end{aligned} \tag{1.25}$$

and

$$-16\pi^2 \, \frac{T_d^{\tilde{f}}}{v_u} = 3\mu Y_t A_t B_0(m_{\tilde{t}_L}, m_{\tilde{t}_R}) + 3\mu Y_b A_b B_0(m_{\tilde{b}_L}, m_{\tilde{b}_R}) + \mu Y_\tau A_\tau B_0(m_{\tilde{\tau}_L}, m_{\tilde{\tau}_R}) \, . \tag{1.26}$$

Note the v_u in the denominator on the left-hand side of (1.26); it signals the $\tan\beta$ enhancement of these contributions to T_d. The $\tan\beta$ enhanced chargino contributions in the limit where $|\mu|$, $|M_2|$ and $|\mu - M_2|$ are all $\gg M_W$ can be written as (neglecting phases in μ and M_2)

$$16\pi^2 \, \frac{T_u^{\chi^\pm}}{v_u} = \frac{2g^2}{M_2^2 - \mu^2} \Big[M_2^2 A_0(M_2) - \mu^2 A_0(\mu) \Big], \tag{1.27}$$

$$16\pi^2 \, \frac{T_d^{\chi^\pm}}{v_u} = 2g^2 \mu M_2 \tan\beta \, B_0(\mu, M_2) \, . \tag{1.28}$$

1.3.3 Threshold corrections to fermion masses

The Super CKM (SCKM) basis for the quark and squark fields is defined as the basis wherein the tree-level running Yukawa couplings in the $\overline{\text{DR}}$ scheme are simultaneously diagonal. In this basis, the (tree level) CKM matrix appears in charged current vertices. The diagonalization is achieved by means of chiral rotations of the superfields Q, U, D, L, E

$$Q_1 \to V_{Q_1}^\dagger Q_1 \quad \text{etc.}, \tag{1.29}$$

so that the Yukawa matrices are redefined according to[3]

$$Y_U \to V_{Q_1}^* Y_U V_U^\dagger \,, \qquad Y_D \to V_{Q_2}^* Y_D V_D^\dagger \,, \qquad Y_E \to V_{L_2}^* Y_E V_E^\dagger \,, \tag{1.30}$$

where the matrices on the right-hand side are now diagonal. Accordingly, the trilinear coupling matrices are rotated as

$$T_U \to V_{Q_1}^* T_U V_U^\dagger \,, \qquad T_D \to V_{Q_2}^* T_D V_D^\dagger \,, \qquad T_E \to V_{L_2}^* T_E V_E^\dagger \,, \tag{1.31}$$

and the sfermion mass matrices as

$$m_Q^2 \to V_{Q_2} m_Q^2 V_{Q_2}^\dagger \,, \qquad m_U^2 \to V_U^T m_Q^2 V_U^* \,, \tag{1.32}$$

$$m_L^2 \to V_{L_2} m_Q^2 V_{L_2}^\dagger \,, \qquad m_D^2 \to V_D^T m_Q^2 V_D^* \,, \tag{1.33}$$

$$m_E^2 \to V_E^T m_Q^2 V_E^* \,. \tag{1.34}$$

Note that, in the following, the SCKM basis and the original basis will not be distinguished notationally. It should always be clear from context which basis is meant.

The masses of quarks and leptons are consequently given at tree level (in the $\overline{\text{DR}}$ scheme) by

$$(m_u)_i = \frac{v_u}{\sqrt{2}}(Y_U)_{ii} \qquad (m_d)_i = \frac{v_d}{\sqrt{2}}(Y_D)_{ii} \qquad (m_\ell)_i = \frac{v_d}{\sqrt{2}}(Y_E)_{ii} \tag{1.35}$$

where $v_u = v \sin\beta$, $v_d = v \cos\beta$, $v \simeq 246$ GeV and the Yukawa couplings are understood to be in the SCKM basis. The experimentally accessible masses are however not the quantities in (1.35), but pole masses or QCD running masses in the $\overline{\text{MS}}$ scheme. Let us first discuss how these quantities are related for arbitrary fermions.

Starting from a running particle mass m defined in a mass-independent renormalization scheme like $\overline{\text{MS}}$ or $\overline{\text{DR}}$, the physical (pole) mass M is found as the pole of the inverse propagator,

$$S(\not{p})^{-1} = \not{p} - m - \Sigma(\not{p}) + i\epsilon \,, \tag{1.36}$$

[3]Note that the indices $1, 2$ on Q and L label the components of the $SU(2)$ doublet here, not the generation.

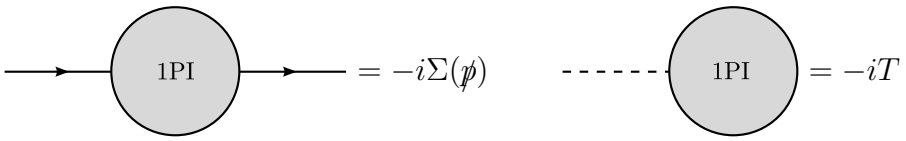

Figure 1.1: Definition of fermion self-energy and scalar tadpole.

where $-i\Sigma(\not{p})$ is given by the sum of 1PI self-energy diagrams with the external propagators removed as shown in figure 1.1. Writing

$$\Sigma(\not{p}) = \Sigma^{LL}(p^2)\,\not{p}P_L + \Sigma^{RR}(p^2)\,\not{p}P_R + \Sigma^{RL}(p^2)\,P_L + \Sigma^{LR}(p^2)\,P_R\,, \tag{1.37}$$

with $\Sigma^{RL} = (\Sigma^{LR})^*$ one finds

$$M = m + \Delta m\,, \tag{1.38}$$

where

$$\Delta m = \frac{M}{2}\left(\Sigma^{LL}(M^2) + \Sigma^{RR}(M^2)\right) + \Sigma^{RL}(M^2)\,. \tag{1.39}$$

This procedure for calculating the pole mass is applicable in the MSSM for heavy fermions like the top quark, the gluino, the charginos or neutralinos, but also for colourless light particles light the charged leptons. For the light (i.e. lighter than m_t) quarks, however, it is not applicable since their pole masses are not well-defined quantities; since α_s is strong at these low scales, the gluon contribution to the self-energy has to be resummed. In other words, one should use the $\overline{\rm MS}$ masses instead of the pole masses.

The procedure for matching light quark masses defined in the $\overline{\rm DR}$ scheme within the MSSM onto the masses defined in the $\overline{\rm MS}$ scheme within QCD with 5 flavours of quarks is as follows. First, one subtracts all the contributions to the 1PI quark self-energies except for the gluon and light quark contributions at some matching scale μ_m close to the EW scale, such as M_Z. For consistency reasons, these contributions have to be evaluated in the $\overline{\rm DR}$ scheme. One obtains the running quark mass in the $\overline{\rm DR}$ scheme *within five-flavour QCD*:

$$m^{\overline{\rm DR},\,\rm QCD}(\mu_m) = m^{\overline{\rm DR},\,\rm MSSM}(\mu_m) + \Delta m^{\overline{\rm DR}}(\mu_m) \tag{1.40}$$

where $\Delta m^{\overline{\rm DR}}$ is given by (1.39), but the Σ^{AB} are now understood not to include ordinary QCD loops. Second, the conversion from the $\overline{\rm DR}$ to the $\overline{\rm MS}$ scheme is performed at the one-loop level via [20]

$$m(\mu_m)^{\overline{\rm MS}} = \frac{m_(\mu_m)^{\overline{\rm DR}}}{1 - \frac{\alpha_s}{3\pi}}\,. \tag{1.41}$$

The $\overline{\rm MS}$ mass can now be evolved to scales lower than μ_m by means of the well-known QCD RG equations (RGEs). Numerically, this can be performed at the four-loop level with the public code RunDec [21].

The threshold correction Δm in (1.38) and (1.40) (the subscript and scale dependence will be omitted in the following when it is clear from the context) has a great impact on phenomenology in particular for the down-type quarks and charged leptons when $\tan\beta$ is large. The reason is that, while at the tree-level, these fermions couple only to the down-type Higgs H_d, which has a small VEV in the large $\tan\beta$ regime, they can couple to the up-type Higgs at the loop level in the presence of SUSY breaking (the Hall-Rattazzi-Sarid effect [22]).

These non-holomorphic couplings show up as insertion of the up-type Higgs VEV v_u when the self-energy diagrams contributing to (1.40) are calculated in the mass insertion approximation.

While the full one-loop results for the MSSM fermion self-energies have already been presented in [17], it is instructive to calculate the dominant contributions to the threshold corrections to the down-type quarks and charged leptons in the MIA to understand the behaviour of these quantities under changes of the SUSY parameters.

Writing the bottom and tau masses as

$$m_{b,\tau} = \frac{1}{\sqrt{2}}(v_d\, y_{b,\tau} + v_u\, y'_{b,\tau}) = \frac{v_d}{\sqrt{2}} y_{b,\tau}(1 + \epsilon_{b,\tau}\tan\beta), \tag{1.42}$$

one finds in the MIA, assuming flavour blind soft terms,

$$\epsilon_b^{\tilde{g}} = \frac{g_3^2}{6\pi^2}\,\mu M_3\,\left[-C_0(m^2_{\tilde{b}_L}, m^2_{\tilde{b}_R}, M_3^2)\right], \tag{1.43}$$

$$\epsilon_b^{\tilde{H}} = \frac{y_t^2}{16\pi^2}\,\mu A_t\,\left[-C_0(m^2_{\tilde{t}_L}, m^2_{\tilde{t}_R}, \mu^2)\right], \tag{1.44}$$

$$\epsilon_b^{\tilde{W}} = \epsilon_\tau^{\tilde{W}} = -\frac{3g_2^2}{32\pi^2}\,\mu M_2\,\left[-C_0(m^2_{\tilde{t}}, M_2^2, \mu^2)\right], \tag{1.45}$$

where

$$\epsilon_b = \epsilon_b^{\tilde{g}} + \epsilon_b^{\tilde{H}} + \epsilon_b^{\tilde{W}} + \epsilon_b^{\tilde{B}}\ , \qquad\qquad \epsilon_\tau = \epsilon_\tau^{\tilde{W}} + \epsilon_\tau^{\tilde{B}}\ , \tag{1.46}$$

and the $\tilde{B}$ contributions are usually subleading with respect to the $\tilde{W}$ contributions. The loop function C_0 in (1.43)–(1.45) has dimensions of inverse mass squared, it is finite and strictly negative. Its explicit form is

$$C_0(x,y,z) = -\frac{x\ln x}{(x-y)(x-z)} - \frac{y\ln y}{(y-x)(y-z)} - \frac{z\ln z}{(z-x)(z-y)}\ . \tag{1.47}$$

1.3.4 Renormalization group evolution

The RG evolution of the soft SUSY breaking and superpotential parameters is a crucial ingredient of any phenomenological analyis within a SUSY framework predicting the pattern of these parameters at some high scale, such as the GUT scale.

The RGEs for all the relevant couplings in a general quantum field theory have been presented in [23–25] at the two-loop level and for a general SUSY theory and in particular the MSSM in [26]. For the numerical analyses to be presented in this thesis, a Mathematica code developed by the author for the numerical solution of the full set of coupled two-loop RGEs has been applied. Still, to get an analytic understanding of the results, it is often useful to have only the dominant contributions to the RGEs as well as approximate numerical solutions. Some aspects of this are briefly discussed in appendix B.

1.4 The flavour puzzle

As discussed in the introduction, 13 of the 19 parameters in the SM with massless neutrinos are related to Yukawa couplings and their actual values exhibit peculiar hierarchies which call for a fundamental explanation. Moreover, even the mere fact that there are three sequential generations of fermions is completely unexplained in the SM. In the MSSM, these puzzles persists almost unchanged. In fact, the discussion in the preceding sections showed that there is a large number of flavour violating terms in the soft SUSY breaking Lagrangian which are subject to strong constraints from experiment, since no significant deviation from the SM predictions have been observed in the flavour sector so far.

The strongest assumption one can make on these flavour violating terms is the assumption of minimal flavour violation discussed in section 1.2.2. In that case, the flavour puzzle remains a puzzle of Yukawa couplings, and the soft terms do not introduce any additional flavour violation beyond that. This can be realized if the mechanism of SUSY breaking mediation is flavour blind. On the other hand, the MFV principle is indeed a very strong assumption and by no means established as an experimental necessity.

Concerning the Yukawa couplings themselves, their values are unexplained in the MSSM just as in the SM; however, supersymmetry introduces several new handles how the origin of Yukawa couplings could be better understood. The requirement of two Higgs doublets modifies the relation between Yukawa couplings and fermion masses. The observed fermion mass hierarchies could then be partly due to hierarchical Higgs VEVs rather than hierarchical Yukawa couplings, namely in the large $\tan\beta$ regime. In this regime, loop-induced "wrong-Higgs" couplings of quarks and leptons additionally blur the distinction between flavour structures arising from the Yukawa couplings vs. the soft SUSY breaking sector.

Also the perturbativity and naturalness of the MSSM up to very high scales opens new roads to deal with the flavour puzzle. Grand unification relates the quarks and leptons within a generation and might therefore also relate their Yukawa couplings. Finally, horizontal, i.e. inter-generational, gauge symmetries and their spontaneous breakdown might represent a possible supersymmetric explanation of the flavour

structure observed at low energies.

1.4.1 Mediation of SUSY breaking

Let us have a brief look at how the flavour puzzle is addressed in the two most popular mechanisms of SUSY breaking mediation, gravity and gauge mediation.

Gravity mediation

Once supersymmetry is promoted to a local symmetry, one obtains a supersymmetric effective field theory including gravity called supergravity. If SUSY is broken in a hidden sector, Planck-suppressed non-renormalizable operators should be present that mediate this breaking to the visible sector. Supergravity allows to treat these contributions in a consistent framework.

The $N = 1$ supergravity Lagrangian is fixed by the symmetries up to three functionals: the superpotential as well as the Kähler potential and the gauge kinetic function. Assuming a universal gauge kinetic function and "canonical" Kähler potential, a very simple pattern of soft terms emerges: the constrained MSSM (CMSSM) with

$$\begin{aligned} m^2_{Q,U,D,L,E} &= m_0^2 \, \mathbb{1} \ , & m^2_{H_u} &= m^2_{H_d} = m_0^2 \ . \\ T_{U,D,E} &= A_0 \, Y_{U,D,E} \ , & M_{1,2,3} &= m_{1/2} \ . \end{aligned} \tag{1.48}$$

With the requirement of correct EWSB, the magnitude of the μ term is fixed in this model and the b term can be traded for $\tan\beta$. One is left with three real parameters $\tan\beta$, m_0 and $m_{1/2}$ (exploiting the PQ and R symmetries as discussed in section 1.2.3), one complex one A_0 and the phase of μ.

Although the CMSSM is very appealing due to its simplicity, there is no firm theoretical motivation for choosing these special forms for the Kähler potential and gauge kinetic function. Gravity mediation in general does in fact not lead to universal and flavour blind soft terms unless additional symmetries are introduced specifically for that purpose. One is then lead to so-called SUSY flavour models which will be briefly discussed in section 1.4.2.

Gauge mediation

If the mediation of supersymmetry breaking proceeds entirely via $SU(3)_c \times SU(2)_L \times U(1)_Y$ gauge interactions between hidden sector and visible sector fields, the soft SUSY breaking automatically fulfills the condition of MFV (see section 1.2.2), since gauge interactions are flavour blind.

Phenomenologically, this is of course very welcome since it would explain to a great extent the agreement of precision experiments in the flavour sector with the SM expectations. This is even more true since theories with gauge mediation (GM) generically predict negligible trilinear couplings at the mediation scale since they

are loop-suppressed with respect to the sfermion and gaugino masses. Although the trilinear couplings are regenerated in the RG evolution from the mediation scale down to low energies, the fact the this scale can be quite low in GM models implies that also these RG contributions are generically small. As a consequence, also chirality-violating processes like $B \to X_s\gamma$ or $B_s \to \mu^+\mu^-$, which in general represent powerful constraints on SUSY models even in the absence of non-minimal flavour violation, are usually under control.

While a large number of different phenomenologically viable models of gauge mediation are on the market[4], a very simple and general definition of gauge mediation was suggested in [28]: If one assumes that the visible and hidden sectors decouple in the limit that the gauge couplings $g_i \to 0$, one can encode all the information on the hidden sector required to parametrize the soft terms in a limited number of gauge current correlation functions.

This definition of General Gauge Mediation (GGM) encompasses a large number of existing models, including models with or without messengers and models with a strongly coupled hidden sector. It allows to parametrize the soft terms for gauginos and sfermions as [29]

$$M_k = g_k^2 M B_k\,, \quad (m_F^2)_{ij} = \delta_{ij}\left(g_1^2 Y_F \zeta + \sum_{k=1}^{3} g_k^4 C_2(F,k) A_k\right)\,, \quad (T_{U,D,E})_{ij} = 0\,, \tag{1.49}$$

where $k = 1, 2, 3$ labels the gauge group, $F = Q, U, D, L, E$, while C_2 is the quadratic Casimir of the respresentation of superfield F with respect to gauge group k and Y is the hypercharge. Accordingly, for the Higgs soft masses one has

$$\begin{aligned}(m_{H_{u,d}}^2) &= g_1^2 Y_{H_{u,d}} \zeta + \sum_{k=1}^{2} g_k^4 C_2(H_{u,d},k) A_k \\ &= \pm\frac{g_1^2}{2}\zeta + \frac{3g_1^4}{20} A_1 + \frac{3g_2^4}{4} A_2\,. \end{aligned} \tag{1.50}$$

However, one of the biggest problems in GMSB models is to generate the μ and b terms of a phenomenologically viable size [30, 31]. Therefore, an additional mechanism has to be invoked to generate μ and b and it is reasonable to expect that this mechanism will modify also the GGM relations for the Higgs soft masses (1.50).

In fact, the simple definition of GGM as stated above, i.e. the MSSM and the hidden sector decouple in the limit $g_i \to 0$, does not allow the generation of a b or μ term from soft SUSY breaking interactions at all, since these parameters violate the Peccei-Quinn symmetry and cannot be generated by gauge interactions alone (cf. section 1.2). One therefore either has to extend the definition of GGM to allow

[4] See [27] for an excellent but slightly dated review and collection of references.

for interactions generating sufficient μ and b [28], or one accepts $b = 0$, which is not ruled out *per se*, and assumes that the origin of the superpotential parameter μ is unrelated to the SUSY breaking sector.

In the GGM expressions for the soft masses of sfermions (1.49) and Higgs fields (1.50), a hypercharge D-term appears, which is problematic, since it gives rise to a non-positive definite contribution to the scalar squared masses and can lead to tachyons in the spectrum. To avoid this, it can be forbidden by imposing a discrete symmetry [28, 32].

Let us now have a look at the number of parameters in GGM. In the most general case, with ζ and b nonzero, the are 8 real parameters – $|A_k|$, B_k, ζ and $|b|$ ($|\mu|$ is fixed by the requirement of correct EWSB); $|b|$ can be traded for $\tan\beta$. Concerning phases, there are 5 in total – in A_k, b and μ – but two can be rotated away by making use of the $U(1)_{\mathrm{PQ}}$ and $U(1)_R$ symmetries discussed in section 1.2.1, so there are only 3 physical phases.

Since the seven sfermion and Higgs soft masses are determined by the four real parameters $A_{1,2,3}$ and ζ in this case, there are three relations among them, valid at the mediation scale M:

$$6m_Q^2 + 3m_U^2 - 9m_D^2 - 6m_L^2 + m_E^2 = 0 \ , \tag{1.51}$$

$$m_L^2 = m_{H_d}^2 \ , \tag{1.52}$$

$$3m_Q^2 - 3m_U^2 + 3m_L^2 + 2m_E^2 = 6m_{H_u}^2 \ . \tag{1.53}$$

If $\zeta = 0$, there is an additional relation, $m_{H_u}^2 = m_{H_d}^2$.

If $b = 0$ at the mediation scale, $\tan\beta$ is no longer a free parameter and one has the freedom to remove one more phase; then, the 2 remaining physical phases can be chosen to reside in B_1 and B_2.

In fact, this shows that having $b = 0$ at the mediation scale is not only interesting from a conceptual point of view, being a prediction of the simple definition of GGM, but also has an important phenomenological motivation, strongly ameliorating the SUSY CP problem within gauge mediation: Assuming the gaugino masses to have a common phase at the mediation scale, as is the case for example in the Minimal Gauge Mediation (MGM) model, where the gaugino masses fulfill the GUT relation $M_1/g_1^2 = M_2/g_2^2 = M_3/g_3^2$, the condition $b = 0$ indeed completely solves the CP problem, since there are no CP-violating phases left that cannot be rotated away.

1.4.2 Origin of Yukawa couplings

The puzzling values of the Yukawa couplings in the MSSM superpotential (1.3) mentioned at the beginning of section 1.4 might be an indication that the Yukawas are not fundamental parameters but arise dynamically as VEVs of some more fundamental scalar fields. In that case, a subgroup of the flavour symmetry discussed in section 1.2.1 would be broken spontaneously by these VEVs and the hierarchies in

the Yukawa couplings would be generated by a generalized Froggatt-Nielsen mechanism [33].

Such "SUSY flavour models" are particularly interesting in the context of gravity mediated SUSY breaking since they provide a rationale for the absence of excessive flavour violating terms: in the limit of exact flavour symmetry, the soft terms have to be invariant under this symmetry. After its breaking, the flavour structures in soft terms and Yukawa couplings will be generated by the same mechanism and one can therefore expect some amount of alignment.

On the other hand, although a large number of SUSY flavour models is on the market, it is very difficult to generate soft terms which are exactly of the MFV form. Therefore, another interesting point about SUSY flavour models is typically the presence of non-minimal flavour violating effects and correlations between different processes induced by the flavour symmetry. A comprehensive study of flavour and CP violating effects in some representative SUSY flavour models has been presented by us recently [34].

2 SUSY GUTs with Yukawa unification

Grand Unified Theories (GUTs) aim to explain the origin and different strengths of the three gauge interactions described by the SM and the origin of the peculiar gauge quantum numbers of quarks and leptons (cf. table 1.1).

The SM does not provide an explanation of the patterns of quantum numbers of the various $SU(3)_c$ triplets and singlets and $SU(2)_L$ doublets and singlets. Although the hypercharges of these fields are not arbitrary since all gauge anomalies have to cancel, there remains a freedom to assign continuous hypercharges without spoiling this cancellation. Therefore, the quantization of charge as is evident in the neutrality of the neutron is a mystery and the cancellation of anomalies seems like a miracle in the SM.

The smallest simple group which contains the SM gauge group as a subgroup is $SU(5)$. It is a stunning observation that the $SU(3) \times SU(2) \times U(1)$ decomposition of a $\bar{\mathbf{5}}$ and $\mathbf{10}$ representation of $SU(5)$ gives fields which have precisely the quantum numbers of one generation of quarks and leptons. Moreover, embedding $SU(5)$ in $SO(10)$, both the $\bar{\mathbf{5}}$ and the $\mathbf{10}$ can be embedded in a single 16-dimensional spinor representation which, in addition to the SM fermions, predicts the existence of one SM gauge singlet per generation, which is very welcome for the explanation of the tiny but non-zero neutrino masses.

Another hint for a unified gauge group and a strong motivation for the MSSM and supersymmetric GUTs is the precise apparent gauge coupling unification in the MSSM. Evolving the gauge couplings to high energies, assuming the sparticle masses to lie around the TeV scale, the gauge couplings unify within errors at a scale of about $2 \times 10^{16}\,\mathrm{GeV}$, unlike in the SM, where this unification fails.

In spite of all these virtues, the fact that the GUT symmetry, if it exists at some high scale, has to be broken combined with our ignorance about the breaking scheme makes it very difficult to provide model-independent, testable predictions.

One generic prediction of GUTs is the instability of the proton, since baryon and lepton number are necessarily violated if quarks and leptons share common representations of the gauge group. However, proton decay has not been observed yet, so it only provides bounds on classes of GUT models. In SUSY GUTs, the dominant contribution to the proton decay rate typically comes from dimension-five operators generated by the exchange of colour-triplet Higgsinos. This contribution is however strongly model dependent, so it is difficult to draw general conclusions on the viability of SUSY GUTs [35–37].

A different way to test specific SUSY GUT models is by their predictions for the

masses and mixings of the SM fermions. In $SU(5)$ GUTs, the right-handed down-type quarks and left-handed charged leptons are unified in a $\bar{\mathbf{5}}$ representation. In the minimal model, their Yukawa couplings are thus the same at the GUT scale, $Y_D^T = Y_E$. Unfortunately, this is not phenomenologically viable since it leads to the approximately RG invariant prediction $m_s/m_d = m_\mu/m_e$, which is off by orders of magnitude. However, for the third generation, one observes that the bottom quark and tau lepton masses are similar in magnitude, and moreover that the difference between their running masses decreases as one goes to higher scales, due to the $SU(3)_c$ contributions to the running of the bottom Yukawa coupling. b-τ unification at the GUT scale thus remains a tantalizing possibility.

In $SO(10)$, where all quarks and leptons of one generation share a **16** representation of the gauge group, one could even have a unification of the top, bottom and tau Yukawa couplings at the GUT scale. To explain the large hierarchy between m_t and m_b, this scenario would require large $\tan\beta$, i.e. a large hierarchy between the VEVs of the two MSSM Higgs doublets instead of a large hierarchy of Yukawa couplings.

Whether such Yukawa coupling unification is successful depends however not only on $\tan\beta$, but also on the SUSY spectrum since the relations between the known fermion masses and the Yukawa couplings are affected by potentially large threshold corrections. On the other hand, this dependence implies that the *assumption* of successful Yukawa unification (YU) might allow to make predictions for the SUSY spectrum itself, facilitating robust tests of the YU hypothesis.

It should be stressed that, since Yukawa unification is impossible for the first two generations, even for the third generation it is by no means a necessary ingredient of a realistic GUT model. On the other hand, the third generation plays a special role, in particular in the large $\tan\beta$ regime where all the third generation Yukawa couplings are of $O(1)$. Therefore, it will be the aim of this chapter to investigate the *phenomenological consequences* of an *exact* unification of the b-τ or t-b-τ Yukawa couplings at the GUT scale $M_G \simeq 2 \times 10^{16}\,\text{GeV}$. The discussion will rely on the assumptions that there exists a GUT theory predicting Yukawa unification for the third generation and that the GUT-scale threshold corrections to this unification are negligible. If these assumptions lead to testable predictions at low energies, their falsification or verification could help shed light on the origin of fundamental interactions.

2.1 Yukawa unification in the MSSM

In the MSSM, the third generation Yukawa couplings are given at tree level by

$$y_t = \frac{m_t}{v_u/\sqrt{2}}\,, \qquad\qquad y_{b,\tau} = \frac{m_{b,\tau}}{v_d/\sqrt{2}}\,, \tag{2.1}$$

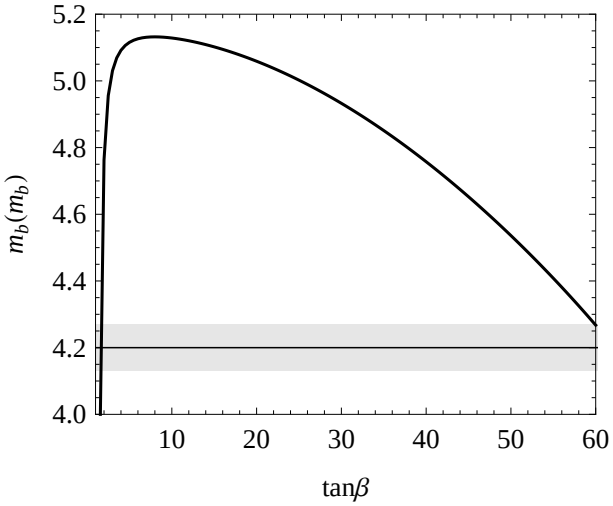

Figure 2.1: Prediction for the bottom quark mass $m_b(m_b)$ in the $\overline{\text{MS}}$ scheme imposing b-τ unification at the GUT scale, $y_b(M_G) = y_\tau(M_G)$, and neglecting threshold corrections to the Yukawa couplings. The gray band indicates the experimentally allowed 1σ range [39].

where $v_u = v \sin\beta$ and $v_d = v \cos\beta$. To explain the large hierarchy $m_t/m_b \sim 50$, Yukawa unification of top and bottom requires a large hierarchy of VEVs, $\tan\beta \sim 50$. However, also the unification of the b and τ Yukawa couplings alone prefers large $\tan\beta$. This can be seen by solving the RG equations for the third generation Yukawa couplings, neglecting threshold corrections and imposing the top and tau Yukawas at low energies to equal their tree-level values (2.1), as well as y_b to equal y_τ at the scale where the gauge couplings unify, $M_G \simeq 2 \times 10^{16}\,\text{GeV}$. The resulting prediction for the bottom quark mass depending on the value of $\tan\beta$, shown in figure 2.1, turns out to be generically too large unless $\tan\beta \lesssim 1$ or $\tan\beta \gtrsim 60$; since the very low $\tan\beta$ solution is precluded by the upper bound on the mass of the lightest Higgs boson set at LEP [38], b-τ unification prefers large $\tan\beta$.

In the case of t-b-τ unification, $\tan\beta \simeq 50$ is fixed and it can be seen from figure 2.1 that m_b is too large with respect to its measured value $m_b(m_b) = (4.2 \pm 0.07)\,\text{GeV}$ [39]. However, going beyond the tree level, the prediction for m_b can be strongly modified due to the $\tan\beta$ enhanced threshold corrections arising from the loop-induced "wrong-Higgs" couplings discussed in section 1.3.3. The question of successful Yukawa unification then turns into the question of the region in SUSY parameter space where the low-energy threshold corrections to m_b are sufficiently *negative* to obtain the correct m_b.

Indeed, it is precisely this correlation between the SUSY couplings as well as spectrum and the success of YU that will allow to make testable predictions from the hypothesis of YU.

To understand which of these regions potentially leading to successful YU are, let us recall the main contributions to the threshold-corrected b quark mass already discussed in section 1.3.3,

$$m_b = \frac{v_d}{\sqrt{2}} y_b (1 + \epsilon_b \tan\beta) \ . \tag{2.2}$$

Assuming for simplicity the sbottom masses to be equal and degenerate with the gluino mass, as well as the stop masses to be equal and degenerate with the Higgsino mass, the contributions to ϵ_b from from gluino-sbottom and chargino-stop loops read, in the mass insertion approximation (cf. (1.43)–(1.44)),

$$\epsilon_b^{\tilde{g}} = \frac{g_3^2}{6\pi^2}\,\mu M_3\,\frac{1}{2m_{\tilde{b}}^2}, \qquad\qquad \epsilon_b^{\tilde{\chi}^\pm} = \frac{y_t^2}{16\pi^2}\,\mu A_t\,\frac{1}{2m_{\tilde{t}}^2} \tag{2.3}$$

The sign of the gluino contribution is given by the sign of the μ term, and the sign of the chargino contribution by the sign of (μA_t). To understand which of these contributions is dominant, one can solve the RG equations approximately to obtain the values of the relevant parameters at low energies, starting from some values at the GUT scale. Assuming a universal trilinear coupling A_0 and a universal gaugino mass $m_{1/2}$ at the GUT scale, the low-energy value of A_t is given by

$$A_t \simeq -2.0\, m_{1/2} + 0.23\, A_0, \tag{2.4}$$

and the gluino mass by

$$M_3 \simeq 2.6\, m_{1/2}. \tag{2.5}$$

Due to the comparably large coefficients of $m_{1/2}$ and the parametric suppression of the chargino contribution, the gluino contribution thus typically dominates, prompting μ to be negative to obtain a negative overall correction to m_b. However, $\mu < 0$ is strongly disfavoured by the measurement of the muon anomalous magnetic moment as will be discussed in section 2.2.4.

There are two obvious possibilities to remedy this problem. The first is to introduce non-universal gaugino masses. In that case, eq. (2.4) generalizes to $A_t \approx -0.2M_2 - 1.8M_3 + 0.23A_0$ and a hierarchy $M_2 \gg M_3$ can be invoked to enhance the negative chargino contributions with respect to the gluino contributions. This possibility has been studied in [40] in the context of gaugino mediation and in [41] in the context of a left-right symmetric model. The second possibility is to assume a hierarchy $-A_0 \gg m_{1/2}$, so that the gluino mass is small and the large negative stop trilinear is not dominantly generated by RG effects proportional to $m_{1/2}$, but is present already at the GUT scale.

Another requirement on the parameter space leading to succesful YU is the need for Higgs splitting. The soft SUSY breaking Higgs soft masses have to obey $m_{H_d}^2 > m_{H_u}^2$ at the EWSB scale (which is usually assumed to be $m_{\rm SUSY} = \sqrt{m_{\tilde{t}_1} m_{\tilde{t}_2}}$

to minimize logarithmic corrections to the effective potential) if $\tan\beta > 1$. Usually, this splitting is realized radiatively in the MSSM, even if $m^2_{H_d} = m^2_{H_u}$ at some high scale, since $m^2_{H_u}$ is driven towards negative values more strongly by the top Yukawa coupling compared to $m^2_{H_d}$, whose running is mainly driven by the bottom and tau Yukawas. However, for $\tan\beta \simeq 50$, the third generation Yukawa couplings all become comparable, the radiative splitting mechanism becomes weaker and consequently EWSB with universal $m^2_{H_{u,d}}$ becomes more difficult [42].

Indeed, in [43, 44] the MSSM with universal sfermion masses, universal gaugino masses, universal trilinear couplings and non-universal Higgs masses (the "NUHM") was found to allow for successful YU in the region with

$$\tan\beta \simeq 50, \quad -A_0 \approx 2\, m_{16}, \quad \mu, m_{1/2} \ll m_{16}\ . \tag{2.6}$$

However, the large $\tan\beta$ and large trilinear couplings in this scenario can lead to dangerous effects in FCNC observables. Indeed, the above solution to YU was only possible by assuming a SUSY contribution to the $B \to X_s\gamma$ decay twice as large as the SM one [45], a solution which is nowadays strongly disfavoured by the data on the inclusive $B \to X_s\ell^+\ell^-$ decay [46, 47].

This tension highlights the importance of FCNCs as constraints on Yukawa unified models. Therefore, the next section will briefly review the most important flavour constraints in the MFV MSSM at large $\tan\beta$.

2.2 Flavour physics at large $\tan\beta$

The most stringent flavour constraints on the MSSM with MFV, no new sources of CP violation and large $\tan\beta$ currently come from helicity suppressed $b \to s$ transitions and from the tree-level flavour changing charged current decay $B \to \tau\nu$. An important flavour conserving precision constraint is represented by the anomalous magnetic moment of the muon.

The part of the $\Delta B = \Delta S = 1$ effective Hamiltonian most sensitive to NP effects reads

$$\mathcal{H}_{\text{eff}} = -\frac{4\,G_F}{\sqrt{2}} V_{tb}V_{ts}^* \sum_{i=7,8,9,10,P,S} (C_i\mathcal{O}_i + C_i'\mathcal{O}_i')\,, \tag{2.7}$$

where the relevant operators are given by

$$\mathcal{O}_7 = \frac{e^2}{16\pi^2} m_b(\bar{s}\sigma_{\mu\nu}P_R b)F^{\mu\nu}, \qquad \mathcal{O}_8 = \frac{g_3^2}{16\pi^2} m_b(\bar{s}\sigma_{\mu\nu}T^a P_R b)G^{\mu\nu\,a}, \tag{2.8}$$

$$\mathcal{O}_9 = \frac{e^2}{16\pi^2}(\bar{s}\gamma_\mu P_L b)(\bar{\ell}\gamma^\mu \ell), \qquad \mathcal{O}_{10} = \frac{e^2}{16\pi^2}(\bar{s}\gamma_\mu P_L b)(\bar{\ell}\gamma^\mu\gamma_5 \ell), \tag{2.9}$$

$$\mathcal{O}_S = \frac{e^2}{16\pi^2} m_b(\bar{s}P_R b)(\bar{\ell}\ell), \qquad \mathcal{O}_P = \frac{e^2}{16\pi^2} m_b(\bar{s}P_R b)(\bar{\ell}\gamma_5 \ell), \tag{2.10}$$

and the chirality-flipped operators $\mathcal{O}'_i$ are obtained from (2.8)–(2.10) by making the replacement $P_L \leftrightarrow P_R$.

2.2.1 $B \to X_s\gamma$

The inclusive radiative $B \to X_s\gamma$ [48] decay is among the most powerful contraints on the MSSM in view of its precise experimental measurement

$$\mathrm{BR}(B \to X_s\gamma)_{\mathrm{exp}}^{E_\gamma > 1.6\ \mathrm{GeV}} = (3.52 \pm 0.25) \times 10^{-4}\ , \tag{2.11}$$

and its good agreement with the SM NNLO prediction [49]

$$\mathrm{BR}(B \to X_s\gamma)_{\mathrm{SM}} = (3.15 \pm 0.23) \times 10^{-4}\ . \tag{2.12}$$

In a general NP theory, the partonic decay rate is proportional to

$$\Gamma(b \to s\gamma) \propto |C_7^{\mathrm{eff}}(\mu_b)|^2 + |C'_7(\mu_b)|^2\ , \tag{2.13}$$

where $C_7^{\mathrm{eff}}(\mu_b) = C_7^{\mathrm{eff,\ SM}}(\mu_b) + C_7^{\mathrm{NP}}(\mu_b)$ and C'_7 vanishes in the SM (C_7^{eff} will also be discussed in section 4.1.1). The NP contributions to the Wilson coefficients $C_7^{(\prime)\mathrm{NP}}$ at the low scale μ_b are sensitive to $C_{7,8}^{(\prime)\mathrm{NP}}$ at the matching scale. For the full set of one-loop contributions to $C_{7,8}^{(\prime)}$ in the MSSM see [50, 51].

In the MFV MSSM, the contributions to the primed operators are strongly suppressed since there are no right-handed currents. The Wilson coefficients of the unprimed operators, $C_{7,8}$, receive contributions from charged Higgs, chargino, neutralino and gluino loops. The charged Higgs contributions always interefere constructively with the SM contribution; the neutralino contributions are usually subleading. The gluino contributions are particularly relevant in the presence of non-minimal sources of flavour violation, but can also play a role in the MFV MSSM [52]. The dominant contribution to $C_{7,8}$ in the MFV MSSM with large $\tan\beta$ is then typically given by $\tan\beta$ enhanced chargino contributions. Assuming a common SUSY mass $\tilde{m}$, it can be written in the MIA as [53]

$$C_{7,8}^{\tilde{\chi}^\pm} = -\frac{\tan\beta}{1+\epsilon_b \tan\beta}\ \frac{m_t^2}{\tilde{m}^2}\ \frac{A_t\mu}{\tilde{m}^2} f_{7,8}(x_\mu)\ . \tag{2.14}$$

where the loop functions can be found in the appendix of [53].

The two crucial points for the following analysis are that the chargino contribution (2.14) is $\tan\beta$ enhanced and that its sign – with the loop functions being strictly positive – is given by the sign of μA_t.

Since the $B \to X_s\gamma$ branching ratio is only sensitive to the magnitude of C_7^{eff} and not to its sign, one could conceive a scenario where the chargino contributions to C_7 are so large (and negative) that they overcompensate the SM contribution, leading

again to a branching ratio in agreement with the experimental measurement. Indeed, such a scenario was found earlier to be favoured by models with YU. However, it has been shown in [46] that this is ruled out at more than 2σ by the measurement of the inclusive $B \to X_s \ell^+ \ell^-$ branching ratio *unless* there are sizable corrections to the Wilson coefficients C_9 and C_{10}, which is however not the case in the scenarios to be considered in this chapter. The sign of the $b \to s\gamma$ amplitude will thus always be SM-like.

2.2.2 $B_s \to \mu^+\mu^-$

The decay $B_s \to \mu^+\mu^-$ is strongly helicity suppressed in the SM, with a predicted branching ratio of [54]

$$\mathrm{BR}(B_s \to \mu^+\mu^-) = (3.2 \pm 0.2) \times 10^{-9}. \tag{2.15}$$

It has not been observed experimentally yet and the most recent experimental upper bound[1] still lies, at the 95% confidence level, one order of magnitude above the SM [48, 56, 57]:

$$\mathrm{BR}(B_s \to \mu^+\mu^-) < 4.3 \times 10^{-8}\,. \tag{2.16}$$

In a generic NP model, the branching ratio is given by

$$\mathrm{BR}(B_s \to \mu^+\mu^-) = \tau_{B_s} f_{B_s}^2 m_{B_s} \frac{\alpha_{\mathrm{em}}^2 G_F^2}{16\pi^3} |V_{tb}V_{ts}^*|^2 \sqrt{1 - \frac{4m_\mu^2}{m_{B_s}^2}} \left[|S|^2 \left(1 - \frac{4m_\mu^2}{m_{B_s}^2}\right) + |P|^2 \right], \tag{2.17}$$

where

$$S = \frac{m_{B_s}^2}{2}(C_S - C_S'), \qquad P = \frac{m_{B_s}^2}{2}(C_P - C_P') + m_\mu (C_{10} - C_{10}'). \tag{2.18}$$

In the MSSM with large $\tan\beta$, the branching ratio can be strongly enhanced by a contribution to the (pseudo)scalar Wilson coefficients $C_{S,P}$ from Higgs penguin diagrams which grow as $\tan^6\beta$ [58, 59]. Assuming a common SUSY mass $\tilde{m}$, one finds in the MIA [53]

$$C_{S,P} = \mp \frac{m_\mu}{4M_A^2} \frac{m_t^2}{M_W^2 s_w^2} \frac{\tan^3\beta}{(1+\epsilon_b \tan\beta)(1+\epsilon_0 \tan\beta)(1+\epsilon_\ell \tan\beta)} \frac{\mu A_t}{\tilde{m}^4} C_0(\tilde{m}^2, \tilde{m}^2, \mu^2)\,. \tag{2.19}$$

where the loop function has been given in (1.47). Just as the chargino contribution to C_7 in (2.14), this contribution is proportional to μA_t.

[1] In the numerical analysis of capters 2 and 3.2, the latest *published* upper bound from the CDF collaboration, $\mathrm{BR}(B_s \to \mu^+\mu^-) < 5.8 \times 10^{-8}$ [55], was used. The more recent and slightly more stringent preliminary bound presented here does however not affect the conclusions of these analyses.

2.2.3 $B^+ \to \tau^+\nu$

The tree level decay $B^+ \to \tau^+\nu$ is a sensitive probe of models with an extended Higgs sector [60]. In the MSSM with large $\tan\beta$, its branching ratio can differ significantly from the SM prediction [61, 62]. Tree level charged Higgs contributions interfere destructively with the SM ones and lead to

$$R_{B\tau\nu} = \frac{\mathrm{BR}(B^+ \to \tau^+\nu)}{\mathrm{BR}(B^+ \to \tau^+\nu)_{\mathrm{SM}}} \simeq \left(1 - \frac{m_{B^+}^2}{M_{H^+}^2} \frac{t_\beta^2}{(1+\epsilon_0 t_\beta)(1+\epsilon_\ell t_\beta)}\right)^2 , \tag{2.20}$$

where ϵ_0 is given by ϵ_b *without* the Higgsino contributions and encodes both the $\tan\beta$ enhanced threshold corrections to the b quark Yukawa and to the CKM element V_{ub} [63].

The current experimental world average for the branching ratio of $B^+ \to \tau^+\nu$ reads [64]

$$\mathrm{BR}(B^+ \to \tau^+\nu)_{\mathrm{exp}} = (1.73 \pm 0.35) \times 10^{-4} . \tag{2.21}$$

SM predictions for the branching ratio that rely on fits of the Unitarity triangle result in values roughly 2.5σ below the experimental data [34, 64, 65], leading to severe constraints on the destructively interfering charged Higgs contributions. Assuming the UT fits to be affected by NP as well, a more conservative estimate for the SM contribution to the branching ratio is [34]

$$\mathrm{BR}(B^+ \to \tau^+\nu)_{\mathrm{SM}} = (1.10 \pm 0.29) \times 10^{-4} , \tag{2.22}$$

which implies

$$R_{B\tau\nu} = 1.57 \pm 0.53 . \tag{2.23}$$

Even this conservative estimate represents an important constraint on the MSSM Higgs spectrum in the large $\tan\beta$ region.

2.2.4 The muon $g-2$

The anomalous magnetic moment of the Muon, $a_\mu = \frac{1}{2}(g-2)_\mu$, is predicted in the SM to be [66]

$$a_\mu^{\mathrm{SM}} = (11\,659\,183.4 \pm 4.9) \times 10^{-10} . \tag{2.24}$$

Experimentally, the E821 experiment at BNL however found [67, 68]

$$a_\mu^{\mathrm{exp}} = (11\,659\,208.9 \pm 6.3) \times 10^{-10} , \tag{2.25}$$

leading to a 3.2σ discrepancy [66]

$$\Delta a_\mu = a_\mu^{\mathrm{exp}} - a_\mu^{\mathrm{SM}} = (25.5 \pm 8.0) \times 10^{-10} . \tag{2.26}$$

In the MSSM, a_μ receives SUSY contributions already at the one loop level from chargino-sneutrino and neutralino-slepton loops, allowing easily to account for such

a discrepancy. In the MSSM with large $\tan\beta$, the typically dominant chargino contribuions can be written approximately, assuming a common SUSY mass $\tilde{m}$, as [53, 69, 70]

$$\Delta a_\mu^{\text{SUSY}} = \frac{\alpha_2}{4\pi} m_\mu^2 \frac{t_\beta}{1+\epsilon_\ell t_\beta} \frac{\mu M_2}{\tilde{m}^4} f_4(x_2, x_\mu) \ , \tag{2.27}$$

where the loop function can be found in the appendix of [53]. While this contribution has the right order of magnitude in a large part of MSSM parameter space, a crucial observation is that the sign of it is determined by the sign of μM_2. Thus, if M_2 is positive, the data on $(g-2)_\mu$ disfavour negative μ at more than 3σ.

2.3 A top-down approach to Yukawa unification

Due to the crucial role played by low-energy threshold corrections to fermion masses, the success of Yukawa unification is strongly dependent on the values of soft SUSY breaking parameters. In addition, the low-energy observables like the bottom quark and the constraints arising from measured branching ratios of FCNC processes are afflicted with theoretical and experimental uncertainties.

A common approach to assess the viability of YU is the *bottom-up* approach [40, 71–77], where the low-energy values of the Yukawa couplings have to be fixed to reproduce the experimental central values of the fermion masses. YU at the GUT scale is then never exact, but the departure from exact YU can be quantified depending on the point in MSSM parameter space. An advantage of this approach is that some amount of unification can be sacrificed to accommodate additional constraints, like the dark matter relic density.

In a *top-down* approach [43–45, 47, 78–80], one rather fixes the GUT-scale values of the Yukawa couplings, which allows to impose exact YU throughout the analysis. The low-energy values of fermion masses and FCNC observables are then fitted to their measured values, taking into account all relevant uncertainties, by means of a χ^2 minimization procedure. In addition to being able to impose exact YU, this approach has the advantage that the results are not biased by the current central values of low-energy observables but allows to consistently take into account their existing uncertainties.

This top-down approach will be applied in the subsequent sections to assess the viability of YU in view of FCNC constraints.

2.3.1 Procedure

In the top-down approach to Yukawa unification, all the model parameters, including the Yukawa couplings and soft SUSY breaking parameters, are fixed at the GUT scale. Then, they are evolved down to low energies by means of the RG equations.

At low energies, all the observables, including fermion masses and FCNC processes, are calculated and the value of the χ^2 function evaluated, which is defined as

$$\chi^2[\vec{\vartheta}] \equiv \sum_{i=1}^{N_{\text{obs}}} \frac{(f_i[\vec{\vartheta}] - \mathcal{O}_i)^2}{(\sigma_i^2)_{\text{exp}} + (\sigma_i^2)_{\text{theo}}} \ . \tag{2.28}$$

Here, $\mathcal{O}_i$ indicates the experimental value of an observable and $f_i[\vec{\vartheta}]$ the corresponding theoretical prediction, which is a function of the model parameters collectively indicated with $\vec{\vartheta}$; σ_i are the corresponding experimental and theoretical uncertainties. The χ^2 function then has to be minimized by varying all or some of the input parameters and iterating the procedure until a viable point with low χ^2 is found. The final value of χ^2 then corresponds to a quantitative measure of the fit quality.

The necessary ingredients – input parameters, RG evolution, observables and minimization – will now be discussed in turn.

Input parameters

In principle, all the MSSM parameters discussed in section 1.2.1 (including the ones present in the SM as well) have to be specified at the GUT scale. However, simplifying assumptions on the soft SUSY breaking sector are necessary both from a computational and from a phenomenological point of view.

In the gauge sector, the definition of the GUT scale as the scale of gauge coupling unification reduces the necessary parameters to the GUT scale M_G itself and the unified gauge coupling g_G. However, a GUT-scale threshold correction to the strong gauge coupling can be allowed for, since it is both preferable phenomenologically and can arise in actual GUT models (cf. the review of S. Raby in [39]). One then requires an additional parameter ϵ_3, defined as

$$g_3^2(M_G) = g_G^2\,(1 + \epsilon_3) \ . \tag{2.29}$$

In the Yukawa sector, neglecting for the time being right-handed neutrinos, there are 13 parameters: 3 charged lepton masses, 6 quark masses and the 4 CKM parameters. In the case of t-b-τ (b-τ) unification, this number is of course reduced by 2 (1). If the focus is on third generation Yukawa unification, it is a good approximation to neglect the Yukawa couplings of the first two generations in the RG equations.

When specifying the Yukawa couplings at the GUT scale, one has to make a choice of basis, since the Yukawa Lagrangian is invariant under chiral rotations (cf. sec. 1.2.2). Although these bases for the Yukawa matrices are physically equivalent, Yukawa unification conditions like $(Y_U)_{33} = (Y_D)_{33}$ are not basis invariant. This is relevant if the 23-entries in Y_U or Y_D are sizable *in the basis where the YU conditions hold*. Thus it will be understood in the following that in the basis where the YU conditions hold, the off-diagonal elements are hierarchically suppressed, such that

Sector	#	Parameters
gauge	3	M_G, g_G, ϵ_3
SUSY & SUSY-breaking	7	m_{16}^2, $m_{1/2}$, $m_{H_u}^2$, $m_{H_d}^2$, A_0, $\tan\beta$, μ
3rd generation Yukawa	1	y_3
light generation Yukawa	6	$y_{u,c}$, $y_{d,s}$, $y_{e,\mu}$
CKM	4	λ, A, $\bar{\varrho}$, $\bar{\eta}$
neutrino	1	M_R

Table 2.1: GUT-scale input parameters in the case of t-b-τ YU and NUHM boundary conditions.

the YU conditions are still valid to a good approximation in the basis where either Y_U or Y_D is diagonal. This is indeed realized in many concrete GUT models (e.g. [45, 78]).

In the soft SUSY breaking sector, simplifying assumptions are necessary as mentioned above. Since Higgs splitting is a required ingredient of YU, one of the simplest soft SUSY breaking boundary conditions is the NUHM (non-universal Higgs masses), implying at the GUT scale[2]

$$\begin{aligned} m^2_{Q,U,D,L,E} &= m^2_{16}\,\mathbb{1}\ , & M_{1,2,3} &= m_{1/2}\ , \\ T_{U,D,E} &= A_0\,Y_{U,D,E}\ , & m^2_{H_u} &\neq m^2_{H_d} \neq m^2_{16}\ . \end{aligned} \tag{2.30}$$

The b term can be traded for $\tan\beta$. Finally, the μ term has to be specified.

The total number of input parameters in the case of t-b-τ YU and NUHM boundary conditions is summarized in table 2.1.

RG evolution

Once the boundary conditions for all the relevant input parameters at the GUT scale have been fixed, the Yukawa couplings, gauge couplings and soft SUSY breaking parameters have to be evolved to low energies by numerically solving their RG equations (cf. section 1.3.4). In the numerical analysis of section 2.4, two-loop RGEs are used for Yukawa and gauge couplings and one-loop RGEs for the remaining, dimensionful parameters. In the analysis of section 2.5, two-loop RGEs are used for all parameters.

At low energies, the EWSB conditions have to be imposed and the threshold corrections to fermion masses calculated as described in sections 1.3.2 and 1.3.3,

[2]The 16 in m_{16} stems from the fact that the fields in question originate from a 16-dimensional spinor representation in $SO(10)$ GUTs. This parameter is also frequently denoted m_0.

respectively. The pseudoscalar Higgs pole mass is caculated follwing [18], and the remaining Higgs masses using FeynHiggs [81–84].

An important point in the RG evolution is the possible contribution from neutrino Yukawa couplings in the presence of right-handed neutrinos [85–87]. Right-handed neutrinos are predicted e.g. in $SO(10)$ as part of the 16-dimensional spinor representation containing also one generation of quarks an leptons; and they are necessary to generate light neutrino masses by means of the see-saw mechanism.

In specific models predicting the pattern of quark, charged lepton and neutrino Yukawa matrices at the GUT scale (such as the DR model [45, 78] studied in [47]), one has to determine the masses of the heavy (mostly right-handed) neutrino mass eigenstates, construct effective theories with appropriate numbers of heavy neutrinos above/below these scales and integrate out the neutrino Yukawa contributions to the RGEs step by step (see also [17]). In this analysis however, where the focus is on third generation Yukawa unification, the details of this procedure are less important; assuming the 33 entry of the neutrino Yukawa matrix to be unified with the top Yukawa at the GUT scale, it will simply be assumed in the following that $(Y_\nu)_{ij} = y_t \delta_{i3} \delta_{j3}$ at M_G and the right-handed neutrio mass scale M_R will be treated as a free parameter in the χ^2 analysis.

Let us now have a look at the impact of the neutrino Yukawa couplings on the RGEs. First of all, they enter in the RGEs of up-type quark and charged lepton Yukawas and tend to drive these couplings to smaller values. In the leading-log approximation, the difference between the values of the top and tau Yukawa couplings at low energies in the presence of neutrino Yukawa contributions and the values they would take in the absence of right-handed neutrinos is

$$y_t - y_t^{0\nu} = y_\tau - y_\tau^{0\nu} = -\frac{1}{16\pi^2}\, y_t(M_G)\, \log\left(\frac{M_G}{M_R}\right) . \tag{2.31}$$

From the top-down point of view, this percent level change in Yukawa couplings can be compensated by adjusting accordingly the GUT-scale value of the Yukawa coupling and $\tan\beta$, which in turn affects the value of the b quark Yukawa coupling y_b at low energies.

In the soft sector, the neutrino Yukawa contributions leave the largest impact on the left-handed slepton doublet mass term m_L^2 and on the up-type Higgs mass term $m_{H_u}^2$. In the leading-log approximation and with the boundary conditions (2.30), (2.43), their low-energy values are modified according to [85, 87]

$$\left(m_L^2\right)_{ij} - \left(m_L^2\right)_{ij}^{0\nu} = -\frac{1}{16\pi^2}\left(4m_{16}^2 + 2m_{H_u}^2 + 4A_U^2\right)(Y_\nu^\dagger Y_\nu)_{ij} \log\left(\frac{M_G}{M_R}\right) , \tag{2.32}$$

$$m_{H_u}^2 - (m_{H_u}^2)^{0\nu} = -\frac{1}{16\pi^2}\left(4m_{16}^2 + 2m_{H_u}^2 + 4A_U^2\right) \mathrm{Tr}(Y_\nu^\dagger Y_\nu) \log\left(\frac{M_G}{M_R}\right) , \tag{2.33}$$

where the quantities on the right-hand side are defined at the GUT scale. According to (2.32), the presence of right-handed neutrinos leads to lighter left-handed sleptons at low energies; however, this does not have any relevant impact on the mechanism ensuring the success of YU. The off-diagonal components of (2.32) give rise to lepton flavor violating decays [85], but definite predictions can only be made in models predicting $(Y_\nu^\dagger Y_\nu)_{ij}$. Eq. (2.33) shows that the neutrino Yukawa contributions drive $m_{H_u}^2$ to smaller values. However, this can be easily compensated by raising the value of $m_{H_u}^2$ at the GUT scale, which is possible in the setup of non-universal Higgs masses. However, this change in $m_{H_u}^2$ induced by right-handed neutrino effects is by far not sufficient to explain or to generate the large $m_{H_u}^2$-$m_{H_d}^2$ splitting required for successful YU.

Observables

The observables entering the χ^2 function can be divided into three classes. First, known SM parameters like fermion masses and gauge couplings have to be added to fit the GUT-scale values of the gauge and Yukawa couplings. Second, additional low-energy constraints like measured FCNC branching ratios are added. Third, lower bounds on the masses of as yet unobserved particles or upper bounds on the branching ratios of as yet unobserved decays are added to the χ^2 in the form of suitably smoothened step functions, yielding a "penalty" if a bound is violated.

In the first class of observables, there are the 9 quark and charged lepton masses and the 4 measured CKM parameters (to fit the Yukawa couplings) as well as the Z boson mass M_Z, Fermi constant G_F, electromagnetic fine-structure constant α_em and the strong coupling constant $\alpha_s(M_Z)$ to fit $g_{1,2,3}$ and the Higgs VEVs (essentially fixing a combination of μ, $m_{H_{u,d}}^2$ and $\tan\beta$). The values of these observables and their experimental uncertainties are shown in table 2.2.

In the second class, there are the FCNC constraints most relevant in the MSSM at large $\tan\beta$ with no new sources of flavour and CP violation, which are shown in table 2.3.

In the third class, there are the lower bounds on the masses of the lightest Higgs boson and the sparticles shown in table 2.4 and the upper bound on the branching ratio of $B_s \to \mu^+\mu^-$.

In principle, the anomalous magnetic moment of the muon discussed in section 2.2.4 could also be added to the χ^2 function. However, it was already found in [44] that in the region leading to successful YU, the SUSY contributions to a_μ are typically too small to account for the 3.2σ discrepancy. On the other hand, the presence of NP in a_μ has not been established beyond doubt yet. Still, in the numerical analysis, $\mu > 0$ was imposed to ensure that at least the sign of the contributions to a_μ is the right one.

Observable	Value(σ_{exp})	Observable	Value(σ_{exp})
M_W	80.398(25)	M_t	173.1(1.3)
M_Z	91.1876(21)	$m_b(m_b)$	4.20(7)
$10^5 G_\mu$	1.16637(1)	M_τ	1.777(0)
$1/\alpha_{\text{em}}$	137.036(0)		
$\alpha_s(M_Z)$	0.1176(20)		

Table 2.2: Flavor conserving observables [39] used in the fit. Dimensionful quantities are expressed in powers of GeV.

Observable	Value(σ_{exp})(σ_{theo})	
$\Delta M_s/\Delta M_d$	35.1(0.4)(3.6)	[48, 88]
10^4 BR($B \to X_s\gamma$)	3.52(25)(46)	[48]
10^6 BR($B \to X_s\ell^+\ell^-$)	1.60(51)(40)	[89, 90]
10^4 BR($B^+ \to \tau^+\nu$)	1.40(40)(26)	[39]

Table 2.3: Flavor-changing observables used in the fit. The BR($B \to X_s\ell^+\ell^-$) refers to the dileption invariant mass range $q^2 \in [1, 6]$ GeV^2.

χ^2 minimization

For any given set of the input parameters in table 2.1, the χ^2 function can now be evaluated containing all the flavour-conserving and flavour-changing observables and the bounds discussed above. The χ^2 is then minimized using `MIGRAD`, which is part of the `CERNlib` library [91].

2.4 b-τ unification vs. flavour data

In [17, 47], a predictive $SO(10)$ SUSY GUT model with t-b-τ Yukawa unification [45, 78] was studied in the light of all relevant data on FCNCs in the quark sector.

Observable	Lower bound	Observable	Upper bound	
M_{h^0}	114.4	BR($B_s \to \mu^+\mu^-$)	5.8×10^{-8}	[55]
$M_{\tilde{\chi}^+}$	104			
$M_{\tilde{t}}$	95.7			

Table 2.4: Bounds imposed in the fit. Since all scenarios considered in the following have universal gaugino masses and $\mu \gg m_{1/2}$, the neutralino and gluino mass bounds can be omitted since they are always weaker than the chargino mass bound. For the $B_s \to \mu^+\mu^-$ bound, cf. the comment in the footnote on page 39.

It was found that the simultaneous description of EW observables as well as fermion masses and mixings *and* all the FCNC processes considered is impossible unless the squark masses are pushed well above the limits allowed by naturalness and within reach of LHC.

Although these tensions are partly due to the Yukawa textures predicted by the model's flavour symmetry, an important role is played by the requirement of exact t-b-τ YU, the implications for SUSY parameters space discussed in section 2.1 (in particular $\tan\beta \simeq 50$ and large trilinear couplings), and the ensuing large effects in flavour physics. It will be shown in this section that indeed t-b-τ YU in the MSSM with NUHM soft SUSY breaking boundary conditions is strongly disfavoured by FCNC constraints unless sfermion masses are raised well above the TeV scale.

One possibility to weaken the FCNC bounds is to lower $\tan\beta$. However, this is only possible if the unification of the top and bottom Yukawa couplings is broken, so that the full Yukawa unification is relaxed to b-τ unification, occurring, e.g., in $SU(5)$. Such breaking of t-b unification is actually also a general possibility in $SO(10)$ SUSY GUTs once all the representations needed for a realistic GUT-breaking sector are taken into account. For example, the "minimal breaking scheme" introduced by Barr and Raby [92] requires the presence of a $\mathbf{16}'_H$ spinor. In this framework, the MSSM Higgs doublet H_d can naturally be a mixture between a doublet contained in the same $\mathbf{10}_H$ representation as the doublet H_u and one doublet contained in this $\mathbf{16}'_H$ spinor, since the two have the same quantum numbers. One then has [37, 93, 94]

$$\begin{aligned} H_u &= H(\mathbf{10}_H) \ , \\ H_d &= \overline{H}(\mathbf{10}_H)\cos\gamma + \overline{H}(\mathbf{16}'_H)\sin\gamma \ . \end{aligned} \tag{2.34}$$

Consequently, the Yukawa unification relation $y_t = y_b$ is effectively broken to

$$\frac{y_b}{y_t} \simeq \cos\gamma \ . \tag{2.35}$$

At the EW scale, this relation leads to a value of $\tan\beta \lesssim 50$ parametrically smaller than in the exact unification case, depending on the amount of mixing in the second of eqs. (2.34).

However, even if this allows to lower $\tan\beta$, it was shown in section 2.1 that also b-τ unification with $\tan\beta < 50$ requires sizable negative threshold corrections to m_b. In fact, these corrections have to be larger than in the full YU case. Therefore, SUSY GUT models with b-τ unification maintain most of their predictivity, and the ISMH relations eq. (2.6) should still be approximately satisfied.

2.4.1 Numerical analysis

The aim of this analysis is a χ^2 fit, as described in section 2.3.1, of SUSY GUTs with b-τ unification and NUHM soft SUSY breaking boundary conditions (2.30) at

Observable	Exp.	Fit	Pull
M_W	80.403	80.56	0.4
M_Z	91.1876	90.73	**1.0**
$10^5\ G_\mu$	1.16637	1.164	0.3
$1/\alpha_{\rm em}$	137.036	136.5	0.8
$\alpha_s(M_Z)$	0.1176	0.1159	0.8
M_t	170.9	171.3	0.2
$m_b(m_b)$	4.20	4.28	**1.1**
M_τ	1.777	1.77	0.4
10^4 BR$(B \to X_s\gamma)$	3.55	2.72	**1.6**
10^6 BR$(B \to X_s\ell^+\ell^-)$	1.60	1.62	0.0
$\Delta M_s/\Delta M_d$	35.05	32.4	0.7
10^4 BR$(B^+ \to \tau^+\nu)$	1.41	0.726	**1.4**
10^8 BR$(B_s \to \mu^+\mu^-)$	< 5.8	3.35	–
		total χ^2:	**8.78**

Table 2.5: Example of successful fit in the region with b-τ unification. Dimensionful quantities are expressed in powers of GeV. Higgs, lightest stop and gluino masses are pole masses, while the rest are running masses evaluated at M_Z.

the GUT scale. The results of this analyis have been published in [79].

Input parameters

For simplicity, the Yukawa couplings are parametrized as

$$Y_{U,N} = \begin{pmatrix} 0 & 0 & 0 \\ 0 & 0 & 0 \\ 0 & 0 & y_{t,\nu_\tau} \end{pmatrix}, \qquad Y_{D,E} = \begin{pmatrix} 0 & 0 & 0 \\ 0 & 0 & 0 \\ 0 & 0 & y_{b,\tau} \end{pmatrix}, \tag{2.36}$$

during the RG evolution. Only at low energies, where the threshold corrections to Yukawa couplings and the observables are evaluated, are the light generation Yukawas and the CKM taken into account, i.e. they are not part of the fitting procedure. This turns out to be a good approximation in the setup considered, as was checked explicitly in the numerical analysis. The right-handed neutrinos are integrated out at a common scale M_R as discussed above.

The total number of input parameters entering the χ^2 is then 12: the 10 parameters in the first two rows of table 2.1 as well as $y_b = y_\tau$ and $y_t = y_{\nu_\tau}$.

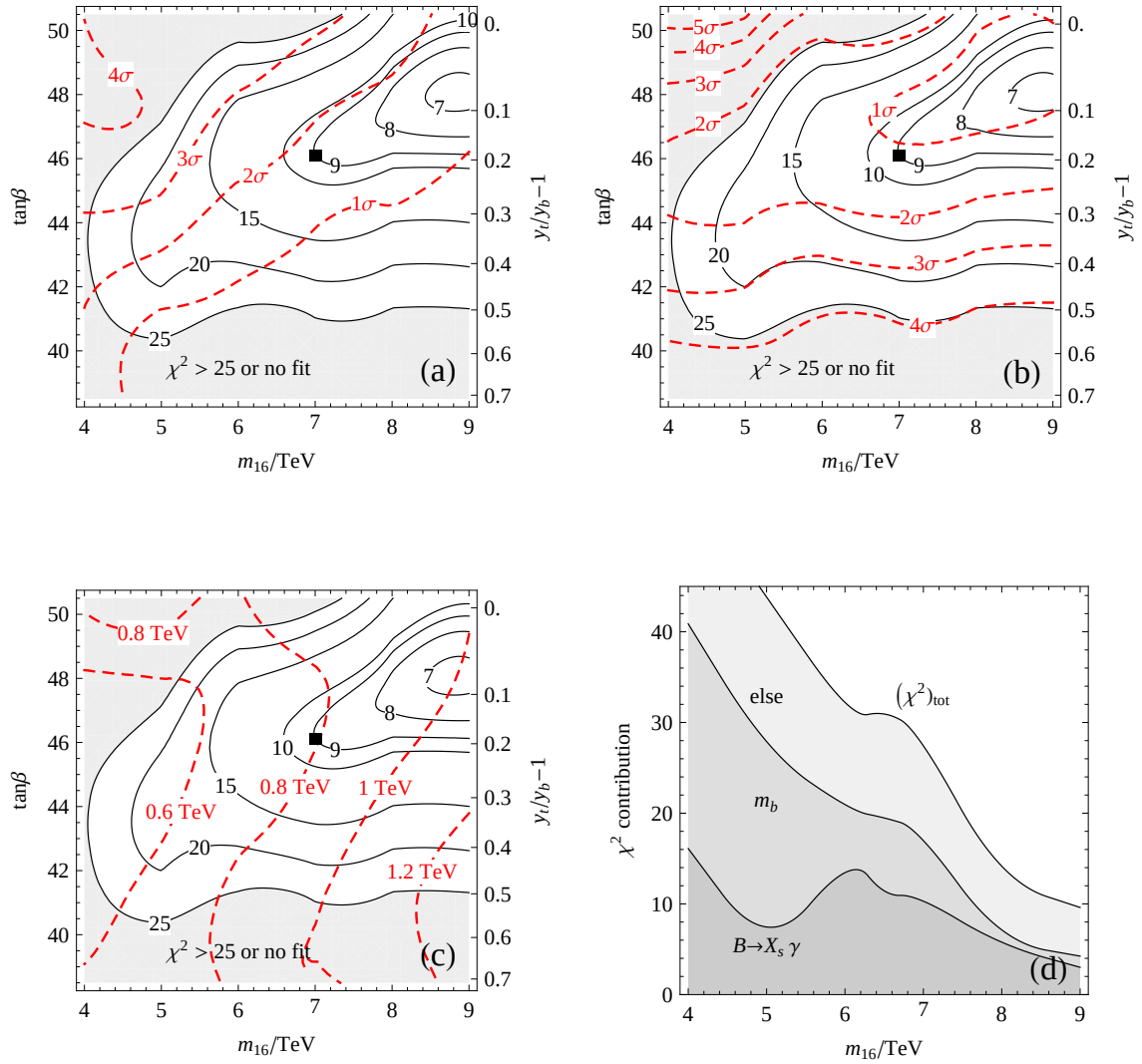

Figure 2.2: Panels (a)-(c): χ^2 contours (solid lines) in the m_{16} vs. $\tan\beta$ plane. Superimposed as dashed lines are the pulls for BR($B \to X_s\gamma$) (panel (a)) and for m_b (panel (b)) and the lightest stop mass contours (panel (c)). Panel (d): χ^2 contributions vs. m_{16} in the special case of exact Yukawa unification.

Input parameters		Mass predictions	
m_{16}	7000	M_{h^0}	121.5
μ	1369	M_{H^0}	585
$M_{1/2}$	143	M_A	586
A_0	-14301	M_{H^+}	599
$\tan\beta$	46.1	$m_{\tilde{t}_1}$	783
$1/\alpha_G$	24.7	$m_{\tilde{t}_2}$	1728
$M_G/10^{16}$	3.67	$m_{\tilde{b}_1}$	1695
$\epsilon_3/\%$	-4.91	$m_{\tilde{b}_2}$	2378
$(m_{H_u}/m_{16})^2$	1.616	$m_{\tilde{\tau}_1}$	3297
$(m_{H_d}/m_{16})^2$	1.638	$m_{\tilde{\chi}_1^0}$	58.8
$M_R/10^{13}$	8.27	$m_{\tilde{\chi}_2^0}$	117.0
λ_u	0.608	$m_{\tilde{\chi}_1^+}$	117.0
λ_d	0.515	$M_{\tilde{g}}$	470

Table 2.6: Input parameters and SUSY spectrum for the fit reported in table 2.5. Dimensionful quantities are expressed in powers of GeV.

Fit results

The results of the analysis are shown in the four panels of figure 2.2. Panels (a) to (c) report contours of constant χ^2 (shown as solid black lines) in the m_{16} vs. $\tan\beta$ plane. Since t-b-τ unification requires $\tan\beta \simeq 50$, smaller $\tan\beta$ corresponds to a parametric departure from $y_t/y_b = 1$. While the relation between y_t/y_b is not simply linear, due to the RG evolution, and depends on the Yukawa threshold corrections, one finds that for the region of interest, the approximate expression

$$\left.\frac{y_t}{y_b}\right|_{M_G} = 1 - 2.3\left(\frac{\tan\beta}{50} - 1\right) + 3.6\left(\frac{\tan\beta}{50} - 1\right)^2 \tag{2.37}$$

holds. This relation is used to show the departure of y_t/y_b from 1 on the right-hand axes of panels (a) to (c). The top border of the plots thus corresponds to full t-b-τ unification. In panels (a) and (b), the superimposed red dashed contours show the deviations of $\mathrm{BR}(B \to X_s\gamma)$ and m_b from their experimental central values in units of the total error, in panel (c) they show the mass of the lighter stop.

The χ^2 contours in panels (a)–(c) highlight a region of successful fits for $m_{16} \gtrsim 7$ TeV and $46 \lesssim \tan\beta \lesssim 48$, corresponding to a moderate breaking of t-b unification, with $0.2 \gtrsim (y_t/y_b - 1) \gtrsim 0.1$. The interesting region emerges as a compromise between $B \to X_s\gamma$ and m_b, pushing $\tan\beta$ to lower and larger values, respectively. In this region, the mass of the lighter stop is roughly between 800 GeV and 1 TeV. Interestingly enough, the χ^2 value deteriorates quickly in the limit of $y_t/y_b \to 1$, i.e. in the t-b-τ YU limit.

Panel (d) shows the χ^2 contributions from $\mathrm{BR}(B \to X_s\gamma)$, m_b and the remaining observables vs. m_{16} in the special case of $y_t/y_b = 1$, corresponding to exact t-b-τ Yukawa unification. For $m_{16} \lesssim 9$ TeV, the χ^2 contribution from $B \to X_s\gamma$ alone is no less than roughly 4, corresponding to no less than 2σ deviation from its experimental value. For lower values of m_{16}, fit quality becomes so bad that the minimization algorithm prefers to sacrifice the prediction for m_b in favour of the $\mathrm{BR}(B \to X_s\gamma)$ constraint. These observations show that indeed exact t-b-τ YU is strongly disfavoured by the FCNC constraints unless the sfermions are decoupled well beyond the TeV scale.

An example of a fit in the interesting region is reported in tables 2.5 and 2.6 and shown in panels (a)–(c) as a black square.

2.4.2 Conclusions

The preceding numerical analysis has shown two important facts: First, t-b-τ unification is only possible at the price of decoupling the sfermions, placing them beyond the reach of the LHC. Second, exact b-τ unification is compatible with all FCNC constraints and is very predictive as for the implied SUSY spectrum; the lighter stop mass is around 1 TeV, the gluino mass around 400 GeV, the LSP is an almost pure Bino with a mass of order 60 GeV and $\tan\beta$ lies between 46 and 49.

These conclusions are valid within the MSSM with NUHM soft SUSY breaking boundary conditions at the GUT scale.

2.5 Non-universal soft terms and t-b-τ Yukawa unification

The analysis in section 2.4 revealed that t-b-τ Yukawa unification in the context of NUHM soft SUSY breaking boundary conditions is disfavoured by the constraints from flavour physics, unless the SUSY spectrum is decoupled, with the lightest squark mass well above 1 TeV. The purpose of this section is to analyze departures from the simple NUHM boundary conditions (2.30) and their impact on YU, to answer the question whether non-universalities can remedy the tension between YU and FCNCs.

An immediate possibility is to give up gaugino mass universality at the GUT scale. Indeed, even with gauge coupling unification, GUTs do not in general require gaugino mass unification. As mentioned in section 2.1, a hierarchy $M_2 \gg M_3$ can be sufficient to avoid the problematic large trilinear couplings implied by eq. (2.6). Since this setup was already studied in [40, 41], it will not be considered here, and gaugino masses will be assumed to be universal at M_G throughout this section.

What remains, then, is to reduce the amount of universality in the sfermion sector. Sfermion masses and trilinear couplings should however not deviate too much from

Minimal Flavour Violation (cf. section 1.2.2), in order not to violate bounds from flavour physics.

Let us recall the form of the sfermion mass matrices and trilinear coupling matrices in the MFV MSSM, neglecting powers of Yukawa couplings greater than two. One has

$$\left(m_Q^2\right)^T = \tilde{m}^2 \left[a_1 \mathbb{1} + b_1 Y_U Y_U^\dagger\right] , \tag{2.38}$$

$$\left(m_U^2\right)^T = \tilde{m}^2 \left[a_2 \mathbb{1} + b_5 Y_U^\dagger Y_U\right] , \qquad T_U = A\, a_4\, Y_U , \tag{2.39}$$

$$\left(m_D^2\right)^T = \tilde{m}^2 \left[a_3 \mathbb{1} + b_6 Y_D^\dagger Y_D\right] , \qquad T_D = A\, a_5\, Y_D , \tag{2.40}$$

$$\left(m_L^2\right)^T = \tilde{m}^2 \left[a_6 \mathbb{1} + b_{13} Y_E Y_E^\dagger\right] , \tag{2.41}$$

$$\left(m_E^2\right)^T = \tilde{m}^2 \left[a_7 \mathbb{1} + b_{14} Y_E^\dagger Y_E\right] , \qquad T_E = A\, a_8\, Y_E . \tag{2.42}$$

In the NUHM (as in the constrained MSSM), one has $a_i = 1$, $b_i = 0$, $\tilde{m} = m_{16}$ and $A = A_0$.

The following departures from this universality, while still being compatible with MFV, are now conceivable: 1. non-zero (possibly non-universal) b_i, 2. non-universal $a_{1,2,3,6,7}$, 3. non-universal $a_{4,5,8}$.

If we are interested in the impact on YU, off-diagonal elements of Yukawa couplings are less important for the moment. Then, option 1. basically corresponds to splitting the sfermion masses of the third generation from the first two generations. It is interesting, however, that the mechanism leading to successful YU, as described in section 2.1, is essentially determined by quantities related to the third squark generation, such as the stop and sbottom spectrum; furthermore, conditions (2.6) anyway lead to a large hierarchy between third and first/second generation squarks, by means of a radiatively generated inverse scalar mass hierarchy [95]. Therefore, a generational splitting induced by non-zero b_i does not at first sight seem like a promising approach to reconcile YU with FCNCs, so it will not be considered in the following.

Option 2., i.e. non-universal generation-independent sfermion mass parameters, could have a profound impact on YU, since it would allow an arbitrary splitting between stop and sbottom masses, which is crucial for the threshold corrections to m_b as discussed in section 2.1. A full analysis of YU in this framework, taking into account the constraints from flavour physics, does not exist but could prove interesting.

In the following, option 3. will instead be investigated in detail: non-universal trilinear couplings. For simplicity (and since L and D share a common representation of the GUT group both in $SU(5)$ and $SO(10)$), we will still assume $a_5 = a_8$, so that the trilinear couplings read

$$T_U = A_U Y_U , \qquad T_D = A_D Y_D , \qquad T_E = A_D Y_E . \tag{2.43}$$

The remaining SUSY breaking parameters are as in (2.30).

2.5.1 Impact of non-universal trilinear couplings

The solution to Yukawa unification first discussed in [43, 44] and also invoked in the analysis of section 2.4 features large negative trilinear couplings $A_0 \sim -2m_{16}$ (cf. eq. (2.6)) for two reasons: First, a large negative stop trilinear leads to sizable negative threshold corrections to m_b, as is required by YU (cf. eq. (2.3) and the subsequent discussion); Second, large trilinear couplings give rise to negative RG contributions to the third-generation sfermion masses at low energies, permitting an inverted scalar mass hierarchy (ISMH) with heavy first and second generation sfermion masses and light third generation sfermion masses.

The first of these motivations still holds in the case of non-universal trilinear couplings and suggests that $A_U \lesssim -m_{16}$ is still necessary in this case. The second one, i.e. the RG induced reduction of sfermion masses, is the most important new feature of this scenario: If $A_U \neq A_D$, the RG induced effects on the third generation sfermion masses are different for up-type and down-type squarks, allowing in principle not only an ISMH, but also a splitting between the stop and sbottom spectrum even larger than in the universal case. This is crucial for YU since a heavy sbottom spectrum will suppress the unwanted positive gluino contributions to m_b with respect to the negative chargino ones.

To see this effect numerically, consider the approximate solutions to the RG equations of the 33 entries of the squark mass matrices. Assuming $\tan\beta \approx 50$ and neglecting gaugino mass contributions (anticipating the condition $m_{1/2} \ll m_{16}, A_{U,D}$), their low-energy values can be approximately written in terms of the GUT-scale parameters as

$$\left(m_Q^2\right)_{33} \approx 0.51\, m_{16}^2 - 0.12\, m_{H_u}^2 - 0.09\, m_{H_d}^2 - 0.02\, A_U^2 - 0.02\, A_D^2 \,, \quad (2.44)$$

$$\left(m_U^2\right)_{33} \approx 0.49\, m_{16}^2 - 0.22\, m_{H_u}^2 - 0.01\, m_{H_d}^2 - 0.06\, A_U^2 + 0.01\, A_D^2 \,, \quad (2.45)$$

$$\left(m_D^2\right)_{33} \approx 0.55\, m_{16}^2 + 0.01\, m_{H_u}^2 - 0.21\, m_{H_d}^2 + 0.01\, A_U^2 - 0.05\, A_D^2 \,. \quad (2.46)$$

As is apparent from eq. (2.45), a very light right-handed stop can be obtained by appropriately adjusting $m_{H_u}^2$ and A_U^2 at the GUT scale. In the universal case, $A_U^2 = A_D^2 \equiv A_0^2$, a sizable A_0 also leads to a reduction of $(m_D^2)_{33}$ and $(m_Q^2)_{33}$. Instead, in the non-universal case, the choice $A_D^2 \ll A_U^2$ allows to maintain a light right-handed stop, while preventing negative RGE contributions to the right-handed sbottom and left-handed squark masses. As a result, this mechanism permits to obtain a strong mass hierarchy

$$\left(m_U^2\right)_{33} \ll \left(m_Q^2\right)_{33} < \left(m_D^2\right)_{33} , \quad (2.47)$$

implying[3]

$$m_{\tilde{t}_R} \ll m_{\tilde{t}_L} \approx m_{\tilde{b}_L} < m_{\tilde{b}_R}. \tag{2.48}$$

While this hierarchy is also present in the universal case, it can be greatly amplified in the trilinear splitting scenario if A_D^2 is reduced: this leads to only a mild increase of $m_{\tilde{t}_L}$ and $m_{\tilde{b}_L}$, but a strong increase of $m_{\tilde{b}_R}$, while leaving $m_{\tilde{t}_R}$ almost unaffected.

2.5.2 Numerical analysis

The aim of this analysis is a χ^2 fit, as described in section 2.3.1, of SUSY GUTs with exact t-b-τ unification and soft SUSY breaking boundary conditions characterized by

$$\begin{aligned} m^2_{Q,U,D,L,E} &= m^2_{16}\,\mathbb{1}\ , \qquad M_{1,2,3} = m_{1/2}\ , \\ T_U &= A_U Y_U\ , \qquad T_{D,E} = A_D Y_{D,E}\ , \qquad m^2_{H_u} \neq m^2_{H_d} \neq m^2_{16}\ , \end{aligned} \tag{2.49}$$

at the GUT scale. The results of this analysis have been published in [80].

Input parameters

In contrast to the analysis discussed in section 2.4, in this analysis the full 3×3 form of the Yukawa coupling matrices is taken into account. The third generation Yukawa couplings are parametrized by a single parameter y_3 due to the assumption of full YU. The treatment of right-handed neutrinos is the same as in section 2.4. In the soft sector, conditions (2.49) require one additional parameter with respect to the NUHM (2.30). For simplicity, the universal sfermion mass m_{16} was fixed to 4 TeV throughout this analysis.

χ^2 fits where then performed for fixed values of μ and A_D, while A_U and all the other input parameters were subject to variation by the minimization program.

Fit results

The left-hand panel of fig. 2.3 displays the lines of constant χ^2 in the μ vs. A_D plane. The lowest values for the χ^2 function are obtained for remarkably large values of $\mu \approx 3.5$ to 4.5 TeV, which is of the order of m_{16}, here set to 4 TeV. The χ^2 contours are roughly symmetric to the axis $A_D = 0$, with a slight preference for small positive A_D. For too large μ, the χ^2 starts deteriorating again. In this region, the negative corrections to m_b in fact start being so large that the mechanism described in section 2.5.1 has to be tamed to prevent m_b from dropping below 4.2 GeV.

The right-hand panel shows the contribution to the χ^2 function solely from the BR($B \to X_s\gamma$) constraint, backdropped by the total χ^2 contours for comparison.

[3] Note that the LR mixing terms in the squark mass matrices do not play a role in this discussion, since $m^2_{16} \gg m_t A_t$ and $\gg m_b \mu \tan\beta$.

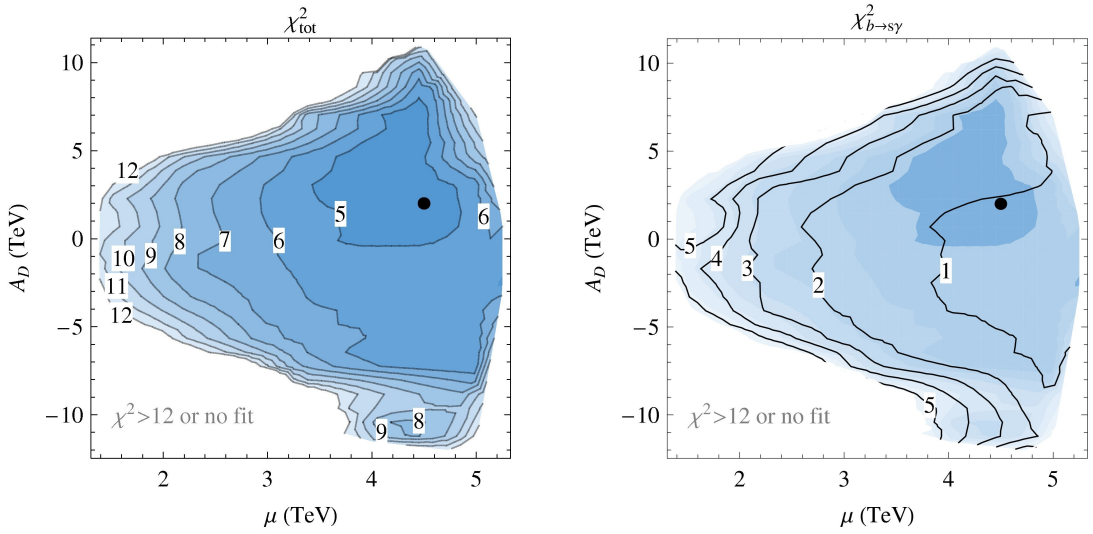

Figure 2.3: Left: lines of constant χ^2 in the μ vs. A_D plane, with $m_{16} = 4$ TeV. Right: contributions to the χ^2 function from BR($B \to X_s\gamma$). The black dot represents the example fit reported in tables 2.7–2.8.

Large values of μ are not only preferable for enhancing the threshold corrections to m_b (once the mechanism described in section 2.5.1 has ensured that the overall sign of these corrections is *negative*), but, remarkably enough, they lead at the same time to a *suppression* of chargino contributions to the $b \to s\gamma$ amplitude (see [52] for a discussion on this point), therefore preventing a large destructive interference with the SM contribution. This is why the BR($B \to X_s\gamma$) constraint only dominates the χ^2 for small μ. It should be stressed again that the solution where the SUSY contributions are so large that they flip the sign of the $b \to s\gamma$ amplitude, which is in principle allowed in the fitting procedure, is strongly disfavoured since it implies a too large branching ratio of $B \to X_s\ell^+\ell^-$ with respect to the experimental measurement [46].

From the left-hand panel of fig. 2.4, one can see that the preferred region points to $A_U \approx -2.5\, m_{16}$, and in particular to a sizable A_U-A_D splitting. The limit $A_D \to A_U$ corresponds to the lower leftmost part of the plot with small μ, where no successful fits have been found, reflecting the bad phenomenological performance of YU in the case of universal trilinears discussed in section 2.4.

The right-hand panel of fig. 2.4 shows that the universal gaugino mass $m_{1/2}$ is very small, but increases with increasing A_D. Its smallness is due to the requirement of a light gluino mass to suppress the gluino corrections to m_b, as discussed in section 2.1. In fact, $m_{1/2}$ is always fitted close to its lowest allowed value, set by the LEP lower bound on the mass of the lightest chargino (see table 2.4), which is an almost pure Wino, due to the large μ. If only one-loop RGEs for the gaugino masses were used,

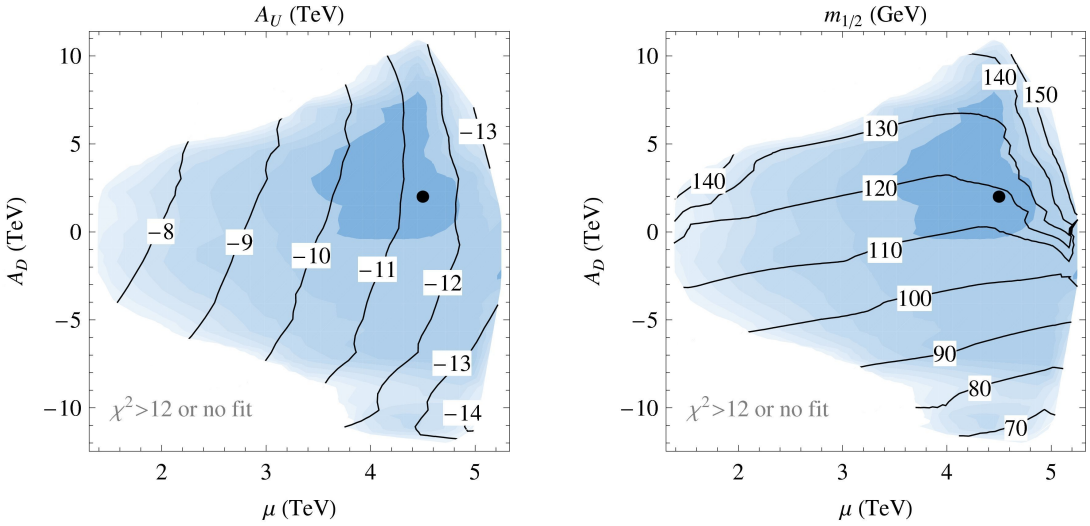

Figure 2.4: Lines of constant A_U (left, in TeV) and $m_{1/2}$ (right, in GeV) at the GUT scale.

$M_2 > 104$ GeV would imply $m_{1/2} \gtrsim 132$ GeV. However, due to the conditions $|A_{U,D}| \gg m_{1/2}$, two-loop effects become important in the running of the gaugino masses. These two-loop contributions are responsible both for the possibility of having $m_{1/2}$ less than 132 GeV and for the rise of $m_{1/2}$ with A_D. This effect always ensures a light chargino. For positive A_D and $\mu > 4$ TeV, there is a steep rise in $m_{1/2}$. In this region with large χ^2, i.e. bad fit performance, the threshold corrections to m_b become too large, as mentioned above, such that the pressure for a small gluino mass is removed.

Fig. 2.5 shows the values of the Higgs soft masses $m^2_{H_{u,d}}$ at the GUT scale in the μ vs. A_D plane. The low-scale value of $m^2_{H_u}$ is fixed by the EWSB conditions. At large $\tan\beta$, these conditions require $m^2_{H_u} \approx -|\mu|^2$ to hold at the EW scale. Its value at the scale M_Z can be expressed approximately in terms of GUT-scale parameters as

$$m^2_{H_u}(M_Z) = -0.74\, m^2_{16} + 0.56\, m^2_{H_u} + 0.06\, m^2_{H_d} - 0.11\, A^2_U + 0.01\, A^2_D \ , \qquad (2.50)$$

which makes clear why $m^2_{H_u}$ at the GUT scale is basically independent of A_D. For $m^2_{H_d}$, on the other hand, one has the approximate relation

$$m^2_{H_d} - m^2_{H_u} \approx m^2_A + m^2_Z \qquad (2.51)$$

at the EW scale, effectively setting a lower bound on $m^2_{H_d}$ for a given value of μ. On the other hand, $m^2_{H_d}$ is also bounded from above because a too large value would drive the sbottom masses smaller, cf. eq. (2.46), which is unfavourable for YU.

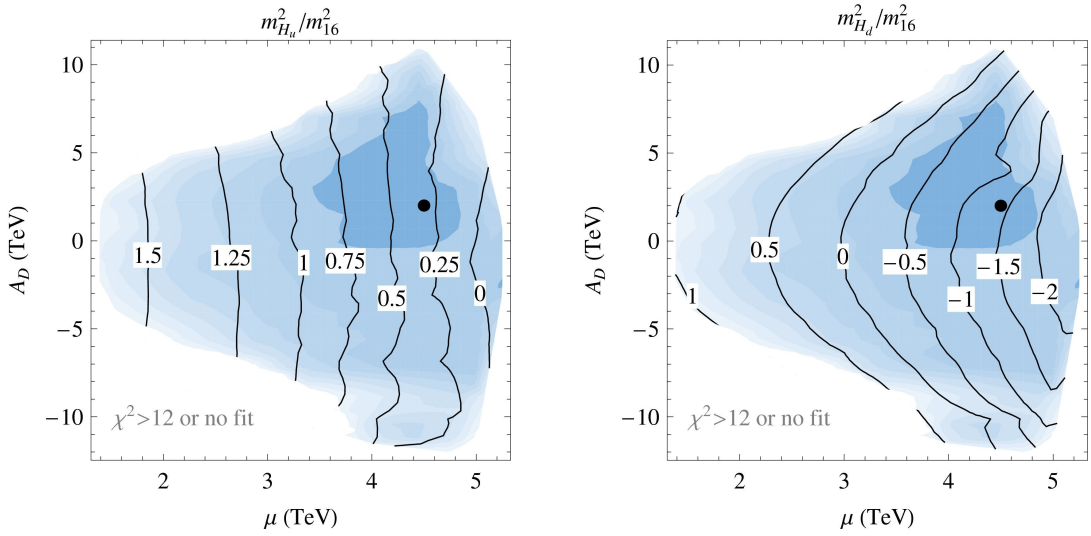

Figure 2.5: Lines of constant Higgs soft masses $m^2_{H_{u,d}}$ at the GUT scale, normalized to the universal sfermion mass m_{16}.

Expressing the low-scale value of $m^2_{H_d}$ finally in terms of GUT-scale parameters as

$$m^2_{H_d}(M_Z) = -0.81\, m^2_{16} + 0.06\, m^2_{H_u} + 0.52\, m^2_{H_d} + 0.01\, A_U^2 - 0.14\, A_D^2 \tag{2.52}$$

explains the dependence of $m^2_{H_d}$ on A_D shown in the right-hand panel of fig. 2.5.

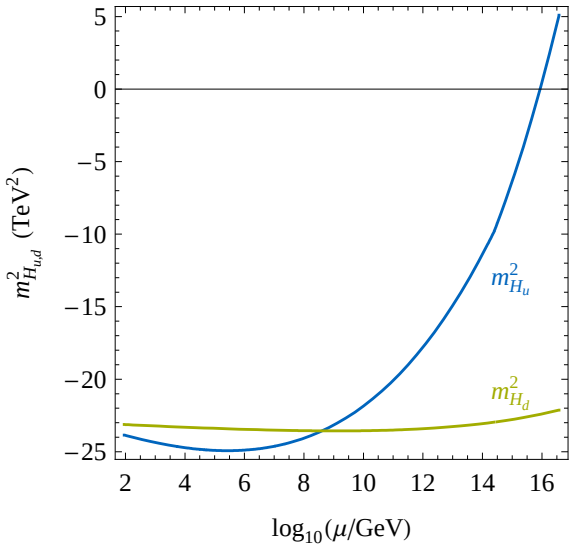

Figure 2.6: RG evolution of the parameters $m^2_{H_{u,d}}$ for the example fit in tables 2.7–2.8.

The values for the Higgs soft masses chosen by the fit are qualitatively very different from the case of universal trilinear couplings, where $m^2_{H_{u,d}} \simeq 2m^2_{16}$. As discussed at the end of section 2.1, EWSB at large $\tan\beta$ is helped by a GUT-scale Higgs splitting, since the similarity of up- and down Yukawa couplings hampers the usual radiative splitting mechanism. However, the Yukawa-driven RG contributions to the running of $m^2_{H_{u,d}}$ are in fact proportional to trilinear couplings. In the case of non-universal trilinears, $m^2_{H_u}$ and $m^2_{H_d}$ can therefore run very differently. This is also apparant from the last terms of eqs. (2.50) and (2.52). In fact, in the successful region in the μ vs. A_D plane, $m^2_{H_d}$ is negative already at the GUT scale and stays almost constant throughout the RG evolution. An example point demonstrating this running is shown in figure 2.6.

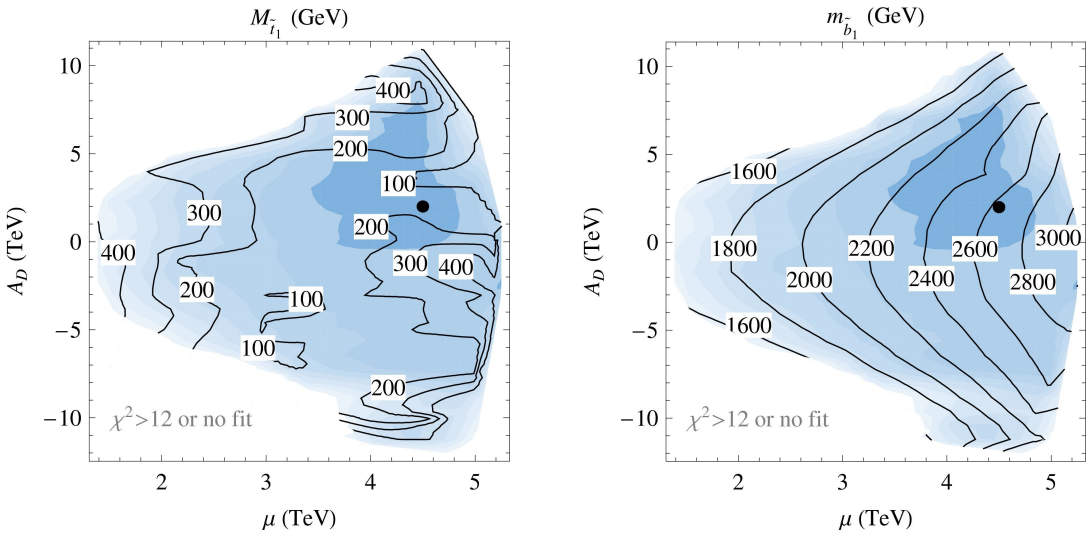

Figure 2.7: Values of the lighter stop mass (left) and the lighter bottom mass (right) chosen by the fit.

Fig. 2.7 shows the masses of the lighter stop and sbottom and highlights the large stop-sbottom splitting facilitated by the mechanism described in section 2.5.1. The stop mass is in fact as light as is allowed by the experimental lower bound, except for the region at small μ, where the $\mathrm{BR}(B \to X_s\gamma)$ constraint pushes for a heavier stop, and at too large μ, where the negative threshold corrections to m_b have to be tamed. The sbottom, on the other hand, is very heavy, its mass increasing with increasing μ (i.e. *decreasing* $m^2_{H_u}$, cf. fig. 2.5) and decreasing $|A_D|$, both of which can be readily understood by looking at eq. (2.44) since the lighter sbottom is predominantly left-handed.

Table 2.7 lists the fitted values for the observables entering the χ^2 function for an example fit belonging to the region with lowest χ^2. The input values for this example fit are reported in the left panel of table 2.8, next to the resulting spectrum

Observable	Exp.	Fit	Pull
M_W	80.398	80.58	0.5
M_Z	91.1876	90.65	**1.2**
$10^5\ G_\mu$	1.16637	1.164	0.4
$1/\alpha_{\rm em}$	137.036	136.7	0.5
$\alpha_s(M_Z)$	0.1176	0.1176	0.0
M_t	173.1	172.7	0.3
$m_b(m_b)$	4.20	4.22	0.3
M_τ	1.777	1.78	0.1
10^4 BR$(B \to X_s\gamma)$	3.52	3.04	0.9
10^6 BR$(B \to X_s\ell^+\ell^-)$	1.60	1.63	0.0
$\Delta M_s/\Delta M_d$	35.1	33.9	0.3
10^4 BR$(B^+ \to \tau^+\nu)$	1.40	0.93	**1.0**
10^8 BR$(B_s \to \mu^+\mu^-)$	< 5.8	2.01	–
		total χ^2:	**4.05**

Table 2.7: Example of fit in the region with successful YU. The pull in the last column is defined as the square root of the χ^2 contribution.

Input parameters		Spectrum predictions	
m_{16}	4000	M_{h^0}	126
μ	4500	M_{H^0}	1109
$m_{1/2}$	113.8	M_A	1114
A_D	2000	M_{H^+}	1115
A_U	-11321	$M_{\tilde{t}_1}$	192
$\tan\beta$	49.8	$m_{\tilde{t}_2}$	2656
$1/\alpha_G$	24.7	$m_{\tilde{b}_1}$	2634
$M_G/10^{16}$	3.77	$m_{\tilde{\tau}_1}$	3489
$\epsilon_3/\%$	-3.8	$m_{\tilde{\chi}_1^0}$	53.3
$(m_{H_u}/m_{16})^2$	0.32	$m_{\tilde{\chi}_2^0}$	104.1
$(m_{H_d}/m_{16})^2$	-1.38	$m_{\tilde{\chi}_1^+}$	104.1
y_t	0.66	$m_{\tilde{g}}$	321
$M_R/10^{14}$	2.6		

Table 2.8: Input parameters and spectrum predictions for the example fit reported in table 2.7. All masses and massive input parameters are in units of GeV.

predictions. This example fit is also represented in figures 2.3–2.7 as a dot.

2.5.3 Conclusions

The above analysis confirms the result of section 2.4 that YU is disfavoured for $A_U = A_D$ by an interplay between the corrections to the bottom quark mass and the FCNC constraints, but also shows that the trilinear splitting scenario indeed gives rise to a viable solution featuring exact YU and being compatible with all relevant constraints. This can be achieved by $|A_D|^2 \ll |A_U|^2$ and large $\mu \approx m_{16}$ (but not too large). Interestingly enough, the recovery of phenomenological viability is not obtained by invoking a decoupling of the sparticle spectrum, but it instead seems to *require* parts of this spectrum to be very close to their experimental lower bounds.

3 Signatures of Minimal Flavour Violation

3.1 Minimal Flavour Violation and the SUSY CP problem

The principle of Minimal Flavour Violation (MFV), stating that the Yukawa couplings are the only spurions breaking the MSSM flavour symmetry, is a powerful symmetry principle to ensure that the flavour structure of the MSSM soft SUSY breaking sector is sufficiently similar to the SM flavour structure in order not to be in disagreement with the precise experimental flavour data. However, as already mentioned in section 1.2.2, the MFV principle does not forbid CP-violating phases beyond the CKM one. While it is of course possible to *assume* that no CP violation beyond the CKM phase is present, as was done e.g. in [10], this is not guaranteed by the MFV breaking of the flavour symmetry. In fact, since the Yukawa spurions themselves violate CP, it does not seem very natural to assume CP conservation apart from the CKM phase.

In the general MSSM, we saw in section 1.2.3 that there are 12 *flavour blind* phases that can be chosen to be the phases of the μ term, two gaugino masses and 9 diagonal elements of the trilinear coupling matrices. The b term and one gaugino mass (usually the gluino mass) can be made real by making use of the PQ and R symmetries. Additionally, there are in total 33 phases related to flavour non-diagonal couplings.

In the MFV MSSM, without making the assumption that all CP violation arises from the CKM phase, the flavour blind phases of the μ term and the gaugino masses can still be present; In the trilinear terms, the situation is different however: recalling the MFV expansion of the squark and slepton trilinear couplings,

$$T_U = A\left(a_4\mathbb{1} + b_7 Y_D Y_D^\dagger + c_7 Y_U Y_U^\dagger + c_8 Y_U Y_U^\dagger Y_D Y_D^\dagger + c_9 Y_D Y_D^\dagger Y_U Y_U^\dagger\right) Y_U\,, \tag{3.1}$$

$$T_D = A\left(a_5\mathbb{1} + b_8 Y_U Y_U^\dagger + c_{10} Y_D Y_D^\dagger + c_{11} Y_U Y_U^\dagger Y_D Y_D^\dagger + c_{12} Y_D Y_D^\dagger Y_U Y_U^\dagger\right) Y_D\,, \tag{3.2}$$

$$T_E = A\left(a_8\mathbb{1} + b_{15} Y_E Y_E^\dagger\right) Y_E\,, \tag{3.3}$$

all the a_i and b_i coefficients can be complex, but all terms except for the ones proportional to a_i are proportional to at least three powers of Yukawa couplings and therefore suppressed, in particular if $\tan\beta$ is small.

The only additional phases present in the MFV MSSM reside in highly suppressed terms in the expansion of sfermion squared masses, i.e. the coefficients b_3, c_3 and c_6 in eqs. (1.10)–(1.12), but they will not play a role in the following.

To recapitulate, the MFV MSSM in general contains CP violating phases in the μ term, two gaugino masses and the three overall coefficients $a_{4,5,6}$ in the trilinear couplings; these will be referred to as flavour blind phases in the following. In addition, there are phases in the expansion coefficients of trilinear couplings and sfermion masses, which are suppressed by increasing powers of Yukawa couplings.

Of course, the flavour blind phases are problematic from a phenomenological perspective: they generically lead to unacceptably large amounts of CP violation that would have to show up e.g. in electric dipole moments. This is the essence of the SUSY CP problem and it is has to be stressed that the MFV MSSM suffers from this problem just as the completely general MSSM. Before suggesting a mechanism to ameliorate this problem, let us review the most important experimental constraints on flavour blind CP violating phases: electric dipole moments (EDMs).

3.1.1 SUSY and electric dipole moments

A fundamental particle can only have an electric dipole moment if both parity P and time reversal invariance T are violated. This can be easily seen by noting that the EDM term in the nonrelativistic Hamiltonian of a particle in an electric field,

$$H = -d\,\mathbf{E}\cdot\frac{\mathbf{S}}{S}\,, \tag{3.4}$$

is odd under both P and T. Assuming the conservation of CPT, which holds for any local Lorentz invariant quantum field theory with a hermitian Hamiltonian, T violation implies CP violation. The relativistic generalization of (3.4) for fermions is then the CP violating operator

$$\mathcal{L} = -d\,\frac{i}{2}\bar{\psi}\sigma^{\mu\nu}\gamma_5\psi F_{\mu\nu}\,. \tag{3.5}$$

EDMs are therefore precision observables of fundamental CP violation, and EDM searches already set powerful bounds on CP violation in theories beyond the SM (see [96] for a comprehensive review).

Experimentally, not the fundamental particle EDMs are measured but the EDMs of constituent systems like atoms or hadrons. Atomic EDMs are divided into two different classes: the ones of paramagnetic atoms – i.e. atoms with an unpaired electron – like thallium (Tl), are mostly sensitive to the electron EDM. The ones of diamagnetic atoms like mercury (Hg) receive contributions from both quark and lepton EDMs as well as from the quark chromoelectric dipole moments (CEDMs), the QCD analogue of (3.5),

$$\mathcal{L} = -\tilde{d}\,\frac{i}{2}g_3\bar{\psi}\sigma^{\mu\nu}\gamma_5\psi G_{\mu\nu}\,. \tag{3.6}$$

EDM	Current bound
$\lvert d_n \rvert$	$< 2.9 \times 10^{-26}$ @ 90% C.L [98]
$\lvert d_{\mathrm{Hg}} \rvert$	$< 3.1 \times 10^{-29}$ @ 95% C.L [99]
$\lvert d_e \rvert$	$< 1.6 \cdot 10^{-27}$ @ 90% C.L [100]

Table 3.1: Experimental upper bounds and future sensitivities of the three most constraining EDMs in units of $e\,$cm.

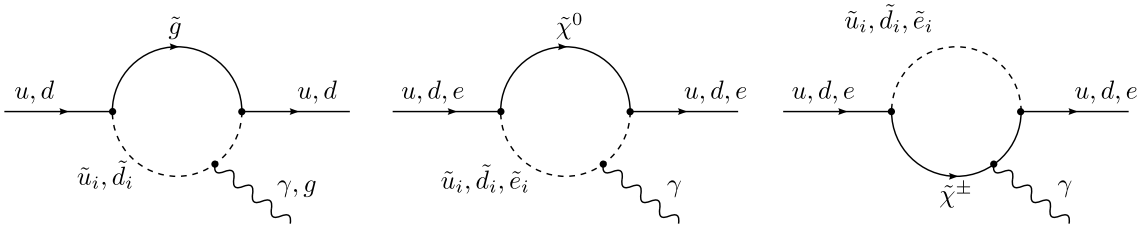

Figure 3.1: One-loop gluino, neutralino and chargino contributions to first generation quark and lepton (C)EDMs.

Finally, the experimentally most important hadron EDM is the neutron EDM, which is sensitive to the quark EDMs and CEDMs. The current experimental exclusion bounds are listed in table 3.1.

In the SM, there are two potential sources of CP violation that can generate (C)EDMs: the QCD vacuum angle θ and the CKM phase. The absence of any evidence for a nonzero fundamental particle EDM puts very strong bounds on θ and gives rise to the strong CP problem; this problem persists in the MSSM and calls for an independent solution. It will be assumed in the following that $\theta = 0$ holds exactly. The CKM phase on the other hand is known to be sizable, but only gives rise to tiny contributions to the EDMs, since it always involves a flavour changing charged quark current. For example, the CKM contribution to the electron EDM arises first at the four-loop level [97].

In the MSSM, the large number of new potential sources of CP violation discussed in secion 1.2.3 can in principle lead to large enhancements of the EDMs with respect to their (tiny) SM expectations, and indeed the current experimental upper bounds on the EDMs in table 3.1 strongly constrain CP violating phases in the MSSM, in particular the flavour blind ones.

In the presence of flavour blind phases, EDMs can be generated in the MSSM already at the one-loop level through the chargino and neutralino diagrams shown in figure 3.1. If the μ term and trilinear parameters are complex, as

$$\mu = |\mu|\, e^{i\phi_\mu} \ , \qquad\qquad T_{U,D,E} = |A|\, e^{i\phi_A}\, Y_{U,D,E} \ , \tag{3.7}$$

the contributions to the electron EDM, for instance, can be written approximately, assuming all SUSY particles to have a common mass $\tilde{m}$, as

$$d_e = \left(\frac{100\,\text{GeV}}{\tilde{m}}\right)^2 \left[\left(\frac{\sin\phi_\mu}{4\times10^{-5}}\right)\left(\frac{\tan\beta}{10}\right) + \left(\frac{\sin\phi_A}{3\times10^{-3}}\right)\right] \times 10^{-27}\; e\,\text{cm}\,, \quad (3.8)$$

putting very strong constraints on ϕ_μ and ϕ_A.

3.1.2 MFV without flavour blind CP violation

In view of the strong constraints on flavour blind phases stemming from the non-observation of EDMs, it is clear that some mechanism is required to explain the suppression of these phases in the MFV MSSM. Instead of making the extreme assumption that the CKM phase is the only source of CP violation in the MFV MSSM, an interesting alternative has been suggested in [101, 102]: If CP is conserved in the limit of *flavour blindness*, but broken by the higher order terms in the MFV expansion, the most dangerous flavour blind phases, i.e. the phases of μ, the gaugino masses and $a_{4,5,6}$ are absent, but phases in the higher order MFV coefficients can still lead to interesting signals in low energy CP violation experiments.

While this approach might seem *ad hoc* at first, it is in fact very similar to what happens in SUSY flavour models based on the Froggatt-Nielsen mechanism [33], which are much more ambitious than MFV since their aim is to explain the origin of Yukawa couplings and solve the SUSY flavour problem at the same time. In these models, CP is usually assumed to be conserved in the flavour symmetric limit, and CP violation only arises from terms breaking the flavour symmetry.

Similarly, the assumption of MFV with CP conservation in the limit of flavour blindness is a phenemenologically motivated one, but could originate from a more fundamental theory relating the mechanisms of the breaking of flavour and CP. However, a crucial ingredient that has to be specified is the scale at which this breaking occurs. The MFV expansion of the soft terms (1.10)–(1.17) is RG invariant [11, 103], since the beta functions of Yukawa couplings respect the MFV principle. However, the assumption of real expansion parameters $a_{4,5,6}$ is not RG invariant, since the expansion parameters mix among each other and can be generated in the RG evolution even if they are zero at some scale.

The discussion will thus proceed in two steps: First, the consequences of imposing the assumption of CP conservation in the limit of flavour blindness *at low energies* will be investigated; in this case, RG effects are of course irrelevant. Second, the same assumption on CP phases will be assumed to hold *at the GUT scale* $M_G \simeq 2\times10^{16}\,\text{GeV}$. In this case, large RG effects are present and the phenomenology will be quite different from the low energy scenario. Clearly, any intermediate flavour (and CP) breaking scale will then lead to results interpolating between the two extreme cases.

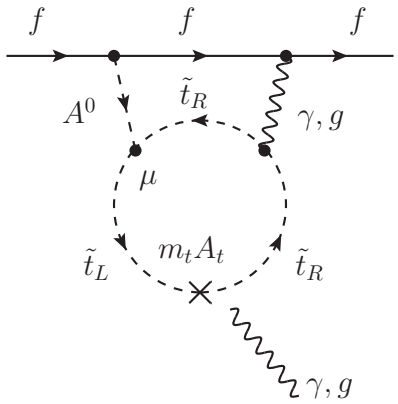

Figure 3.2: Two-loop Barr-Zee type diagram generating an EDM for quarks ($f = q$) and leptons ($f = \ell$) when $\mathrm{Im}(\mu A_t) \neq 0$.

MFV at low energies

If the assumption that CPV in the MFV MSSM arises only through terms breaking the flavour blindness is imposed at the EW scale, then the μ term and the gaugino masses are real at low energies and CPV beyond the CKM phase arises only from the b_i and c_i coefficients in the trilinear terms (3.1)–(3.3) (neglecting the highly suppressed b_3, c_3 and c_6 in the squark mass matrices).

The crucial observation is now that the imaginary parts of diagonal elements of the trilinear coupling matrices are hierarchically suppressed, since they are proportional to at least three powers of Yukawa couplings. For example, one has

$$(T_U)_{33} = a_4\, y_t + b_7\, y_b^2 y_t + c_7\, y_t^3 + O(y^5)\,, \tag{3.9}$$

compared to

$$(T_U)_{11} = a_4\, y_u + b_7\, y_d^2 y_u + c_7\, y_u^3 + O(y^5)\,, \tag{3.10}$$

with a_4 real, so that e.g. at small $\tan\beta$, $\mathrm{Im}((T_U)_{33})/\mathrm{Im}((T_U)_{11}) \simeq m_u^3/m_t^3$. Accordingly, one has $(T_D)_{33} \gg (T_D)_{11,22}$ and $(T_E)_{33} \gg (T_E)_{11,22}$.

This suppression has the immediate consequence that the one-loop contributions to the EDMs of first generation fermions are well under control in this scenario, since they require a nonvanishing phase in the trilinear couplings of the first generation (or in the μ term or the gaugino masses, which are real in this scenario).

Still, sizable contributions to the EDMs can be generated at the two loop level from contributions which are directly proportional to the third generation trilinear couplings. Then, the additional loop suppression factor is easily compensated by the lifted suppression of imaginary parts of trilinear couplings. The dominant two-loop contribution turns out to arise from a Barr-Zee type diagram shown in figure 3.2.

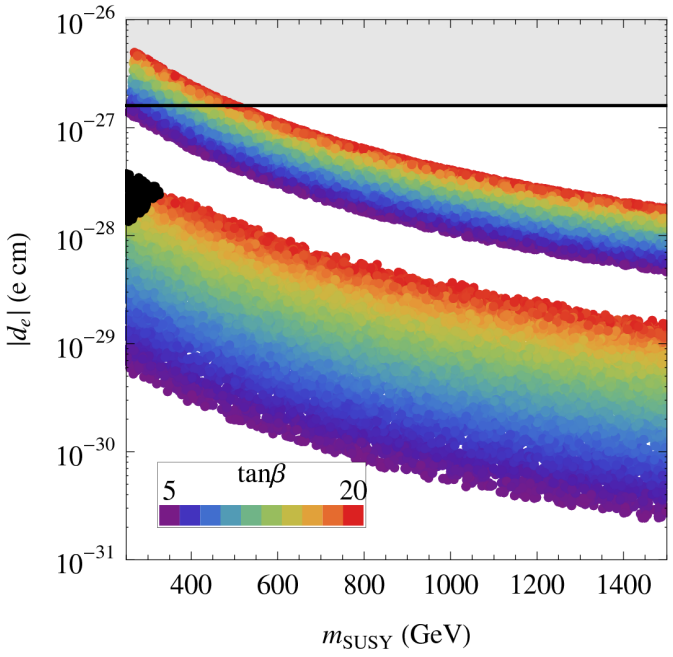

Figure 3.3: Predictions for the electron EDM in a MFV framework defined at the EW scale. The upper band corresponds to the scenario where $T_U = A_U(\mathbb{1}+c_7 Y_U Y_U^\dagger)Y_U$ with $c_7 = i$, while the lower band refers to the scenario where $T_U = A_U(\mathbb{1} + b_7 Y_D Y_D^\dagger)Y_U$ with $b_7 = i$. In both cases, the black points are excluded by the constraints from B physics processes.

While these diagrams contribute both to lepton EDMs and to quark (C)EDMs, the most constraining observable turns out to be the electron EDM.

To assess the phenomenological viability of the low-scale MFV scenario numerically, one can now concentrate on simple benchmark scenarios: since the dominant EDM contribution arises from a Barr-Zee type diagram proportional to the stop trilinear, the most important phases are the ones in the expansion of T_U (3.1). Fig. 3.3 shows the prediction for the electron EDM, compared to the experimental exclusion bound, versus a common SUSY mass m_{SUSY} that was assumed for simplicity, for two scenarios with different complex flavour structures in the up-squark trilinear couplings:

$$\text{i) } T_U = A_U\,(\mathbb{1} + i\,Y_U Y_U^\dagger)\,Y_U\,, \quad \text{i.e. } c_7 = i, b_7 = 0\,, \tag{3.11}$$

$$\text{ii) } T_U = A_U\,(\mathbb{1} + i\,Y_D Y_D^\dagger)\,Y_U\,, \quad \text{i.e. } c_7 = 0, b_7 = i\,, \tag{3.12}$$

where $A_U = A\,a_4$ is real. In both cases, the EDM is well under control, but can reach experimentally visible levels.

MFV at the GUT scale

As mentioned above, while the MFV expansion itself is RG invariant, the ansatz that CPV arises only from terms breaking the flavour blindness is not, since phases in the complex parameters in eq. (3.1)–(3.3) can be generated through the RG evolution from the GUT scale to the EW scale.

In particular, the imaginary parts of the first generation trilinear terms, which are highly suppressed by their cubic dependence on the fermion masses at the input scale (as discussed in the previous section), can become sizable.

This can be illustrated by an approximate solution to the RG equation of the first-generation up-squark trilinear A_u,

$$A_u(M_Z) \approx A_u(M_G) - \left(0.41 y_t^2 a_4 - 0.03 y_b^2 a_5 + 0.05 y_t^2 y_b^2 b_7 + 0.11 y_t^4 c_7\right) A - 2.8 m_{1/2}\,. \tag{3.13}$$

The ansatz described at the beginning of section 3.1.2 amounts to assuming $m_{1/2}$ and $a_{4,5}$ real but b_7 and c_7 complex, while the GUT scale value $A_u(M_G)$ is nearly real due to the cubic suppression discussed above. As can be seen from (3.13), a sizable imaginary part can be induced in $A_u(M_Z)$ through the terms proportional to b_7 and c_7, with potentially dangerous effects for EDMs. However, this effect competes with a large real contribution to A_u induced by $SU(3)$ interactions and proportional to $m_{1/2}$.

Similarly, the stop trilinear coupling, which drives the dominant two-loop contributions to the EDMs, can be expressed at low energies as

$$\begin{aligned} A_t(M_Z) \approx A_t(M_G) - \big(&0.81 y_t^2 a_4 + 0.09 y_b^2 a_5 - 0.04 y_t^2 y_b^2 b_7 - 0.10 y_t^4 c_7 \\ &+0.03 y_t^2 y_b^2 b_8 + 0.01 y_b^4 c_{10}\big) A - 2.2 m_{1/2}\,. \end{aligned} \tag{3.14}$$

In this case, already the value at the GUT scale $A_t(M_G)$ can have a sizeable phase, since it is not suppressed by small Yukawa couplings as can be seen from eq. (3.9). However, this phase is strongly reduced by the last term of (3.14), since the assumption of CP conservation in the limit of flavour blindness dictates $m_{1/2}$ to be real.

A more subtle, but nevertheless crucial, effect regards the phase of the μ term. The basic ansatz of CP conservation in the limit of flavour blindness requires μ to be real at the GUT scale. Then, since the phase of μ is RG invariant, it remains real at low energies. But then one has to worry about the phase of the b term: As was first discussed in section 1.2.3, one has the freedom to make use of a combined PQ and R phase transformation to make the b term real *at the EWSB scale*, to ensure that the Higgs VEVs are real. But the phase of b is *not* RG invariant; on the contrary, it can pick up a large phase in the presence of complex trilinear terms. Thus, the phenomenologically necessary assumption that b is real at the EW scale requires, in the presence of complex trilinear terms, a *complex* b term at the GUT scale. This

clashes with the initial assumption of a CP conserving theory at the GUT scale in the absence of flavour breaking.

The solution to this conundrum can be obtained by a change of basis. Assuming μ and b to start out real at the GUT scale, μ will remain real and b become complex at the EW scale. By exploiting the $U(1)_{\mathrm{PQ}}$ phase transformation, which amounts to an equal phase shift in μ and b (cf. the spurion charges in table 1.2), b can be made real, as required by EWSB, but then μ will be complex!

As a consequence of this mechanism, the μ term acquires an effective CPV phase through RG effects in our scenario, giving rise to additional one-loop contributions to EDMs. It should be stressed that this mechanism is not restricted to MFV models, but is at work in all models predicting complex A terms, but real μ and b terms at the GUT scale.

For the numerical assessment of its phenomenological viability, also in the GUT scale scenario it is most instructive to restrict oneself to phases only in T_U at the input scale, since the RG effects are driven most strongly by the stop trilinear.

The results of a scan where the same MFV terms in T_U as in eq. (3.11)–(3.12) (this time at the GUT scale) have been switched on and assumed to be purely imaginary are shown in fig. 3.4. m_{SUSY} in this case refers to CMSSM-like SUSY breaking boundary conditions with $Aa_4 = A_0 = m_0 = m_{1/2} \equiv m_{\mathrm{SUSY}}$. The scenario with $c_7 = i$ is ruled out for all values of $\tan\beta$ even for a sizable SUSY scale. The scenario with $b_7 = i$, however, is allowed at small to intermediate $\tan\beta$ even for a quite low SUSY scale.

3.1.3 Conclusions

The principle of MFV is an elegant solution to the SUSY flavour problem, but it does not solve the SUSY CP problem that is evident in the absence of any nonzero fundamental particle EDM. In this section, it was suggested that this tension could be resolved if the MSSM is CP invariant in the limit of flavour blindness and CP is only broken by the terms breaking the flavour symmetry. This solution is particularly interesting since it predicts viable *and* observable effects in CP violating observables. If the scale of flavour breaking is low, this is possible even with $O(1)$ phases of the MFV coefficients in question; if the scale is as high as the GUT scale, some additional suppression of the phases in the most important coefficient is necessary since the μ term acquires an effective phase through RG effects. This effect, which is sometimes overlooked, is relevant for a much wider class of models.

As a final comment, the scenarios considered in this section also have a rich and interesting B physics phenomenology, with the effects being very similar to the model with hierarchical, complex A terms studied in [34].

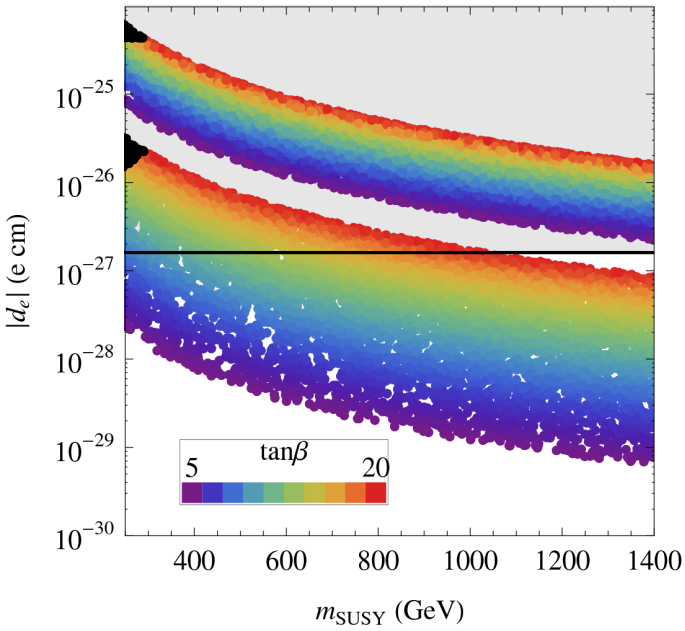

Figure 3.4: Predictions for the electron EDM in MFV framework defined at the GUT scale assuming the boundary conditions $T_U = A_U(\mathbb{1} + c_7 Y_U Y_U^\dagger)Y_U$ with $c_7 = i$ (upper band) and $T_U = A_U(\mathbb{1} + b_7 Y_D Y_D^\dagger)Y_U$ with $b_7 = i$ (lower band).

3.2 Gauge mediation and large $\tan\beta$

In section 3.1, the important role of the b term for the phenomenology of CP violation in the MSSM was highlighted. As already mentioned in section 1.4.1, in theories with gauge mediation of SUSY breaking, it is quite natural to obtain a vanishing b term at the mediation scale, a predicition which is welcome to ameliorate the SUSY CP problem. But $b = 0$ has another important consequence: it implies a vanishing VEV for the down-type Higgs doublet H_d.

Of course, $v_d = 0$ is not viable phenomenologically, but $b = 0$ is not a RG invariant condition, since the b term is SUSY breaking and therefore not protected by the SUSY non-renormalization theorem. So even if $b = 0$ at the mediation scale M, it is nonzero at low energies and H_d acquires a nonzero VEV. But if the scale M is low enough, the radiatively generated VEV for H_d is small, i.e. $\tan\beta$ is large [104, 105].

Since the fermion masses are given at tree level by a product of a Yukawa coupling and a Higgs VEV, small v_d in principle requires large Yukawa couplings for the down-type quarks and charged leptons. However, interestingly enough, due to the loop induced couplings to the up-type Higgs discussed in section 1.3.3, there are large corrections to these masses arising at the one loop level which modify this relation

between fermion masses and Yukawa couplings.

These large corrections are welcome since otherwise, the large Yukawa couplings required at very large values of $\tan\beta$ would lead to a breakdown of perturbativity. Indeed, in [106], it was suggested that the MSSM contains a paramater region dubbed "uplifted SUSY", where $b = 0$ at some high scale, $\tan\beta$ is very large and the down-type quark and charged lepton masses are dominantly generated from loop-induced couplings to the uptype Higgs, allowing to keep their Yukawas perturbative.

An interesting question that arises is *how large* $\tan\beta$ can be before the perturbativity of the Yukawa sector breaks down. In addition, large values of $\tan\beta$ give rise to enhanced flavour violating processes, even with a completely flavour-blind soft sector. The purpose of this section is thus to investigate the phenomenological viability of very large $\tan\beta$ in view of the flavour constraints.

3.2.1 Perturbativity of Yukawa couplings

The Yukawa couplings of the third generation fermions are given at tree level by

$$y_t = \frac{m_t}{v \sin\beta/\sqrt{2}} , \qquad y_{b,\tau} = \frac{m_{b,\tau}}{v \cos\beta/\sqrt{2}} , \tag{3.15}$$

with $v \approx 246$ GeV. In the large $\tan\beta$ limit, $1/\cos\beta \approx \tan\beta$ and demanding the Yukawas to be less than $\sqrt{4\pi} \approx 3.54$ at a scale of, say, 1 TeV, would set an upper bound on $\tan\beta$ of roughly 250. However, as discussed in section 1.3.3, the tree-level relations (3.15) can be strongly modified at large $\tan\beta$, so this bound is not strict.

Irrespective of the size of low-energy threshold corrections, the bound on Yukawas at low energies is stronger if one requires them to be perturbative to some high energy scale. The RG equations for the Yukawa couplings have the general form

$$\frac{dy_i}{dt} = \frac{y_i}{16\pi^2} \sum_{j,k} (a_i\, y_j^2 - b_k\, g_k^2) \tag{3.16}$$

with positive coefficients a_i, b_i, so if the Yukawa couplings are large enough (larger than their IR quasi-fixed points), their beta functions are positive, so they will grow with the renormalization scale and eventually hit a Landau pole at some scale[1]. As a consequence, the higher the scale until where the Yukawa couplings are supposed to remain perturbative, the stronger the upper bound on their value at low energies (and consequently on $\tan\beta$).

Before considering the actual low-energy values of the Yukawa couplings in the presence of threshold corrections, it is instructive to solve the RG equations for

[1] Taking into account the two-loop beta functions, the Yukawa couplings have an apparent UV fixed point instead of a Landau pole. However, this fixed point disappears once three-loop contributions are taken into account and simply signals the breakdown of perturbation theory for $y \gg \sqrt{4\pi}$ [107].

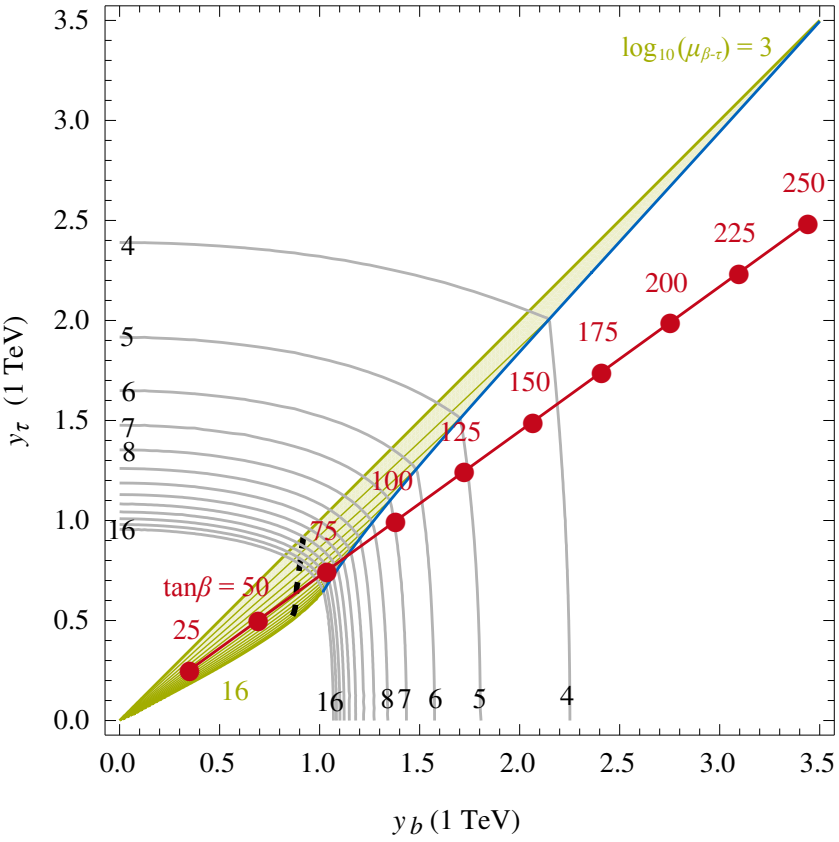

Figure 3.5: Scale $\mu_{\max}$ between 10^4 and 10^{16} GeV at which the bottom (below the blue line) or the tau (above the blue line) Yukawa coupling exceeds the perturbativity limit $\sqrt{4\pi}$, depending on their value at 1 TeV. The gray contours show $\log_{10}(\mu_{\max})$. The red line indicates the values of $y_{b,\tau}$ in the absence of threshold corrections, for fixed values of $\tan\beta$ between 25 and 250. The green shaded area indicates the region where perturbative b-τ Yukawa unification occurs between the TeV scale (uppermost green line) and 10^{16} GeV (lowermost green line). On the black dashed line, full t-b-τ unification takes place.

arbitrary low-energy values and determine the scale at which one of the Yukawas becomes non-perturbative. Since the first and second generation Yukawa couplings are irrelevant for this discussion and the top Yukawa is fairly insensitive to threshold corrections and independent of $\tan\beta$, one can simply determine a scale $\mu_{\max}$, in terms of y_b and y_τ at low energies, where either y_b or y_τ exceeds $\sqrt{4\pi}$. Figure 3.5 shows contours of $\log(\mu_{\max})$ in the plane of y_b and y_τ, fixed for definiteness at the 1 TeV scale.

Of course, the actual low-energy values of $y_{b,\tau}$ have to be the ones reproducing

the known bottom and tau masses. At the tree level, i.e. neglecting threshold corrections, they are simply given by eq. (3.15) and there is an unambiguous relation between $\tan\beta$ and the non-perturbativity scale $\mu_{\max}$, which is shown in fig. 3.5 as well. In this limit, perturbativity up to the GUT scale implies $\tan\beta \lesssim 75$, for instance. However, beyond the tree level, threshold corrections will strongly modify this relation, and it will be the aim of sections 3.2.3 and 3.2.2 to quantify the "true" $\mu_{\max}$ for points in the MSSM parameter space.

It should also be emphasized that perturbativity up to the GUT scale is not strictly necessary, even in GUTs. To explain the peculiar hierarchies present in the Yukawa couplings, SUSY theories of flavour typically assume that the Yukawas are generated from the VEVs of dynamical flavon fields by means of the Froggatt-Nielsen mechanism [33]. While the scale at which this occurs is frequently assumed to be the GUT scale, a much lower flavour breaking scale is not forbidden.

Figure 3.5 also shows the regions in the y_b-y_τ plane leading to b-τ Yukawa unification at some scale between 1 TeV and 10^{16} GeV, The fact that the red tree-level line does not intersect the green 10^{16} GeV b-τ contour reflects the fact discussed in chapter 2 that b-τ unification at the GUT scale requires sizable threshold corrections to y_b. The Yukawa values where complete third generation Yukawa unification, i.e. t-b-τ unification, is possible, are also indicated in the figure.

3.2.2 General Gauge Mediation and large $\tan\beta$

As mentioned in section 1.4.1, $b = 0$ can naturally arise in theories with gauge mediation of SUSY breaking since the b term breaks the Peccei-Quinn symmetry, which his however preserved by gauge interactions. In addition, the gauge mediation scale can be naturally much lower than the GUT scale, so the running of the b term to low energies can be quite short. Due to these facts, it seems natural to consider the framework of very large $\tan\beta$ in the context of general gauge mediation (GGM).

The GGM parameter space consist of the parameters B_k, A_k (where $k = 1, 2, 3$), ζ and b; $|\mu|$ is fixed by the requirement of correct EWSB. b can be traded for $\tan\beta$. It will be assumed in the following that there are no CP violating phases beyond the CKM phase; this is automatically fulfilled in GGM if the B_k are universal at some scale and $b = 0$. Therefore, the B_k will be assumed to be universal at the mediation scale in the following, even when the condition $b = 0$ will not be imposed.

Concerning the hypercharge D-term ζ, since the two Higgs doublets differ in gauge quantum numbers only by the sign of their hypercharge, the GGM relations (1.50) for the Higgs soft masses $m^2_{H_{u,d}}$ show that $\zeta = 0$ would imply $m^2_{H_u} = m^2_{H_d}$. As was discussed already section 2.1 in the context of Yukawa unification, such condition is problematic in the large $\tan\beta$ regime since it obstructs radiative EWSB. Therefore, ζ should be allowed to be nonzero in GGM with large $\tan\beta$.

In fact, from a purely phenomenological perspective, the parameters A_1, A_2 and ζ in (1.49)–(1.50) can be traded for $m^2_L \equiv m^2_{H_d}$, $m^2_{H_u}$ and m^2_E, which can be viewed as

independent free parameters in that case. This parametrization is most transparent to avoid tachyonic sleptons from the outset. The squark masses are then determined in terms of these three parameters and A_3, and tachyonic squarks can in principle always be avoided by choosing A_3 sufficiently large.

To understand the required magnitude of the Higgs splitting, it is useful to note that in the large $\tan\beta$ limit, one approximately has, at the EWSB scale,

$$m_{H_d}^2 - m_{H_u}^2 \approx m_A^2 + m_Z^2 \ , \tag{3.17}$$

so a heavy Higgs spectrum requires a large splitting. In addition, the value of $m_{H_u}^2$ at low energies is related to the size of the μ parameter since

$$-m_{H_u}^2 \approx |\mu|^2 + \frac{1}{2} m_Z^2 \ . \tag{3.18}$$

Interestingly enough, while a nonzero Higgs splitting allows to obtain a heavier Higgs spectrum by means of eq. (3.17), $m_{H_d}^2$ has to be positive at the mediation scale to avoid a charge breaking vacuum since it is tied to the left-handed slepton masses by means of (1.52). Combining eqs. (3.17) and (3.18), one thus obtains an upper bound on the magnitude of μ,

$$|\mu|^2 < m_A^2 + \frac{1}{2} m_Z^2 \ , \tag{3.19}$$

which is valid at the mediation scale, but should be expected to still hold approximately at low energies if the mediation scale is low.

3.2.3 Numerical analysis

Section 3.2.1 demonstrated at which scales the perturbativity of the Yukawa sector breaks down, depending on the values of the third generation Yukawa couplings at low energies. Since the tree-level relations (3.15) between the bottom quark and tau lepton masses and Yukawa couplings can be strongly modified in the large $\tan\beta$ regime, the actual low energy values strongly depend on the soft SUSY breaking parameters.

The purpose of this section is to perform a numerical analyis to determine the values of the third generation Yukawa couplings in the presence of threshold corrections at very large $\tan\beta$, and consequently to determine their non-perturbativity scale μ_{max} by means of the relation between y_b, y_τ and μ_{max} demonstrated in fig. 3.5.

This analysis will proceed in two steps. First, the flavour blind SUSY parameters will be scanned directly at low energies and the Yukawa couplings and non-perturbativity scale determined in a bottom-up approach. Second, an analogous analyis will be performed in the context of GGM with a low mediation scale. since GGM with a low mediation scale leads to approximately flavour blind soft terms at low energies, this second step can be viewed as a special case of the first one.

Low-energy approach

To avoid dangerous effects on flavour and CP violating observables at very large $\tan\beta$, let us consider the flavour-blind and CP-conserving subspace of the full MSSM parameter space, i.e.

$$m^2_{Q,U,D,L,E} = \widetilde{m}^2_{Q,U,D,L,E} \times \mathbb{1} \ , \tag{3.20}$$

$$T_{U,D,E} = A_{U,D,E}\, Y_{U,D,E} \ , \tag{3.21}$$

with real m_i^2 and A_I at low energies, as well as a real μ term and real gaugino masses. The gaugino masses M_1 and M_2 can be treated as independent and with an arbitrary sign, while M_3 can always chosen to be positive (cf. section 1.2.3).

In addition to the parameters in eqs. (3.20)–(3.21) and the gaugino masses, also the pseudoscalar Higgs mass M_A, μ and $\tan\beta$ are free parameters in this setup. They are scanned in the ranges

$$\widetilde{m}_{Q,U,D,L,E} \in [0,2] \text{ TeV}, \qquad A_{U,D,E} \in [-0.5, 0.5] \text{ TeV}, \tag{3.22}$$

$$\mu \in [-2,2] \text{ TeV}, \qquad M_A \in [0,2] \text{ TeV}, \tag{3.23}$$

$$M_1 \in [-1,1] \text{ TeV}, \qquad M_2 \in [-2,2] \text{ TeV}, \qquad M_3 \in [0,6] \text{ TeV}, \tag{3.24}$$

for fixed, large values of $\tan\beta = (50, 100, 150, 200)$. The magnitude of the trilinear couplings $A_{U,D,E}$ is chosen small to soften possible constraints coming from $B_s \to \mu^+\mu^-$ and $B \to X_s\gamma$. In addition, small values of the trilinear couplings naturally arise in the gauge mediation scenario to be considered in section 3.2.2.

In the numerical scan, points violating existing lower bounds on sparticle and Higgs masses, as well as points violating the perturbativity condition $y_{b,\tau} < \sqrt{4\pi}$ at the EWSB scale $m_{\text{SUSY}} = \sqrt{m_{\tilde{t}_1} m_{\tilde{t}_2}}$ have been discarded. For the surviving points, the constraints from the branching ratios of $B \to X_s\gamma$, $B_s \to \mu^+\mu^-$ and $B \to \tau\nu$ and from the muon anomalous magnetic moment have been imposed.

Figure 3.6 shows the results for the bottom and tau Yukawa couplings in the presence of threshold corrections for the four different values of $\tan\beta$, superimposed on the $\mu_{\max}$ contours of fig. 3.5. The plots on the left (right) contain points with $\tan\beta = 50, 150$ ($\tan\beta = 100, 200$) and in the first (second) row the Wino mass M_2 is positive (negative). Light gray points are excluded at the 2σ level by the flavour constraints, while dark gray ones are excluded by $(g-2)_\mu$ alone at the 3σ level. The coloured points finally fulfill all imposed constraints and indicate the corresponding values of μ through the colour.

The four "lobes" of points correspond to the different signs of (μ, M_2) and meet at the (y_b, y_τ) values in absence of threshold corrections (cf. fig. 3.5). Points left of it correspond to positive threshold corrections to y_b ($y'_b > 0$ in the notation of eq. (1.42)), points below it to positive threshold corrections to y_τ ($y'_\tau > 0$), etc. The sign of the corrections to y_τ is given by the sign of $(-\mu M_2)$, and the sign of

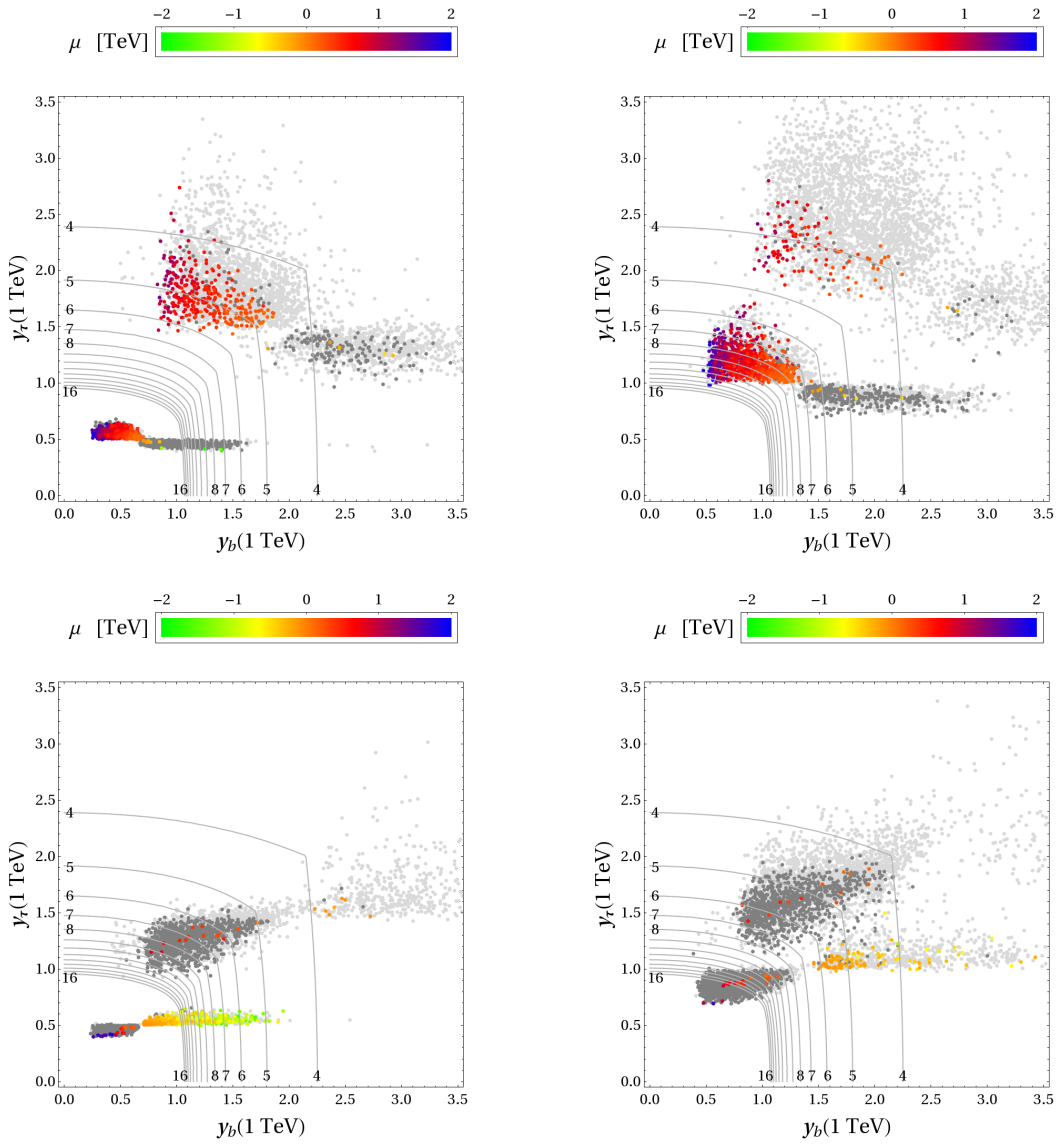

Figure 3.6: Values of the bottom and tau Yukawa couplings at the TeV scale in the low-energy MSSM scan with flavour blind soft terms with $M_2 > 0$ (top row) and $M_2 < 0$ (bottom row). The plots in the left column show the points for $\tan\beta = 50$ below the ones for $\tan\beta = 150$; the plots in the right column show the ones for $\tan\beta = 100$ below the ones for $\tan\beta = 200$. Light gray points are excluded at the 2σ level by the flavour constraints, while dark gray ones are excluded by $(g-2)_\mu$ alone at the 3σ level. Among the coloured points, the ones with smaller values of μ are stacked upon the ones with larger μ. The $\mu_{\max}$ contours are as in fig. 3.5.

the corrections to y_b by the sign of μ, as expected from the dominance of Wino contributions and gluino contributions, respectively, discussed in section 1.3.3.

Almost all the points where $\text{sign}(\mu M_2) = -1$ are ruled out at more than 3σ by the $(g-2)_\mu$ constraint, as was expected from the discussion in section 2.2.4. This rules out positive threshold corrections to y_τ, as would be preferable from the point of view of perturbativity to high scales. The best points in this respect allowed by the $(g-2)_\mu$ constraint are then the ones with positive contributions to y_b and negative contributions to y_τ, i.e. with $\text{sign}(\mu) = \text{sign}(M_2) = +1$.

The size of the threshold corrections to y_b is mainly limited by the maximal possible values of $|\mu|$. Especially for very large $\tan\beta = 150, 200$, $|\mu|$ typically does not exceed 1 TeV. The reason for that is twofold: First, very large values of $\mu \tan\beta$ lead to large left-right mixing entries in the sbottom and stau mass matrices, easily resulting in tachyonic sbottoms or staus. Second, there are sizable sbottom contributions to the lightest Higgs boson mass for large $\mu \tan\beta$ [108]. These contributions are always negative and therefore decrease the lightest Higgs boson mass to values below the LEP bound for too large $\mu \tan\beta$.

General Gauge Mediation

Let us now study the viability of the GGM setup in the very large $\tan\beta$ regime. Since the low-energy analysis showed that the perturbativity scale μ_{max} decreases fastly when $\tan\beta > 50$, a relatively low mediation scale $M = 100$ TeV will be assumed throughout this section for definiteness.

The gaugino mass parameters B_k in (1.49) will be assumed to be independent of the gauge group, implying the usual GUT relations for gaugino masses. The reason for doing so is twofold; First, the solution to the CP problem is facilitated if gaugino masses arise from a single scale, as mentioned in section 3.2.2. Second, the low-energy analysis demonstrated that $M_2 < 0$ requires $\mu < 0$ to meet the $(g-2)_\mu$ bound, which in turn however leads to large positive threshold corrections to y_b and lowers the scale until where y_b remains perturbative. Therefore it is sufficient to consider positive gaugino masses here.

The parameters A_1, A_2 and ζ are traded for m_L^2, m_E^2 and $\Delta m_H^2 = m_{H_d}^2 - m_{H_u}^2$ and scanned in the following ranges,

$$MB_k \in [0,2] \text{ TeV}, \qquad A_3 \in [0,2] \text{ TeV}, \tag{3.25}$$

$$m_L^2 \in [0,2] \text{ TeV}, \qquad m_E^2 \in [0,2] \text{ TeV}, \qquad \Delta m_H^2 \in [0,2] \text{ TeV}. \tag{3.26}$$

Figure 3.7 shows the bottom and tau Yukawa couplings at the TeV scale for fixed $\tan\beta$ values 50, 75 and 100, akin to the plots for the low-energy scan in fig. 3.6. All the points with negative μ are ruled out at more than 3σ by the $(g-2)_\mu$ constraint. For $\tan\beta = 100$, the code did not produce any converged points with correct EWSB for $\mu < 0$. This can be understood from the proximity of the existing points to the

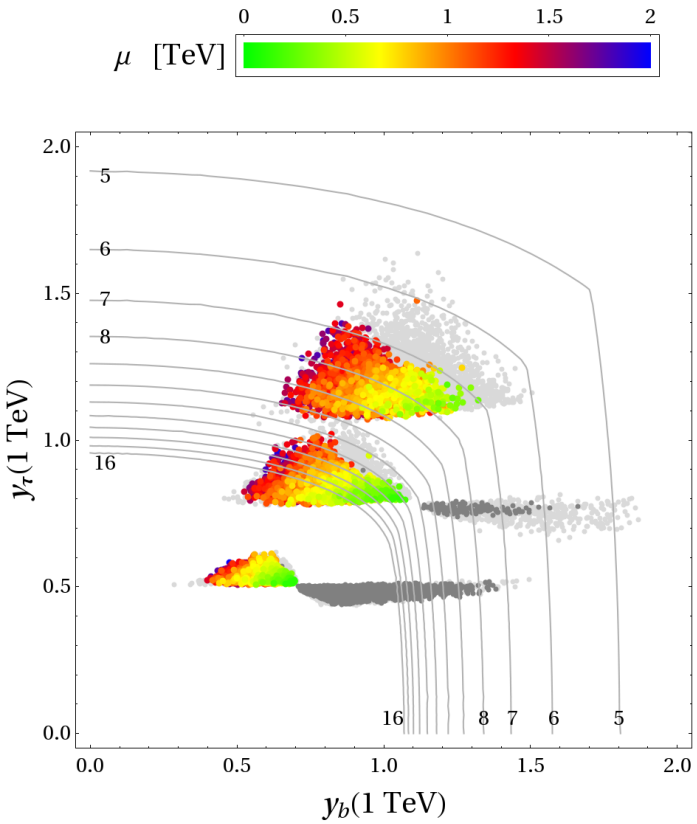

Figure 3.7: Values of the bottom and tau Yukawas at the TeV scale in GGM with $\tan\beta = 50, 75, 100$ (from bottom to top). Light gray points are excluded at the 2σ level by the flavour constraints, while dark gray ones are excluded by $(g-2)_\mu$ alone at the 3σ level. Among the coloured points, the ones with smaller values of μ are stacked upon the ones with larger μ. The $\mu_{\max}$ contours are as in fig. 3.5.

$\mu_{\max} = 10^5$ GeV contour, signaling the non-perturbativity of one Yukawa coupling already at the mediation scale $M = 10^5$ GeV, in which case the calculation becomes unreliable and the code unstable. An attempted scan with $\tan\beta = 150$ accordingly produced no points at all, regardless of the sign of μ. This is also in agreement with the $\tan\beta = 150$ points with $\mu > 0$ in the low-energy plot of fig. 3.6, where all points lie close to or beyond the 10^5 GeV contour.

The other way round, in the regions of parameter space that are preferred from the point of view of Yukawa perturbativity, i.e. where both y_b and y_τ are relatively small, the Higgs mass is always very heavy in GGM and the $B \to \tau\nu$ constraint is automatically fulfilled. This can be understood by combining eqs. (3.17), (3.18) and (1.52) to obtain a relation between the μ term, the left-handed slepton mass

and the pseudoscalar Higgs mass valid at tree level at the mediation scale,

$$m_A^2 = m_L^2 + |\mu|^2 - \frac{1}{2} m_Z^2 \ . \tag{3.27}$$

Since the region with small y_b and y_τ features heavy sleptons (to suppress the positive correction to y_τ) and large μ (to enhance the negative corrections to y_b), eq. (3.27) implies that it also features a heavy Higgs spectrum.

Uplifted SUSY

As discussed at the beginning of section 3.2, a vanishing b term at the mediation scale is a motivation for large or very large $\tan\beta$ (the uplifted SUSY scenario [106]). If $b = 0$ at the mediation scale, $\tan\beta$ is no longer a free parameter but a prediction. Conversely, if $\tan\beta$ is fixed as in the GGM parameter scan, b at the mediation scale turns into a prediction and is not necessarily zero. At tree level, one has $b = m_A^2/\tan\beta$ at low energies. At the loop level, this relation is corrected by the tadpole diagrams discussed in section 1.3.2. Still, the relation $b(M) = 0$ generically requires small pseudoscalar Higgs masses.

Figure 3.8 shows the b term at the mediation scale M against the pseudoscalar Higgs mass M_A. As should be expected from the discussion in section 1.3.2, the loop corrections to the tree-level relation $m_A^2 = b\tan\beta$ roughly scale with μ. In particular, the lower half of the band at $\tan\beta = 50$ corresponds to the points with negative μ and is ruled out at more than 3σ by the $(g-2)_\mu$ constraint. At low $M_A \lesssim 500$ GeV, due to $M_A \approx M_{H^\pm}$, the $B \to \tau\nu$ constraint becomes active and rules out also the points with positive μ. As a consequence, none of the points with $b = 0$ survives.

For $\tan\beta = 75$, the points with $\mu < 0$ have very large y_b (cf. fig. 3.7), leading to large loop corrections to b. These scattered points are however also ruled out by $(g-2)_\mu$. At $M_A \lesssim 750$ GeV, the points are ruled out by $B \to \tau\nu$. For $\tan\beta = 100$, where all points have $\mu > 0$, the bound on M_A rises to almost 1 TeV.

In effect, the combined constraints from $(g-2)_\mu$ and $B \to \tau\nu$ make it virtually impossible to obtain viable scenarios in GGM with $b = 0$ at a mediation scale of 100 TeV.

3.2.4 Conclusions

The main conclusion of the above analysis is that the very large $\tan\beta$ regime is in fact still viable, but this analysis also pointed out the constraints on this scenario arising mainly from the perturbativity of Yukawa couplings, $B \to \tau\nu$, $(g-2)_\mu$, $B \to X_s\gamma$ and $B_s \to \mu^+\mu^-$, exactly the processes that are most relevant for models with Yukawa unifcation, as was discussed in section 2.2.

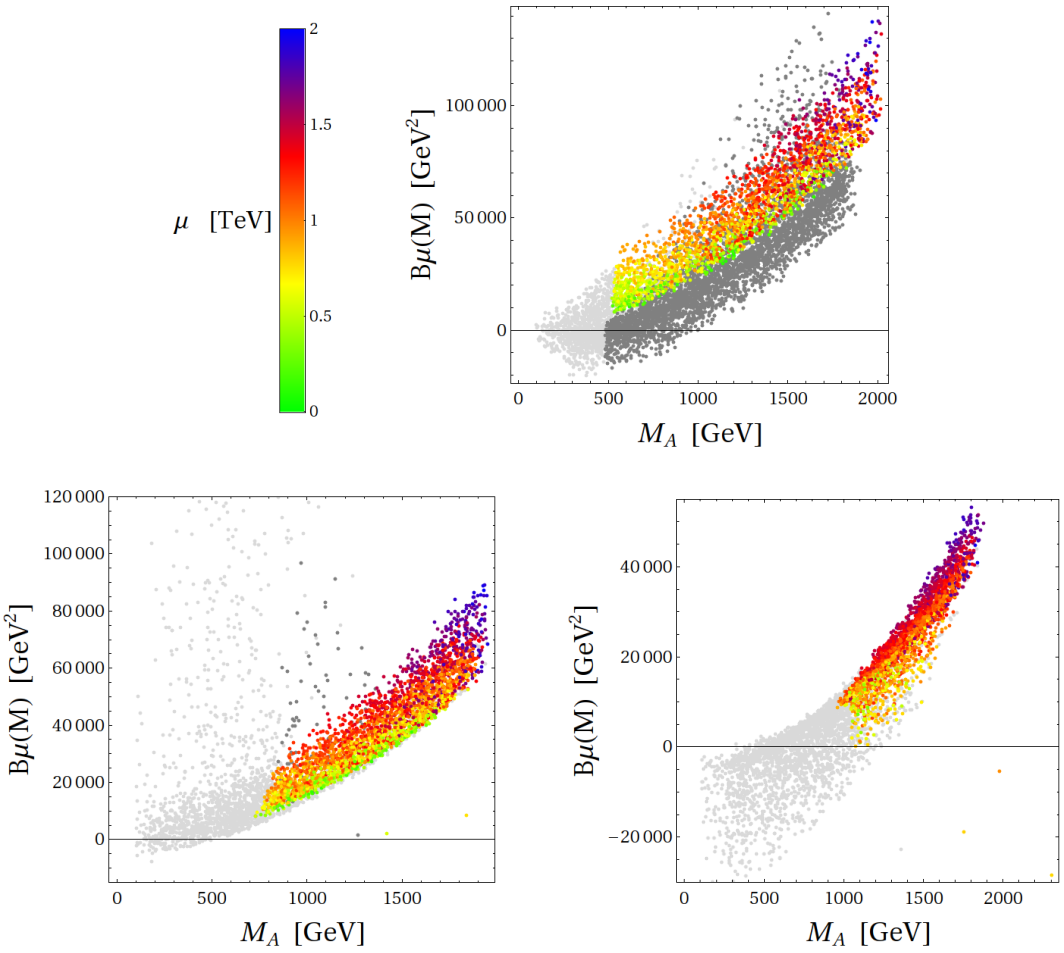

Figure 3.8: b term at the mediation scale $M = 100$ TeV vs. the pseudoscalar Higgs mass M_A for $\tan\beta = 50$ (top), 75 (bottom left) and 100 (bottom right) in the GGM scenario. The light gray points are ruled out by the flavour constraints at the 2σ level, while dark gray ones are excluded by $(g-2)_\mu$ alone at the 3σ level. In particular, the points for low M_A are ruled out by $B \to \tau\nu$.

An important point both for the low-energy scenario and the GGM scenario with a low mediation scale is that the $(g-2)_\mu$ constraint disfavours negative μM_2 and thus disfavours sizable contributions to the tau lepton mass from threshold corrections. While the $B \to X_s\gamma$ and $B_s \to \mu^+\mu^-$ constraints can be relaxed if the trilinear couplings are small, $B \to \tau\nu$ is a crucial constraint even for conservative estimates of the SM uncertainties.

Finally, the analysis of the GGM scenario showed that the condition $b = 0$ at the mediation scale $M = 100$ TeV is only possible for a negative μ parameter or low Higgs masses and correspondingly disfavoured by the combined $(g-2)_\mu$ and

$\mathrm{BR}(B \to \tau\nu)$ constraints. With a higher mediation scale, $b = 0$ remains a valid possibility (cf. [109]) since the larger RG effects lead to stronger deviations from the tree-level relation $b = m_A^2/\tan\beta$. However, a higher mediation scale also lowers the maximal allowed $\tan\beta$ value due to the perturbativity constraints. Consequently, there remains a tension between very large $\tan\beta$ and $b = 0$ in GGM.

Part II

Rare B decays as probes of new physics

4 Angular observables in $B \to K^* \ell^+ \ell^-$ decays

$b \to s$ decays with two leptons in the final state are among the most interesting probes in flavour physics to test the SM and discover or constrain new physics. Compared to the $b \to s\gamma$ transition, they are sensitive to a more diverse number of Wilson coefficients and thus can in principle contain a very rich pattern of new physics effects.

Decays probing the $b \to s\ell^+\ell^-$ transition can be measured either inclusively, i.e. by summing over all final states with strangeness and two leptons, or exclusively, i.e. by "tagging" a particular light meson, like a K or K^*. While inclusive decays are simpler to interpret theoretically, since they are well approximated by the partonic decay, the exclusive ones are more straightforward to obtain experimentally, and indeed at hadron colliders like LHC, an inclusive analysis is very challenging.

Among the exclusive $b \to s\ell^+\ell^-$ decays, $B \to K^*\ell^+\ell^-$ is particularly promising for several reasons. First, the K^* further decays to a kaon and a pion, so the decay of a neutral B^0 only has charged particles in the final state, which are easier to detect at LHC experiments. Second, the four-body final state of $B \to K^*(\to K\pi)\ell^+\ell^-$ gives access to a rich angular distribution containing many observables sensitive to new physics. Third, the CP conjugate modes can be distinguished without tagging the flavour of the B meson, since they can be unambiguously identified merely by means of the kaon and pion charges. This "self-tagging" property allows a clean measurement of various CP asymmetries sensitive to new physics.

First data on $B \to K^*\ell^+\ell^-$ have been accumulated at the B factories BaBar and Belle as well as at the Tevatron, and while they seem to be in agreement with the SM, there is still a lot of room for NP contributions.

One experimental difficulty with $B \to K^*\ell^+\ell^-$ are the resonant contributions due to charmonium production, namely the processes $B \to K^* J/\psi(\to \ell^+\ell^-)$ and $B \to K^*\psi(2S)(\to \ell^+\ell^-)$ occuring around dilepton invariant masses $\sqrt{q^2}$ of 3.1 GeV and 3.7 GeV, respectively. In the following analysis, only the low q^2 region well below the J/ψ threshold will be considered, since in addition to the experimental issues, also theoretical methods like light cone sum rules or QCD factorization rely on expansions only valid at low q^2.

4.1 Theoretical framework

The calculation of the $B \to K^*\ell^+\ell^-$ amplitude poses a number of theoretical challenges. First, it has to be separated into a short-distance part, encoding possible new physics effects, and hadronic matrix elements by means of the operator product expansion. Second, the $B \to K^*$ matrix elements have to be expressed in terms of form factors and these form factors have to be evaluated by means of non-perturbative methods; Third, the contributions to the amplitude which cannot be expressed in terms of form factors have to be estimated. These three ingredients will now be discussed in turn.

4.1.1 Operator product expansion

The effective Hamiltonian for $b \to s\ell^+\ell^-$ transitions can be written as [110]

$$\mathcal{H}_{\text{eff}} = -\frac{4\,G_F}{\sqrt{2}}\left(\lambda_t \mathcal{H}_{\text{eff}}^{(t)} + \lambda_u \mathcal{H}_{\text{eff}}^{(u)}\right), \tag{4.1}$$

where $\lambda_i = V_{ib}V_{is}^*$ and

$$\begin{aligned}
\mathcal{H}_{\text{eff}}^{(t)} &= C_1\mathcal{O}_1^c + C_2\mathcal{O}_2^c + \sum_{i=3}^{6} C_i\mathcal{O}_i + \sum_{i=7,8,9,10,P,S} (C_i\mathcal{O}_i + C_i'\mathcal{O}_i'), \\
\mathcal{H}_{\text{eff}}^{(u)} &= C_1(\mathcal{O}_1^c - \mathcal{O}_1^u) + C_2(\mathcal{O}_2^c - \mathcal{O}_2^u).
\end{aligned}$$

Although $\mathcal{H}_{\text{eff}}^{(u)}$ is highly CKM-suppressed with respect to $\mathcal{H}_{\text{eff}}^{(t)}$, the interference of the two contributions is crucial to obtain non-zero CP asymmetries in $B \to K^*\ell^+\ell^-$ within the SM.

The current-current operators $\mathcal{O}_{1,2}^q$ and QCD penguin operators $\mathcal{O}_{3\ldots6}$ are defined as

$$\mathcal{O}_1^q = 4\,(\bar{s}\gamma_\mu T^a P_L q)(\bar{q}\gamma^\mu T^a P_L b), \qquad \mathcal{O}_2^q = 4\,(\bar{s}\gamma_\mu P_L q)(\bar{q}\gamma^\mu P_L b), \tag{4.2}$$

$$\mathcal{O}_3 = 4\,(\bar{s}\gamma_\mu P_L b)\textstyle\sum_q(\bar{q}\gamma^\mu P_L q), \qquad \mathcal{O}_4 = 4\,(\bar{s}\gamma_\mu T^a P_L b)\textstyle\sum_q(\bar{q}\gamma^\mu T^a P_L q), \tag{4.3}$$

and

$$\mathcal{O}_5 = 4\,(\bar{s}\gamma_{\mu_1}\gamma_{\mu_2}\gamma_{\mu_3} P_L b)\textstyle\sum_q(\bar{q}\gamma_{\mu^1}\gamma^{\mu_2}\gamma^{\mu_3} P_L q), \tag{4.4}$$

$$\mathcal{O}_6 = 4\,(\bar{s}\gamma_{\mu_1}\gamma_{\mu_2}\gamma_{\mu_3} T^a P_L b)\textstyle\sum_q(\bar{q}\gamma^{\mu_1}\gamma^{\mu_2}\gamma^{\mu_3} T^a P_L q). \tag{4.5}$$

In the following, the Wilson coefficients of these operators will be assumed to be unaffected by NP contributions, as is the case in many extensions of the SM. NP effects will then only enter the Wilson coefficients of the radiative and semileptonic operators that already appeared in section 2.2,

$$\mathcal{O}_7 = \frac{e^2}{16\pi^2} m_b(\bar{s}\sigma_{\mu\nu} P_R b)F^{\mu\nu}, \qquad \mathcal{O}_8 = \frac{g_3^2}{16\pi^2} m_b(\bar{s}\sigma_{\mu\nu} T^a P_R b)G^{\mu\nu\,a}, \tag{4.6}$$

$C_1(\mu)$	$C_2(\mu)$	$C_3(\mu)$	$C_4(\mu)$	$C_5(\mu)$
-0.257	1.009	-0.005	-0.078	0.000
$C_6(\mu)$	$C_7^{\text{eff}}(\mu)$	$C_8^{\text{eff}}(\mu)$	$C_9(\mu)$	$C_{10}(\mu)$
0.001	-0.304	-0.167	4.211	-4.103

Table 4.1: SM Wilson coefficients at the scale $\mu = 4.8\,\text{GeV}$, to NNLL accuracy.

$$\mathcal{O}_9 = \frac{e^2}{16\pi^2}(\bar{s}\gamma_\mu P_L b)(\bar{\ell}\gamma^\mu \ell), \qquad \mathcal{O}_{10} = \frac{e^2}{16\pi^2}(\bar{s}\gamma_\mu P_L b)(\bar{\ell}\gamma^\mu\gamma_5 \ell), \tag{4.7}$$

$$\mathcal{O}_S = \frac{e^2}{16\pi^2} m_b(\bar{s}P_R b)(\bar{\ell}\ell), \qquad \mathcal{O}_P = \frac{e^2}{16\pi^2} m_b(\bar{s}P_R b)(\bar{\ell}\gamma_5 \ell). \tag{4.8}$$

Here m_b denotes the running b quark mass in the $\overline{\text{MS}}$ scheme. The chirality-flipped operators $\mathcal{O}_i'$ are obtained from (4.6)–(4.8) by making the replacement $P_L \leftrightarrow P_R$. They are strongly suppressed in the SM, as are the scalar and pseudoscalar operators $\mathcal{O}_{S,P}$.

In matrix elements, C_7, C_8 and C_9 always appear in particular combinations with other Wilson coefficients. It hence proves convenient to define effective coefficients

$$C_7^{\text{eff}} = C_7 - \frac{1}{3}C_3 - \frac{4}{9}C_4 - \frac{20}{3}C_5 - \frac{80}{9}C_6\,, \tag{4.9}$$

$$C_8^{\text{eff}} = C_8 + C_3 - \frac{1}{6}C_4 + 20C_5 - \frac{10}{3}C_6\,, \tag{4.10}$$

$$C_9^{\text{eff}} = C_9 + Y(q^2)\,, \tag{4.11}$$

where the function $Y(q^2)$ can be found e.g. in [110].

Table 4.1 shows the values of the Wilson coefficients to NNLL accuracy in the SM.

4.1.2 Form Factors

The matrix elements of the local operators discussed above between the B initial state and the K^* final state can be expressed in terms of form factors depending on the momentum transfer q^2 between the B and the K^* ($q^\mu = p^\mu - k^\mu$):

$$\begin{aligned}\langle \bar{K}^*(k)|\bar{s}\gamma_\mu(1-\gamma_5)b|\bar{B}(p)\rangle &= \epsilon_{\mu\nu\rho\sigma}\epsilon^{*\nu}p^\rho k^\sigma \frac{2V(q^2)}{m_B + m_{K^*}} - i\epsilon_\mu^*(m_B + m_{K^*})A_1(q^2) \\ &+ i(2p-q)_\mu(\epsilon^*\cdot q)\frac{A_2(q^2)}{m_B + m_{K^*}} + iq_\mu(\epsilon^*\cdot q)\frac{2m_{K^*}}{q^2}\left[A_3(q^2) - A_0(q^2)\right], \end{aligned} \tag{4.12}$$

$$\langle \bar{K}^*(k)|\bar{s}\sigma_{\mu\nu}q^\nu(1+\gamma_5)b|\bar{B}(p)\rangle = T_2(q^2)\left[\epsilon^*_\mu(m_B^2 - m_{K^*}^2) - (\epsilon^*\cdot q)\,(2p-q)_\mu\right] + i\epsilon_{\mu\nu\rho\sigma}\epsilon^{*\nu}p^\rho k^\sigma\, 2T_1(q^2) + T_3(q^2)(\epsilon^*\cdot q)\left[q_\mu - \frac{q^2}{m_B^2 - m_{K^*}^2}\,(2p-q)_\mu\right], \quad (4.13)$$

$$\langle \bar{K}^*|\bar{s}i\gamma_5 b|\bar{B}\rangle = \frac{2m_{K^*}}{m_b + m_s}(\epsilon^*\cdot q)A_0(q^2)\ , \quad (4.14)$$

where ϵ_μ is the polarization vector of the K^* vector meson.

Only seven of these eight form factors are independent since the equations of motion lead to the relation

$$A_3(q^2) = \frac{m_B + m_{K^*}}{2m_{K^*}}\,A_1(q^2) - \frac{m_B - m_{K^*}}{2m_{K^*}}\,A_2(q^2). \quad (4.15)$$

Furthermore, one has $A_0(0) = A_3(0)$ and $T_1(0) = T_2(0)$.

While this definition of form factors will be used throughout this work, an alternative basis [111] can be useful to simplify many expressions, in particular the transversity amplitudes to be discussed below.

The form factors have to be calculated by means of non-perturbative methods. In [112], a calculation based on QCD sum rules on the light cone has been presented. This set of form factors will be used in this analyis. The light cone sum rules (LCSR) calculation of the form factors is valid in the large energy (or large recoil) limit $E_{K^*} \gg \Lambda_{\rm QCD}$; Since the K^* energy is related to the dilepton invariant mass q^2 as

$$E_{K^*} = \frac{m_B^2 + m_{K^*}^2 - q^2}{2m_B}\ , \quad (4.16)$$

large K^* corresponds to small q^2. The form factors are thus only valid in the low q^2 region, which is in practice taken to be $q^2 < 6\,\text{GeV}^2$, below the charm pair production threshold at $q^2 = 4m_c^2$. For the high q^2 region, one has to extrapolate the form factors, making use of physically motivated parametrizations and additional constraints like lattice data and dispersive bounds, see e.g. [111]. This region will not be considered in the following.

4.1.3 QCD factorization

The form factors discussed in the previous section represent a crucial non-perturbative input to the decay $B \to K^*\ell^+\ell^-$; however, there are additional hadronic corrections which cannot be expressed in terms of form factors. The reason is that the *naive factorization* of the matrix element into a hadronic current – containing the form factors – and a leptonic current as

$$\langle \ell^+\ell^-\bar{K}^*\,|\,\mathcal{H}_{\rm eff}\,|\,\bar{B}\rangle \sim \langle \ell^+|\Gamma_1|\ell^-\rangle \times \langle \bar{K}^*|\Gamma_2|\bar{B}\rangle \quad (4.17)$$

is not exact, since the two currents are linked by electromagnetic corrections. Therefore, the full $B \to K^*\ell^+\ell^-$ amplitude contains *non-factorizable* corrections to (4.17).

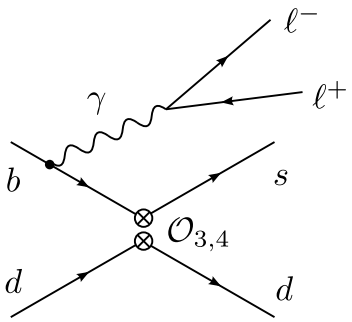

Figure 4.1: Weak annihilation diagram contributing at leading order in α_s to the non-factorizable corrections to $\bar{B}_d \to \bar{K}^{*0}\ell^+\ell^-$. The photon can be attached to any of the four quark legs.

In addition to the large energy limit, another small ratio to expand in is Λ_{QCD}/m_b. In the heavy quark limit, i.e. in the leading order in this ratio (and still in the large energy limit), additional relations between the seven $B \to K^*$ form factors emerge, so that there are only two independent form factors, dubbed "soft" form factors. In this limit, the non-factorizable corrections to $B \to K^*\ell^+\ell^-$ can be calculated systematically by means of the QCD factorization (QCDF) approach [113, 114] as an expansion in α_s.

At leading order in α_s, the only non-factorizable correction to $B \to K^*\ell^+\ell^-$ stems from the weak annihilation diagram shown in figure 4.1. At $O(\alpha_s)$, many more corrections are present and they are consistently taken into account in the numerical analysis following the results of [113, 114].

Starting from the combined heavy quark and large energy limit, one can thus include all corrections of $O((\Lambda/m_b)^0\alpha_s^1)$ (from the NLO QCDF calculation) and some of $O((\Lambda/m_b)^1\alpha_s^0)$ (from using the full set of seven form factors obtained from LCSR as opposed to the two soft form factors in the heavy quark limit). The question is whether there are any additional sizable corrections of $O((\Lambda/m_b)^1\alpha_s^0)$. In [112] it was argued that the bulk of these corrections is indeed included by taking into account the full set of form factors (at least in the case of the neutral $B^0 \to K^{*0}\ell^+\ell^-$ decay where the weak annihilation contribution turns out to be numerically suppressed). In [115], for example, an opposite approach was taken: corrections of $O((\Lambda/m_b)^1\alpha_s^0)$ where dropped altogether, but a conservative theoretical uncertainty accounting for the power suppressed corrections was added.

4.2 Angular distribution

The $B \to K^*(\to K\pi)\ell^+\ell^-$ decay distribution can be described in terms of five kinematical variables: the dilepton invariant mass squared q^2, the K^* invariant mass squared k^2 and the three angles θ_{K^*}, θ_l and ϕ (see fig. 4.2). θ_{K^*} is defined as

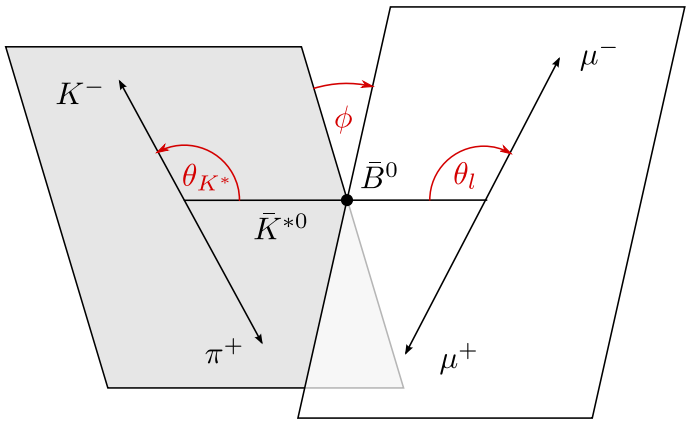

Figure 4.2: Definition of kinematical angles in the $\bar{B}^0 \to \bar{K}^{*0}(\to K^-\pi^+)\ell^+\ell^-$ decay.

the angle between the K and K^* flight directions in the K^* rest frame; θ_l as the angle between the ℓ^- and K^* flight directions in the dilepton center-of-mass frame; and ϕ as the oriented angle between the two planes spanned by the dileptons and the two light mesons, respectively.

The $B \to K\pi$ matrix elements appearing in the amplitude can be easily related to the $B \to K^*$ form factors discussed above if one assumes the intermediate K^* meson to be on-shell. Then, one can make use of the narrow-width approximation $\Gamma_{K^*} \ll m_{K^*}$ and the dependence on the $K^* \to K\pi$ vertex drops out. The on-shell condition $k^2 = m_{K^*}^2$ can be imposed experimentally by appropriate cuts; with k^2 thus fixed, the number of independent kinematical variables is then reduced from five to four.

4.2.1 Decay amplitude

In naive factorization, the matrix element of the effective Hamiltonian (4.1) for the decay $B \to K^*(\to K\pi)\mu^+\mu^-$ can be written as

$$\begin{aligned}\mathcal{M} =& \frac{G_F \alpha}{\sqrt{2}\pi} V_{tb} V_{ts}^* \Bigg\{ \Bigg[\langle K\pi | \bar{s}\gamma^\mu (C_9^{\text{eff}} P_L + C_9' P_R) b | \bar{B} \rangle \\ & - \frac{2m_b}{q^2} \langle K\pi | \bar{s} i\sigma^{\mu\nu} q_\nu (C_7^{\text{eff}} P_R + C_7' P_L) b | \bar{B} \rangle \Bigg] (\bar{\mu}\gamma_\mu \mu) \\ & + \langle K\pi | \bar{s}\gamma^\mu (C_{10} P_L + C_{10}' P_R) b | \bar{B} \rangle (\bar{\mu}\gamma_\mu\gamma_5 \mu) \\ & + \langle K\pi | \bar{s} (C_S P_R + C_S' P_L) b | \bar{B} \rangle (\bar{\mu}\mu) + \langle K\pi | \bar{s} (C_P P_R + C_P' P_L) b | \bar{B} \rangle (\bar{\mu}\gamma_5 \mu) \Bigg\}. \end{aligned} \tag{4.18}$$

To relate the $B \to K\pi$ matrix elements to the $B \to K^*$ form factors, one can

write the squared amplitude as

$$|\mathcal{M}|^2 = \left| \sum_\lambda \mathcal{M}_1^\mu \epsilon_\mu^{*\lambda} \frac{i}{k^2 - m_{K^*}^2 + i m_{K^*}\Gamma_{K^*}} \epsilon_\nu^\lambda \mathcal{M}_2^\nu \right|^2 \tag{4.19}$$

$$= \left| \mathcal{M}_1^\mu \frac{i}{k^2 - m_{K^*}^2 + i m_{K^*}\Gamma_{K^*}} \left(-g_{\mu\nu} + \frac{k_\mu k_\nu}{k^2 - m_{K^*}^2} \right) \mathcal{M}_2^\nu \right|^2 \tag{4.20}$$

where $(\mathcal{M}_1 \cdot \epsilon^{*\lambda})$ is the polarized amplitude for $B \to K^*\ell^+\ell^-$ and $(\mathcal{M}_2 \cdot \epsilon^\lambda)$ the polarized decay amplitude for $K^* \to K\pi$. $\mathcal{M}_2$ can be written formally as

$$\mathcal{M}_2^\nu = -i g_{K^*K\pi} \left(k_1^\nu - k_2^\nu\right) , \tag{4.21}$$

where $g_{K^*K\pi}$ is the $K^*K\pi$ vertex coupling and $k_{1,2}$ the four-momenta of the kaon and pion, respectively. Assuming the K^* to decay resonantly, one can now use the narrow-width approximation to simplify the squared K^* propagator:

$$\left| \frac{i}{k^2 - m_{K^*}^2 + i m_{K^*}\Gamma_{K^*}} \right|^2 \xrightarrow{\Gamma_{K^*} \ll m_{K^*}} \frac{\pi}{m_{K^*}\Gamma_{K^*}} \delta(k^2 - m_{K^*}^2). \tag{4.22}$$

Since the branching ratio of $K^* \to K\pi$ is practically 1, one can write the total K^* decay rate as

$$\Gamma_{K^*} = \frac{m_{K^*}\beta^3}{48\pi}\, g_{K^*K\pi}^2 , \tag{4.23}$$

with

$$\beta = \frac{1}{m_{K^*}^2} \left[m_{K^*}^4 + m_K^4 + m_\pi^4 - 2(m_{K^*}^2 m_K^2 + m_K^2 m_\pi^2 + m_{K^*}^2 m_\pi^2) \right]^{1/2} . \tag{4.24}$$

As a consequence, $g_{K^*K\pi}$ drops out from the amplitude of $B \to K^*(\to K\pi)\ell^+\ell^-$. One can now obtain the amplitude by starting from the $B \to K^*\ell^+\ell^-$ amplitude and replacing the matrix elements of the form

$$\langle \bar{K}^*(k)|J_\mu|\bar{B}(p)\rangle = \epsilon^{*\nu} A_{\nu\mu}, \tag{4.25}$$

where $A_{\nu\mu}$ contains the $B \to K^*$ form factors, by

$$\langle \bar{K}(k_1)\pi(k_2)|J_\mu|\bar{B}(p)\rangle = -D_{K^*}(k^2)\, W^\nu A_{\nu\mu}, \tag{4.26}$$

where [116]

$$|D_{K^*}(k^2)|^2 = g_{K^*K\pi}^2 \frac{\pi}{m_{K^*}\Gamma_{K^*}} \delta(k^2 - m_{K^*}^2) = \frac{48\pi^2}{\beta^3 m_{K^*}^2} \delta(k^2 - m_{K^*}^2), \tag{4.27}$$

$$W^\mu = K^\mu - \frac{m_K^2 - m_\pi^2}{k^2}\, k^\mu, \qquad k^\mu = k_1^\mu + k_2^\mu, \qquad K^\mu = k_1^\mu - k_2^\mu. \tag{4.28}$$

4.2.2 Transversity amplitudes

The $B \to K^*\ell^+\ell^-$ amplitude can be simplified by decompsing it into subamplitudes with definite helicitities of intermediate vector bosons, the *helicity amplitudes*.

Consider the decay $B \to K^*V^*$, with the B meson decaying to an on-shell K^* and a virtual photon or Z boson (which can later decay into a lepton-antilepton pair). The amplitude for this process can be written as

$$\mathcal{M}_{(m,n)}(B \to K^*V^*) = \epsilon^{*\mu}_{K^*}(m)\, M_{\mu\nu}\, \epsilon^{*\nu}_{V^*}(n) \tag{4.29}$$

where $\epsilon^{\mu}_{V^*}(n)$ is the polarization vector of the virtual gauge boson, which can be transverse ($n = \pm$), longitudinal ($n = 0$) or timelike ($n = t$). In the B meson rest frame, the four basis vectors can be written as [117, 118]

$$\epsilon^{\mu}_{V^*}(\pm) = (0, 1, \mp i, 0)/\sqrt{2}, \tag{4.30}$$

$$\epsilon^{\mu}_{V^*}(0) = (-q_z, 0, 0, -q_0)/\sqrt{q^2}, \tag{4.31}$$

$$\epsilon^{\mu}_{V^*}(t) = (q_0, 0, 0, q_z)/\sqrt{q^2}, \tag{4.32}$$

where $q^\mu = (q_0, 0, 0, q_z)$ is the four-momentum vector of the gauge boson. They satisfy the orthonormality and completeness relations

$$\epsilon^{*\mu}_{V^*}(n)\epsilon_{V^*\,\mu}(n') = g_{nn'}, \tag{4.33}$$

$$\sum_{n,n'} \epsilon^{*\mu}_{V^*}(n)\epsilon^{\nu}_{V^*}(n')g_{nn'} = g^{\mu\nu}, \tag{4.34}$$

where $n, n' = t, \pm, 0$ and $g_{nn'} = \mathrm{diag}(+, -, -, -)$.

The K^*, on the other hand, is on shell and thus has only three polarization states, $\epsilon^{\mu}_{K^*}(m)$ with $m = \pm, 0$, which read in the B rest frame

$$\epsilon^{\mu}_{K^*}(\pm) = (0, 1, \pm i, 0)/\sqrt{2}, \tag{4.35}$$

$$\epsilon^{\mu}_{K^*}(0) = (k_z, 0, 0, k_0)/m_{K^*}, \tag{4.36}$$

where $k^\mu = (k_0, 0, 0, k_z)$ is the four-momentum vector of the K^* (note that $k_z = -q_z$). They satisfy the relations

$$\epsilon^{*\mu}_{K^*}(m)\epsilon_{K^*\,\mu}(m') = -\delta_{mm'}, \tag{4.37}$$

$$\sum_{m,m'} \epsilon^{*\mu}_{K^*}(m)\epsilon^{\nu}_{K^*}(m')\,\delta_{mm'} = -g^{\mu\nu} + \frac{k^\mu k^\nu}{m^2_{K^*}}. \tag{4.38}$$

The helicity amplitudes H_0, H_+ and H_- can now be projected out from $M_{\mu\nu}$ by contracting with the explicit polarization vectors in (4.29),

$$H_m = \mathcal{M}_{(m,m)}(B \to K^*V^*), \qquad m = 0, +, -. \tag{4.39}$$

Alternatively, one can work with the transversity amplitudes defined as [119]

$$A_{\perp,\parallel} = (H_{+1} \mp H_{-1})/\sqrt{2}, \quad A_0 \equiv H_0. \tag{4.40}$$

In contrast to the decay of B to two (on-shell) vector mesons, to which this formalism can also be applied, there is an additional transversity amplitude in the case of $B \to K^*V^*$ because the gauge boson is virtual, namely

$$A_t = \mathcal{M}_{(0,t)}(B \to K^*V^*), \tag{4.41}$$

which corresponds to a K^* polarization vector which is longitudinal in the K^* rest frame and a V^* polarization vector which is timelike in the V^* rest frame.[1]

If we now consider the subsequent decay of the gauge boson into a lepton-anti-lepton pair, the amplitude becomes

$$\mathcal{M}(B \to K^*V^*(\to \mu^+\mu^-))(m) \propto \epsilon^{*\mu}_{K^*}(m)\, M_{\mu\nu} \sum_{n,n'} \epsilon^{*\nu}_{V^*}(n)\epsilon^{\rho}_{V^*}(n')\, g_{nn'}\, (\bar{\mu}\gamma_\rho P_{L,R}\mu). \tag{4.42}$$

This amplitude can now be expressed in terms of six transversity amplitudes $A^L_{\perp,\parallel,0}$ and $A^R_{\perp,\parallel,0}$, where L and R refer to the chirality of the leptonic current, as well as the seventh transversity amplitude A_t. The reason that for A_t no separate left-handed and right-handed parts have to be considered can be seen as follows. Noticing that the timelike polarization vector in (4.32) is simply given by $\epsilon^{\mu}_{V^*}(t) = q^\mu/\sqrt{q^2}$, one can see from current conservation,

$$q^\mu(\bar{\mu}\gamma^\mu\mu) = 0, \qquad q^\mu(\bar{\mu}\gamma^\mu\gamma_5\mu) = 2im_\mu(\bar{\mu}\gamma_5\mu), \tag{4.43}$$

that the timelike component of the V^* can only couple to an axial-vector current. In addition, this shows that A_t vanishes in the limit of massless leptons.

Now, having shown that the amplitude of the sequential decay $B \to K^*V^*(\to \mu^+\mu^-)$ can be expressed in terms of seven transversity amplitudes, it is clear that this is true for all contributions of the operators $\mathcal{O}_7^{(\prime)}$, $\mathcal{O}_9^{(\prime)}$ and $\mathcal{O}_{10}^{(\prime)}$ to the decay $B \to K^*(\to K\pi)\mu^+\mu^-$, regardless of whether they originate from virtual gauge boson exchange (i.e. photon or Z penguin diagrams) or from box diagrams.

However, this argument does not hold for transitions mediated not by a vector, but a scalar and pseudoscalar operator. Inspecting eqs. (4.8) and (4.43), one can see that the combination $(\mathcal{O}_P - \mathcal{O}'_P)$ can be absorbed into the transversity amplitude A_t, because it couples to axial-vector currents, just like the timelike component of a virtual gauge boson; But this is *not* possible for the scalar operators $\mathcal{O}_S^{(\prime)}$. Therefore, the inclusion of scalar operators in the decay $B \to K^*(\to K\pi)\mu^+\mu^-$ requires the

[1] Unlike sometimes stated in the literature, A_t does not correspond to a timelike polarization of the K^* meson. As mentioned above, the K^* decays on the mass shell and thus has only three polarization states.

introduction of a an additional, "scalar" transversity amplitude, which we denote A_S.

To summarize, the treatment of the decay $B \to K^*(\to K\pi)\mu^+\mu^-$ by decomposition of the amplitude into seven transversity amplitudes $A_{\perp,\parallel,0}^{L,R}$ and A_t is sufficient as long as the operators $\mathcal{O}_{7,9,10}^{(\prime)}$ and $\mathcal{O}_P^{(\prime)}$ are considered, but has to be supplemented by an additional, eighth transversity amplitude A_S once contributions from scalar operators are taken into account.

Finally, the explicit form of the eight transversity amplitudes (without the non-factorizable corrections mentioned in section 4.1.3) reads

$$\begin{aligned}
A_{\perp L,R} &= N\sqrt{2}\lambda^{1/2}\Bigg[\left[(C_9^{\text{eff}} + C_9^{\text{eff}\prime}) \mp (C_{10}^{\text{eff}} + C_{10}^{\text{eff}\prime})\right]\frac{V(q^2)}{m_B + m_{K^*}} \\
&\quad + \frac{2m_b}{q^2}(C_7^{\text{eff}} + C_7^{\text{eff}\prime})T_1(q^2)\Bigg], \qquad (4.44)\\
A_{\parallel L,R} &= -N\sqrt{2}(m_B^2 - m_{K^*}^2)\Bigg[\left[(C_9^{\text{eff}} - C_9^{\text{eff}\prime}) \mp (C_{10}^{\text{eff}} - C_{10}^{\text{eff}\prime})\right]\frac{A_1(q^2)}{m_B - m_{K^*}} \\
&\quad + \frac{2m_b}{q^2}(C_7^{\text{eff}} - C_7^{\text{eff}\prime})T_2(q^2)\Bigg], \qquad (4.45)\\
A_{0L,R} &= -\frac{N}{2m_{K^*}\sqrt{q^2}}\Bigg\{\left[(C_9^{\text{eff}} - C_9^{\text{eff}\prime}) \mp (C_{10}^{\text{eff}} - C_{10}^{\text{eff}\prime})\right] \\
&\quad \times \left[(m_B^2 - m_{K^*}^2 - q^2)(m_B + m_{K^*})A_1(q^2) - \lambda\frac{A_2(q^2)}{m_B + m_{K^*}}\right] \\
&\quad + 2m_b(C_7^{\text{eff}} - C_7^{\text{eff}\prime})\left[(m_B^2 + 3m_{K^*}^2 - q^2)T_2(q^2) - \frac{\lambda}{m_B^2 - m_{K^*}^2}T_3(q^2)\right]\Bigg\}, \qquad (4.46)\\
A_t &= \frac{N}{\sqrt{q^2}}\lambda^{1/2}\left[2(C_{10}^{\text{eff}} - C_{10}^{\text{eff}\prime}) + \frac{q^2}{2m_\mu}(C_P - C_P')\right]A_0(q^2), \qquad (4.47)\\
A_S &= -N\lambda^{1/2}(C_S - C_S')A_0(q^2), \qquad (4.48)
\end{aligned}$$

where

$$N = V_{tb}V_{ts}^*\left[\frac{G_F^2\alpha^2}{3\cdot 2^{10}\pi^5 m_B^3}q^2\lambda^{1/2}\beta_\mu\right]^{1/2}, \qquad (4.49)$$

with $\beta_\mu = \sqrt{1 - 4m_\mu^2/q^2}$ and $\lambda = \lambda(m_B^2, m_{K^*}^2, q^2)$, with the function

$$\lambda(a,b,c) = a^2 + b^2 + c^2 - 2(ab + bc + ac)\,. \qquad (4.50)$$

4.2.3 Differential decay distribution and angular coefficients

With an on-shell K^*, the four-fold differential decay distribution for $\bar{B}^0 \to \bar{K}^{*0}(\to K^-\pi^+)\mu^+\mu^-$ reads:

$$\frac{d^4\Gamma}{dq^2\, d\cos\theta_l\, d\cos\theta_{K^*}\, d\phi} = \frac{9}{32\pi} I(q^2, \theta_l, \theta_{K^*}, \phi)\,, \tag{4.51}$$

where

$$\begin{aligned} I(q^2, \theta_l, \theta_{K^*}, \phi) = {} & I_1^s \sin^2\theta_{K^*} + I_1^c \cos^2\theta_{K^*} + (I_2^s \sin^2\theta_{K^*} + I_2^c \cos^2\theta_{K^*})\cos 2\theta_l \\ & + I_3 \sin^2\theta_{K^*}\sin^2\theta_l \cos 2\phi + I_4 \sin 2\theta_{K^*}\sin 2\theta_l \cos\phi \\ & + I_5 \sin 2\theta_{K^*}\sin\theta_l \cos\phi \\ & + (I_6^s \sin^2\theta_{K^*} + I_6^c \cos^2\theta_{K^*})\cos\theta_l + I_7 \sin 2\theta_{K^*}\sin\theta_l \sin\phi \\ & + I_8 \sin 2\theta_{K^*}\sin 2\theta_l \sin\phi + I_9 \sin^2\theta_{K^*}\sin^2\theta_l \sin 2\phi\,. \end{aligned} \tag{4.52}$$

The corresponding expression for the CP-conjugated mode $B^0 \to K^{*0}(\to K^+\pi^-)\mu^+\mu^-$ is

$$\frac{d^4\bar{\Gamma}}{dq^2\, d\cos\theta_l\, d\cos\theta_{K^*}\, d\phi} = \frac{9}{32\pi} \bar{I}(q^2, \theta_l, \theta_{K^*}, \phi)\,. \tag{4.53}$$

The function $\bar{I}(q^2, \theta_l, \theta_{K^*}, \phi)$ is obtained from (4.52) by the replacements [116]

$$I^{(a)}_{1,2,3,4,7} \longrightarrow \bar{I}^{(a)}_{1,2,3,4,7}\,, \qquad I^{(a)}_{5,6,8,9} \longrightarrow -\bar{I}^{(a)}_{5,6,8,9}\,, \tag{4.54}$$

where $\bar{I}_i^{(a)}$ equals $I_i^{(a)}$ with all weak phases conjugated.

The angular coefficients I_i in (4.52) can be written in terms of the transversity amplitudes as

$$I_1^s = \frac{(2+\beta_\mu^2)}{4}\left[|A_\perp^L|^2 + |A_\parallel^L|^2 + (L\to R)\right] + \frac{4m_\mu^2}{q^2}\mathrm{Re}\left(A_\perp^L A_\perp^{R*} + A_\parallel^L A_\parallel^{R*}\right), \tag{4.55}$$

$$I_1^c = |A_0^L|^2 + |A_0^R|^2 + \frac{4m_\mu^2}{q^2}\left[|A_t|^2 + 2\mathrm{Re}(A_0^L A_0^{R*})\right] + \beta_\mu^2 |A_S|^2, \tag{4.56}$$

$$I_2^s = \frac{\beta_\mu^2}{4}\left[|A_\perp^L|^2 + |A_\parallel^L|^2 + (L\to R)\right], \tag{4.57}$$

$$I_2^c = -\beta_\mu^2\left[|A_0^L|^2 + (L\to R)\right], \tag{4.58}$$

$$I_3 = \frac{1}{2}\beta_\mu^2\left[|A_\perp^L|^2 - |A_\parallel^L|^2 + (L\to R)\right], \tag{4.59}$$

$$I_4 = \frac{1}{\sqrt{2}}\beta_\mu^2\left[\mathrm{Re}(A_0^L A_\parallel^{L*}) + (L\to R)\right], \tag{4.60}$$

$$I_5 = \sqrt{2}\beta_\mu\left[\mathrm{Re}(A_0^L A_\perp^{L*}) - (L\to R) - \frac{m_\mu}{\sqrt{q^2}}\,\mathrm{Re}(A_\parallel^L A_S^* + A_\parallel^R A_S^*)\right], \tag{4.61}$$

	$m_\mu = 0$	$m_\mu \neq 0$
SM	18	22
SM + $\mathcal{O}_S^{(\prime)}$	20	24

Table 4.2: Number of independent observables in $B \to K^*(\to K\pi)\mu^+\mu^-$, depending on whether lepton mass effects and/or scalar operators are taken into account.

$$I_6^s = 2\beta_\mu \left[\mathrm{Re}(A_\parallel^L A_\perp^{L\,*}) - (L \to R)\right], \tag{4.62}$$

$$I_6^c = 4\beta_\mu \frac{m_\mu}{\sqrt{q^2}} \mathrm{Re}\left[A_0^L A_S^* + (L \to R)\right], \tag{4.63}$$

$$I_7 = \sqrt{2}\beta_\mu \left[\mathrm{Im}(A_0^L A_\parallel^{L\,*}) - (L \to R) + \frac{m_\mu}{\sqrt{q^2}} \mathrm{Im}(A_\perp^L A_S^* + A_\perp^R A_S^*)\right], \tag{4.64}$$

$$I_8 = \frac{1}{\sqrt{2}}\beta_\mu^2 \left[\mathrm{Im}(A_0^L A_\perp^{L\,*}) + (L \to R)\right], \tag{4.65}$$

$$I_9 = \beta_\mu^2 \left[\mathrm{Im}(A_\parallel^{L\,*} A_\perp^L) + (L \to R)\right]. \tag{4.66}$$

4.3 Observables

As discussed in the previous section, the decay $\bar{B}^0 \to \bar{K}^{*0}(\to K^-\pi^+)\mu^+\mu^-$ is completely described in terms of twelve angular coefficient functions $I_i^{(a)}$, which are functions of the dilepton invariant mass squared q^2 and depend on Wilson coefficients, encoding short distance physics from the SM and beyond, as well as on hadronic form factors. The corresponding CP-conjugate mode $B^0 \to K^{*0}(\to K^+\pi^-)\mu^+\mu^-$ gives access to twelve additional observables, the CP-conjugate angular coefficient functions $\bar{I}_i^{(a)}$.

These 24 functions represent the complete set of observables that can be accessed in this decay, with an on-shell intermediate K^*, in the SM and any extension described by the effective Hamiltonian (4.1)–(4.8).

In certain limits, not all of these observables are independent. In the limit of massless leptons, the relations $I_1^s = 3I_2^s$ and $I_1^c = -I_2^c$ hold (and the corresponding relations for the barred coefficients), as can be seen from eqs. (4.55)–(4.58). In the SM, I_6^c vanishes since it is only nonzero if scalar operators are present *and* lepton mass effects are taken into account. The numbers of independent observables in these limits are summarized in table 4.2.

4.3.1 Symmetries and asymmetries

Although the angular coefficient functions $I_i^{(a)}$ and their CP-conjugate counterparts $\bar{I}_i^{(a)}$ form a complete basis of observables and have a clear connection to experiment,

it is useful to choose a different basis for two reasons. First, the $I_i^{(a)}$ and $\bar{I}_i^{(a)}$ are very similar in the SM since they coincide in the limit of exact CP. It therefore makes more sense to separate CP violating and CP conserving effects by considering sums and differences of $I_i^{(a)}$ and $\bar{I}_i^{(a)}$. Second, the angular coefficients are plagued by large theoretical uncertainties due to the form factors, with particularly large uncertainties on the overall normalization of these form factors. Therefore, it is advantageous to consider only ratios of angular coefficients, where such uncertainties cancel to a large extent.

One thus defines CP-averaged angular coefficient functions, normalized to the CP-averaged differential decay distribution,

$$S_i^{(a)} = \left(I_i^{(a)} + \bar{I}_i^{(a)}\right) \Big/ \frac{d(\Gamma + \bar{\Gamma})}{dq^2}\,, \tag{4.67}$$

as well as the corresponding normalized CP asymmetries

$$A_i^{(a)} = \left(I_i^{(a)} - \bar{I}_i^{(a)}\right) \Big/ \frac{d(\Gamma + \bar{\Gamma})}{dq^2}\,. \tag{4.68}$$

Analogously to the situation for angular coefficients discussed above, the $S_i^{(a)}$ and $A_i^{(a)}$ fulfill the conditions $S_1^s = 3S_2^s$, $S_1^c = -S_2^c$ and $A_1^s = 3A_2^s$, $A_1^c = -A_2^c$ in the limit of massless leptons, and S_6^c and A_6^c vanish in the SM. In addition, even for non-zero lepton mass, only three of the four $S_{1,2}^{s,c}$ are independent, which can be seen as follows. The dilepton mass distribution can be expressed in terms of angular coefficients as

$$\frac{d\Gamma}{dq^2} = \frac{3}{4}(2\,I_1^s + I_1^c) - \frac{1}{4}(2\,I_2^s + I_2^c). \tag{4.69}$$

Therefore, due to the normalization (4.67), there is the relation

$$\frac{3}{4}(2\,S_1^s + S_1^c) - \frac{1}{4}(2\,S_2^s + S_2^c) = 1. \tag{4.70}$$

Consequently, the complete set of 24 independent observables (cf. table 4.2) would be given by the twelve $A_i^{(a)}$, eleven $S_i^{(a)}$ and the CP-averaged dilepton mass distribution $d(\Gamma + \bar{\Gamma})/dq^2$. However, the latter is the only observable for which the normalization of the form factors is relevant, so theoretically it is not as clean.

For some observables it is useful to consider their q^2 average. One defines

$$\left\langle S_i^{(a)} \right\rangle = \int_{1\,\mathrm{GeV}^2}^{6\,\mathrm{GeV}^2} dq^2 \left(I_i^{(a)} + \bar{I}_i^{(a)}\right) \Big/ \int_{1\,\mathrm{GeV}^2}^{6\,\mathrm{GeV}^2} dq^2 \frac{d(\Gamma + \bar{\Gamma})}{dq^2}\,, \tag{4.71}$$

$$\left\langle A_i^{(a)} \right\rangle = \int_{1\,\mathrm{GeV}^2}^{6\,\mathrm{GeV}^2} dq^2 \left(I_i^{(a)} - \bar{I}_i^{(a)}\right) \Big/ \int_{1\,\mathrm{GeV}^2}^{6\,\mathrm{GeV}^2} dq^2 \frac{d(\Gamma + \bar{\Gamma})}{dq^2}\,. \tag{4.72}$$

4.3.2 Relation to other observables

Since the observables defined in the previous section form a complete basis for the angular distribution of $\bar{B}^0 \to \bar{K}^{*0}(\to K^-\pi^+)\mu^+\mu^-$ and its CP-conjugate counterpart, well-known observables like the forward backward-asymmetry can be expressed in terms of the $S_i^{(a)}$ and $A_i^{(a)}$. For example, the CP asymmetry in the dilepton mass distribution is given by (see eq. (4.70))

$$A_{\rm CP} = \frac{d(\Gamma - \bar{\Gamma})}{dq^2} \Big/ \frac{d(\Gamma + \bar{\Gamma})}{dq^2} = \frac{3}{4}(2\,A_1^s + A_1^c) - \frac{1}{4}(2\,A_2^s + A_2^c), \tag{4.73}$$

the normalized, CP-averaged forward-backward asymmetry as

$$A_{\rm FB} = \left[\int_0^1 - \int_{-1}^0\right] d\cos\theta_l \frac{d^2(\Gamma - \bar{\Gamma})}{dq^2\, d\cos\theta_l} \Big/ \frac{d(\Gamma + \bar{\Gamma})}{dq^2} = \frac{3}{8}(2\,S_6^s + S_6^c). \tag{4.74}$$

The CP average is numerically irrelevant in the SM, but makes the connection to experiment more transparent. This definition is also complementary to the forward-backward CP asymmetry [120],

$$A_{\rm FB}^{\rm CP} = \left[\int_0^1 - \int_{-1}^0\right] d\cos\theta_l \frac{d^2(\Gamma + \bar{\Gamma})}{dq^2\, d\cos\theta_l} \Big/ \frac{d(\Gamma + \bar{\Gamma})}{dq^2} = \frac{3}{8}(2\,A_6^s + A_6^c). \tag{4.75}$$

Additional well-established observables are the K^* longitudinal and transverse polarization fractions F_L, F_T, which can be written as

$$F_L = -S_2^c, \qquad F_T = 4S_2^s, \tag{4.76}$$

implying the well-known relation $F_T = 1 - F_L$ as a consequence of eq. (4.70) in the limit of vanishing lepton mass.

In Refs. [115, 119], the transverse asymmetries $A_T^{(i)}$ were introduced. They can be expressed in terms of CP-averaged observables as

$$A_T^{(2)} = \frac{S_3}{2\,S_2^s}, \tag{4.77}$$

$$A_T^{(3)} = \left(\frac{4\,S_4^2 + S_7^2}{-2\,S_2^c\,(2\,S_2^s + S_3)}\right)^{1/2}, \tag{4.78}$$

$$A_T^{(4)} = \left(\frac{S_5^2 + 4\,S_8^2}{4\,S_4^2 + S_7^2}\right)^{1/2}. \tag{4.79}$$

Experimentally, the $S_i^{(a)}$ and $A_i^{(a)}$ can be extracted from the angular decay distribution by means of a full angular fit. Analogously to eqs. (4.51)–(4.52), the angular distribution of $d^4(\Gamma + \bar{\Gamma})$ and $d^4(\Gamma - \bar{\Gamma})$, normalized to the CP-averaged dilepton invariant mass distribution, can be written in terms of the $S_i^{(a)}$ and $A_i^{(a)}$, where, due

to eq. (4.54), the CP-averaged decay distribution $d^4(\Gamma + \bar{\Gamma})$ gives access to $S^{(a)}_{1,2,3,4,7}$ and $A^{(a)}_{5,6,8,9}$, while the remaining observables can be obtained from $d^4(\Gamma - \bar{\Gamma})$.

While a full angular analysis requires large statistics, one-dimensional angular distributions are accessible already at B factories. The one-dimensional distributions in the three kinematical angles read

$$\frac{d(\Gamma+\bar{\Gamma})}{d\theta_l\, dq^2}\bigg/\frac{d(\Gamma+\bar{\Gamma})}{dq^2} = \frac{1}{2} + \frac{1}{4}(S_2^c + 2S_2^s)\left(3\cos^2\theta_l - 1\right) + \frac{3}{8}(A_6^c + 6A_6^s)\cos\theta_l\,, \tag{4.80}$$

$$\frac{d(\Gamma+\bar{\Gamma})}{d\theta_{K^*}\, dq^2}\bigg/\frac{d(\Gamma+\bar{\Gamma})}{dq^2} = \frac{3}{16}(3S_1^c - S_2^c)\left(3\cos^2\theta_{K^*} - 1\right) + \frac{3}{4}\left(1 + \cos^2\theta_{K^*}\right)\,, \tag{4.81}$$

$$\frac{d(\Gamma+\bar{\Gamma})}{d\phi\, dq^2}\bigg/\frac{d(\Gamma+\bar{\Gamma})}{dq^2} = \frac{1}{2\pi}\left[1 + S_3\cos(2\phi) + A_9\sin(2\phi)\right]\,. \tag{4.82}$$

In the limit of massless leptons, one can replace

$$(S_2^c + 2S_2^s) \to (1 + 3S_2^c)/2 = (1 - 3F_L)/2 \tag{4.83}$$

$$\text{and}\quad (3S_1^c - S_2^c) \to -4S_2^c = 4F_L \tag{4.84}$$

in eqs. (4.80) and (4.81).

Experimental results for the one-dimensional angular distributions in θ_l and θ_{K^*} have already been presented by the B factories and will be confronted with the corresponding SM predictions in the next section.

4.4 $B \to K^*\mu^+\mu^-$ in the Standard Model

In this section, the predicitions for the $B \to K^*(\to K\pi)\mu^+\mu^-$ angular observables defined above will be presented. These predictions have been published in [112].

4.4.1 Inputs and uncertainties

The dominant uncertainty in most observables stems from the form factors; however, these uncertainties are strongly reduced if only ratios of angular coefficients are considered, as discussed in section 4.3.1. To estimate these uncertainties, three sets of form factors, obtained with different values of the Borel parameter and continuum threshold as discussed in [112], where used. In addition to form factor uncertainties, the renormalization-scale uncertainty is found by varying μ between 4.0 and 5.6 GeV, where μ is the scale at which the Wilson coefficients, α_s and the $\overline{\text{MS}}$ masses are evaluated; the ratio is varied m_c/m_b between 0.25 and 0.33; and the CKM angle γ is varied between 60° and 80°. Finally, several hadronic parameters entering the non-factorizable corrections, afflicted with sizable uncertainties, have to be varied; their values and uncertainties used in the numerical analyis can be found in [112].

Obs.	S_4	S_5	S_6^s
q_0^2 [GeV^2]	$1.94^{+0.12}_{-0.10}$	$2.24^{+0.06}_{-0.08}$	$3.90^{+0.11}_{-0.12}$

Table 4.3: Predictions for the zero positions $q_0^2(S_i^{(a)})$ of S_4, S_5 and S_6^s in the SM.

Obs.	$10^{-2}\times$	Obs.	$10^{-2}\times$
$\langle S_1^s \rangle$	$16.0^{+0.6}_{-0.6}$	$\langle S_5 \rangle$	$-14.2^{+0.8}_{-1.2}$
$\langle S_1^c \rangle$	$79.3^{+0.8}_{-0.8}$	$\langle S_6^s \rangle$	$3.5^{+0.8}_{-1.1}$
$\langle S_2^s \rangle$	$5.3^{+0.2}_{-0.2}$	$\langle S_7 \rangle$	$4.8^{+1.7}_{-1.7}$
$\langle S_2^c \rangle$	$-76.6^{+0.7}_{-0.7}$	$\langle S_8 \rangle$	$-1.5^{+0.6}_{-0.6}$
$\langle S_3 \rangle$	$-0.3^{+0.4}_{-0.3}$	$\langle S_9 \rangle$	$0.1^{+0.1}_{-0.1}$
$\langle S_4 \rangle$	$10.1^{+1.0}_{-1.2}$		

Obs.	$10^{-3}\times$	Obs.	$10^{-3}\times$
$\langle A_1^s \rangle$	$-0.2^{+0.2}_{-0.1}$	$\langle A_5 \rangle$	$-5.7^{+0.6}_{-0.5}$
$\langle A_1^c \rangle$	$6.3^{+0.7}_{-0.8}$	$\langle A_6^s \rangle$	$-4.5^{+0.5}_{-0.4}$
$\langle A_2^s \rangle$	$-0.1^{+0.1}_{-0.0}$	$\langle A_7 \rangle$	$3.4^{+0.4}_{-0.5}$
$\langle A_2^c \rangle$	$-6.1^{+0.7}_{-0.6}$	$\langle A_8 \rangle$	$-2.6^{+0.4}_{-0.3}$
$\langle A_3 \rangle$	$-0.1^{+0.1}_{-0.1}$	$\langle A_9 \rangle$	$0.1^{+0.1}_{-0.1}$
$\langle A_4 \rangle$	$1.5^{+0.2}_{-0.2}$	$\langle A_{\rm CP} \rangle$	$5.9^{+0.6}_{-0.6}$

Table 4.4: Predictions for the integrated CP-averaged angular coefficients $\langle S_i^{(a)} \rangle$ (in units of 10^{-2}) and the integrated CP asymmetries $\langle A_i^{(a)} \rangle$ (in units of 10^{-3}) in the SM.

4.4.2 SM predictions

Figure 4.3 shows the SM predictions for the CP-averaged angular coefficients $S_i^{(a)}$. S_1^s and S_1^c have been omitted since the relations $S_1^s = 3S_2^s$ and $S_1^c = -S_2^c$ are fulfilled up to lepton-mass effects, which amount to at most 1%. $S_{1,2}^{s,c}$ are numerically large; S_4, S_5, S_6^s are similar in magnitude, but are particularly interesting as they each have a zero in q^2. All these observables are seen to have small theory uncertainties, since the normalization results in a cancellation of hadronic uncertainties. Table 4.3 shows the SM predictions for the positions of the zeros of S_4, S_5 and S_6^s. S_3 is numerically small in the SM since it is approximately proportional to the chirality-flipped Wilson coefficient C_7', which is suppressed by a factor m_s/m_b. S_7, S_8 and S_9 are small as well and have a larger error-band as they arise from the imaginary part of the transversity amplitudes. The q^2-integrated $\langle S_i^{(a)} \rangle$ are shown in table 4.4. The last row of fig. 4.3 also shows the CP averaged dilepton mass distribution $d(\Gamma + \bar{\Gamma})/dq^2$ and the observables $A_T^{(3)}$ and $A_T^{(4)}$ defined in [115], which can be related to the observables used here by means of eqs. (4.78) and (4.79).

The corresponding SM predictions for the CP asymmetries are shown in figure 4.4 (again except for $A_1^{s,c}$). In the last row, also the CP asymmetry in the decay distribution, $A_{\rm CP}$ (cf. (4.73)) is shown.

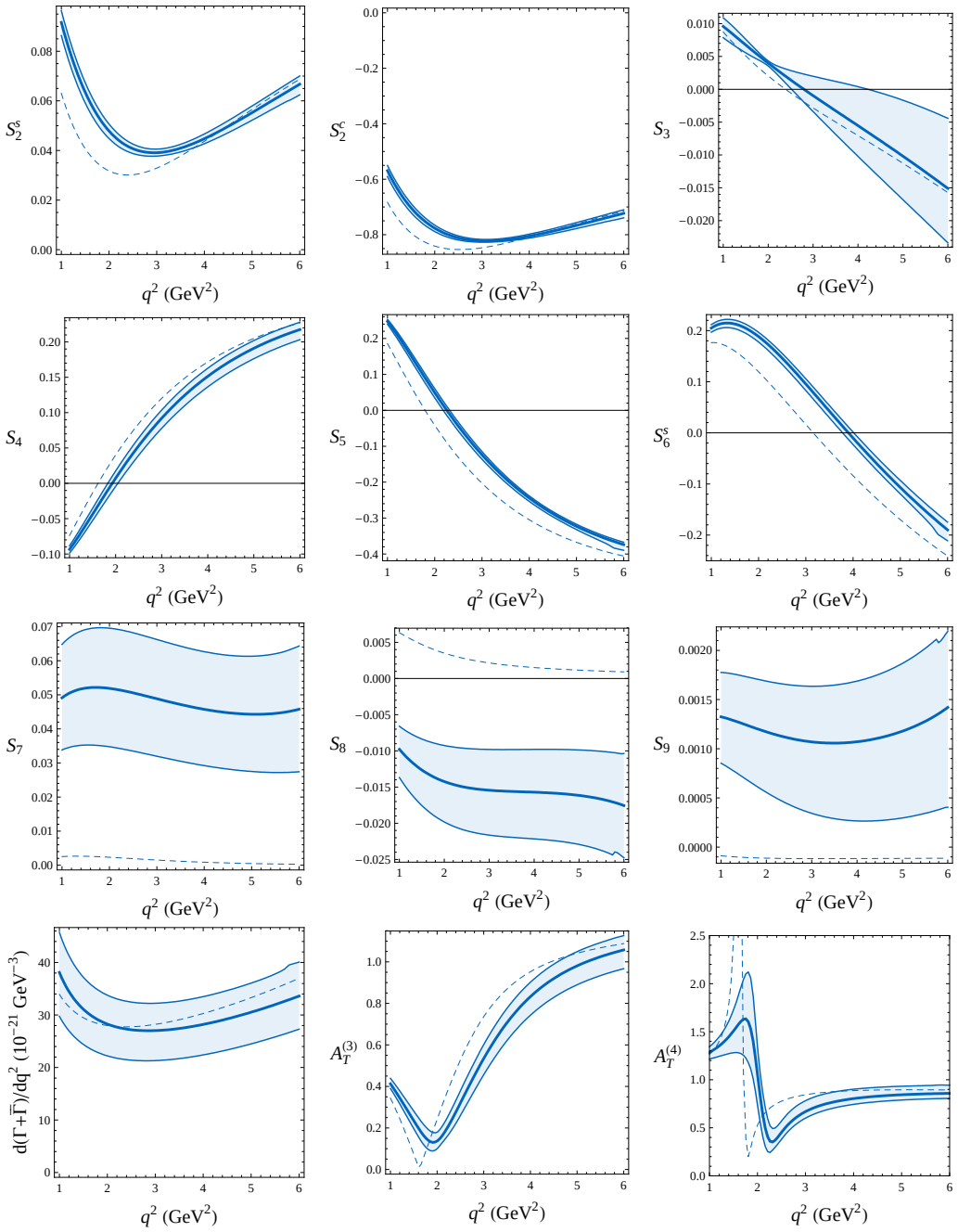

Figure 4.3: CP-averaged angular coefficients $S_i^{(a)}$, CP-averaged dilepton mass distribution $d(\Gamma + \bar{\Gamma})/dq^2$ and transverse asymmetries $A_T^{(3,4)}$ in the SM as a function of q^2. The dashed lines are the leading-order (LO) contributions, obtained in naive factoriation. The thick solid lines are the full next-to-leading order (NLO) predictions from QCD factorization (QCDF).

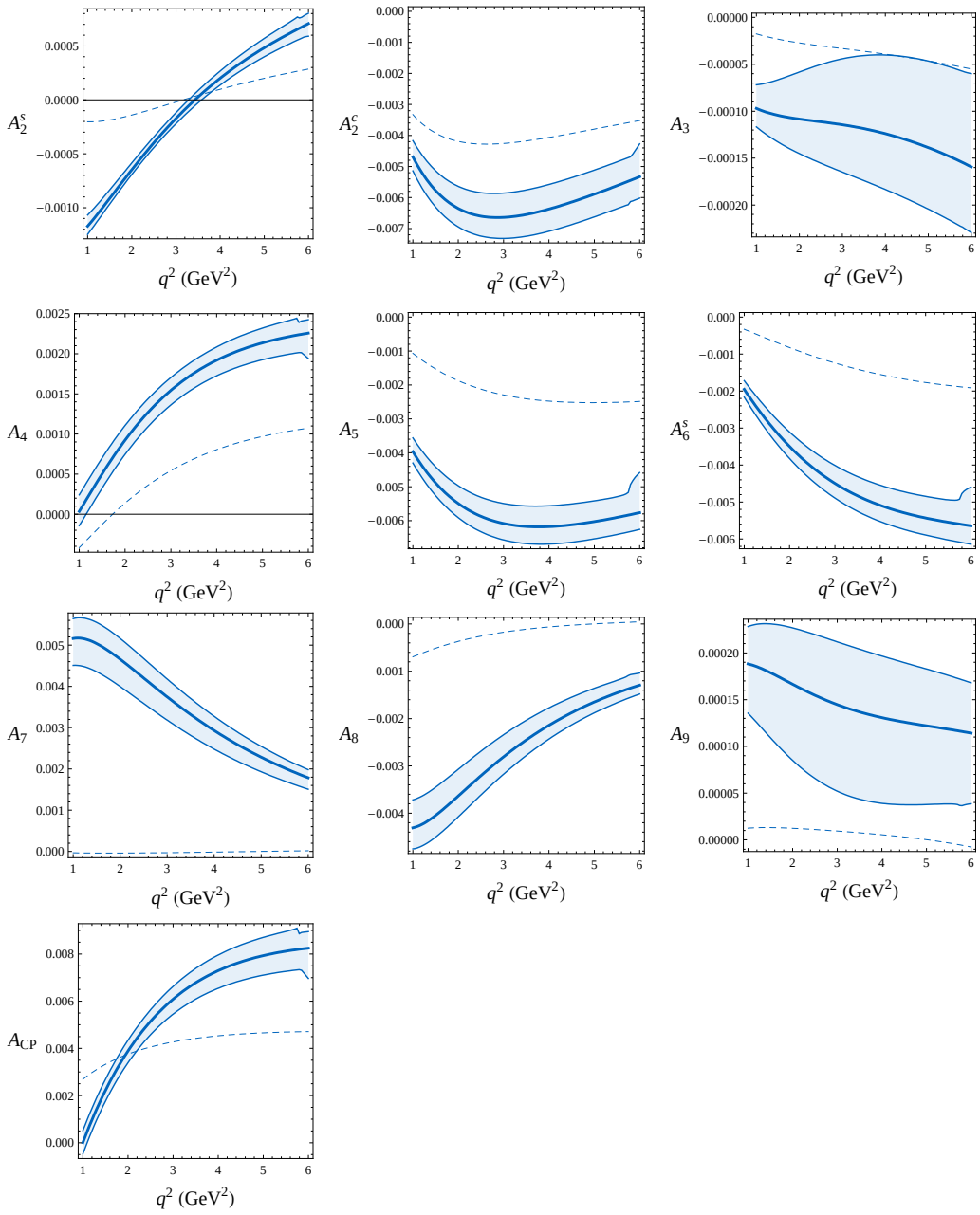

Figure 4.4: CP asymmetries $A_i^{(a)}$ and $A_{\rm CP}$ in the SM as a function of q^2. The meaning of the curves and bands is as in Fig. 4.3.

4.4.3 Confrontation with experiment

Experimental results on one-dimensional angular distributions of $B \to K^*(\to K\pi)\ell^+\ell^-$ have been published by the BaBar [121], Belle [122] and CDF [123] collaborations. Due to the limited statistics in all three experiments (384×10^6 $B\bar{B}$ events at BaBar, 657×10^6 at Belle[2] and an integrated luminosity of 4.4 fb^{-1} at CDF), quite large q^2 bins were used. Unfortunately, the low q^2 bin is chosen to extend down to 0.1 GeV^2 in the BaBar analysis, which makes it difficult to compare to the theory results shown here due to the possible contributions from low lying resonances mentioned above.

The Belle and CDF analyses give the results for the observables $F_L = -S_2^c$, $A_{\rm FB} = 3S_6^s/4$ (assuming S_6^c to be negligible) and for the branching ratio. The Belle collaboration additionally measures the isospin asymmetry

$$A_I = \frac{(\tau_{B^+}/\tau_{B^0}) \times \mathrm{BR}(K^{*0}\ell^+\ell^-) - \mathrm{BR}(K^{*\pm}\ell^+\ell^-)}{(\tau_{B^+}/\tau_{B^0}) \times \mathrm{BR}(K^{*0}\ell^+\ell^-) + \mathrm{BR}(K^{*\pm}\ell^+\ell^-)} \,. \tag{4.85}$$

A_I vanishes in the limit of naive factorization, so it is quite hard to estimate theoretically in view of unknown power suppressed corrections to QCD factorization. The branching ratio is also of limited use since the overall normalization of the form factors, and thus the amplitude, is still plagued by sizable uncertainties.

An interesting point is that the CP asymmetry A_9 and the CP averaged S_3, which are both tiny in the SM but can be greatly enhanced in presence of NP in right-handed currents, could be extracted from a one-dimensional angular distribution in the angle ϕ, see eq. (4.82). No experimental results on this distribution have been published so far.

The q^2 bins in the Belle analysis which can be directly compared to the SM predictions are the $[1, 6]$ GeV^2 bin and the $[2, 4.3]$ GeV^2 bin. The latter bin is also present in the CDF analysis. The corresponding results for $\langle S_2^c \rangle$ and $\langle S_6^s \rangle$ are compared to the SM predictions in figures 4.5 and 4.6, respectively.

4.5 New Physics sensitivity

4.5.1 General considerations

New physics enters the $B \to K^*\ell^+\ell^-$ observables by modifying the Wilson coeffcients of the operators $\mathcal{O}^{(\prime)}_{7\ldots10,S,P}$ in (4.6)–(4.8). The sensitivity of the 24 observables to these Wilson coefficients is diverse, and not all of them are equally interesting as probes of NP.

[2]To relate the number of $B\bar{B}$ events $N_{B\bar{B}}$ at B factories to their integrated luminosity $\mathcal{L}$, note that $N_{B\bar{B}} = \mathcal{L}\sigma_{b\bar{b}}$, and the cross section for the process $e^+e^- \to \Upsilon(4S) \to B\bar{B}$ at a center of mass energy of 10.58 GeV (the $\Upsilon(4S)$ pole) is $\sigma_{b\bar{b}} = 1.10$ nb [124].

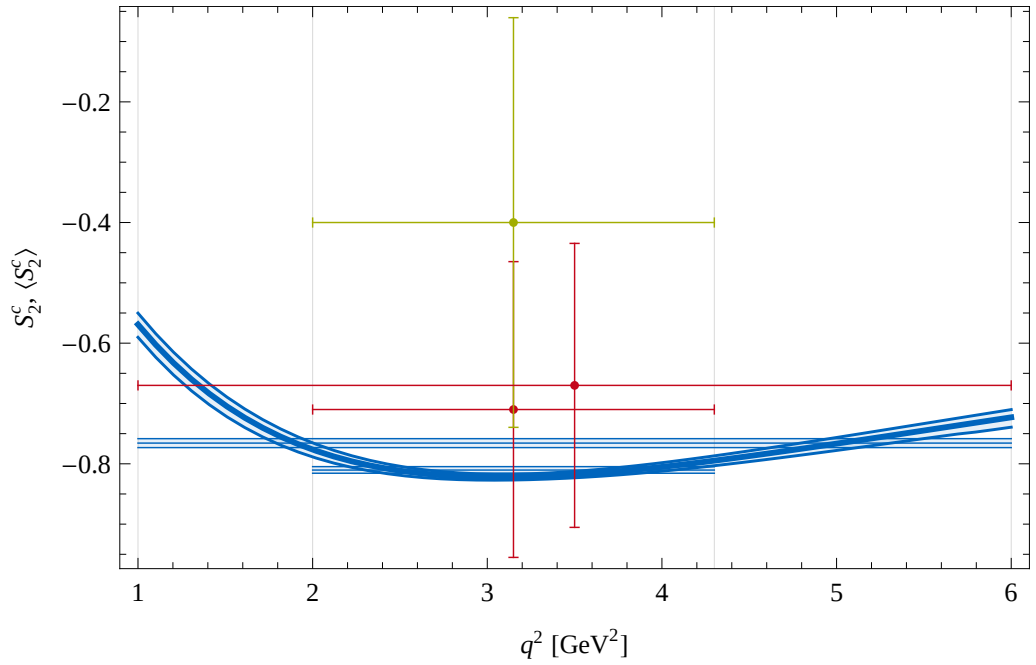

Figure 4.5: Predictions for $\langle S_2^c \rangle$ in the SM for the q^2 bins $[1, 6]$ GeV^2 and $[2, 4.3]$ GeV^2 (blue horizontal bands) compared to the corresponding experimental measurements at Belle [122] (red error bars) and CDF [123] (green error bar), superimposed on the SM prediction of $S_2^c(q^2)$.

Concerning the scalar and pseudoscalar operators, it turns out that $C_P^{(\prime)}$ are numerically irrelevant, while the combination $C_S - C_S'$ can in principle be accessed in the observable S_6^c. These issues will be discussed in detail in section 4.5.2.

Among the other CP averaged angular coefficients, the observables $S_{3,4,5}$, $S_6^c \approx \frac{4}{3} A_{\rm FB}$ and $S_2^c = -F_L$ are particularly interesting (note that in the limit of massless leptons, $S_1^{s,c}$ and S_2^s are not independent observables). S_3 is proportional to C_7' at leading order [125] and is thus a very sensitive probe of right-handed currents. S_4, S_5 and S_6^s each have a zero in q^2 in the SM, but the position of this zero can be modified (or removed) in the presence of NP. $S_{7,8,9}$ are less interesting since they depend on the imaginary parts of the transversity amplitudes, see (4.64)–(4.66), and are zero in the limit of naive factorization. Thus, they are plagued by large uncertainties and are weakly sensitive to new physics.

On the other hand, the CP asymmetries $A_{7,8,9}$ are strongly sensitive to NP. This can be understood by noting that they are odd under a naive time reversal transformation and not suppressed by small strong phases as is discussed in [126]. Similarly to S_3, A_9 requires right-handed currents to be nonvanishing and it can be extracted from the one-dimensional angular distribution in the angle ϕ, see (4.82). Therefore, S_3 and A_9 could in principle already be constrained by current B factory and

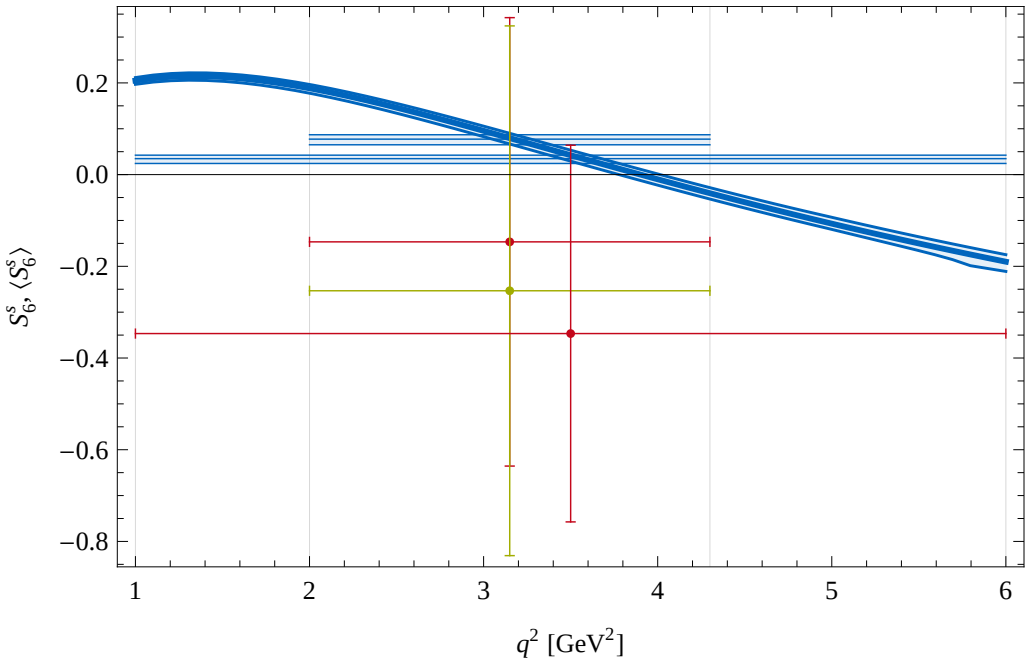

Figure 4.6: Predictions for $\langle S_6^s \rangle$ in the SM for the q^2 bins $[1, 6]$ GeV^2 and $[2, 4.3]$ GeV^2 (blue horizontal bands) compared to the corresponding experimental measurements at Belle [122] (red error bars) and CDF [123] (green error bar), superimposed on the SM prediction of $S_6^s(q^2)$.

Tevatron experiments.

Table 4.5 summarizes the main dependencies of the most interesting observables on the Wilson coefficients.

4.5.2 Impact of scalar currents

In section 4.2.2, it was shown that the scalar and pseudoscalar operators $\mathcal{O}_{S,P}^{(\prime)}$ only have an impact on the angular distribution of $B \to K^*(\to K\pi)\mu^+\mu^-$ if lepton-mass effects are taken into account. In particular, there are two new observables, S_6^c and A_6^c, which are proportional to the difference $(C_S - C_S')$ of the Wilscon coefficients of the scalar operator and its chirality-flipped counterpart. The aim of this section is to investigate the allowed room for new physics in the Wilson coefficients $C_{S,P}^{(\prime)}$ and the possible impact on the $B \to K^*(\to K\pi)\mu^+\mu^-$ observables.

The most stringent constraint on the Wilson coefficients $C_{S,P}^{(\prime)}$ comes from the measurement of $B_s \to \mu^+\mu^-$, which was discussed in section 2.2.2. Considering the experimental bound in Eq. (2.16), the formulae (2.17)–(2.18) imply the approximate bounds

$$|C_S - C_S'| \lesssim 0.12 \text{ GeV}^{-1}, \qquad -0.09 \text{ GeV}^{-1} \lesssim C_P - C_P' \lesssim 0.15 \text{ GeV}^{-1}, \tag{4.86}$$

Observable	mostly affected by
$S_{1,2}^{s,c}$	$C_7^{(\prime)}$, $C_9^{(\prime)}$, $C_{10}^{(\prime)}$
S_3	C_7', C_9', C_{10}'
S_4	$C_7^{(\prime)}$, $C_{10}^{(\prime)}$
S_5	$C_7^{(\prime)}$, C_9, C_{10}'
S_6^s	C_7, C_9
A_7	$C_7^{(\prime)}$, $C_{10}^{(\prime)}$
A_8	$C_7^{(\prime)}$, $C_9^{(\prime)}$, C_{10}'
A_9	C_7', C_9', C_{10}'
S_6^c	$C_S - C_S'$

Table 4.5: The most interesting angular observables in $B \to K^*\mu^+\mu^-$ and the Wilson coefficients they are most sensitive to.

barring large NP contributions to the Wilson coefficients $C_{10}^{(\prime)}$.

Now, inspecting the formulae for the angular coefficients, Eqs. (4.55)–(4.66), one can see that the only terms in which $C_S^{(\prime)}$ and $C_P^{(\prime)}$ are not suppressed by the lepton mass enter in the angular coefficient I_1^c. However, due to the small size of the Wilson coefficients themselves, see (4.86), these terms turn out to be numerically irrelevant in general once the bound from $B_s \to \mu^+\mu^-$ is taken into account.

Since the pseudoscalar operators do not contribute to any other angular coefficient, this implies that they are indeed irrelevant in the phenomenological study of $B \to K^*(\to K\pi)\mu^+\mu^-$. For the scalar operators, however, the situation is different, because of the new angular coefficient I_6^c, Eq. (4.62), which is directly proportional to the real part of $(C_S - C_S')$ and thus vanishes in the SM. So, although numerically small, this angular coefficient is an appealing observable because any measurement of a non-zero value would constitute an unambiguous signal of scalar currents at work.

This is in contrast to the process $B_s \to \mu^+\mu^-$, where a large enhancement of the branching ratio compared to the SM could be caused by both scalar and pseudoscalar currents. In addition, the measurement of a non-zero S_6^c (the CP-averaged counterpart of I_6^c) would allow to determine the sign of $\mathrm{Re}(C_S - C_S')$. In fact, by a combined study of $B_s \to \mu^+\mu^-$ and the observable S_6^c, one would be able to constrain the relative sizes of the scalar and pseudoscalar Wilson coefficients, which can serve to distinguish different models of NP. For example, in the MSSM, the ratio of C_S and C_P is

$$\frac{C_P}{C_S} \approx -\frac{M_{A^0}^2}{M_{H^0}^2} \approx -1 \tag{4.87}$$

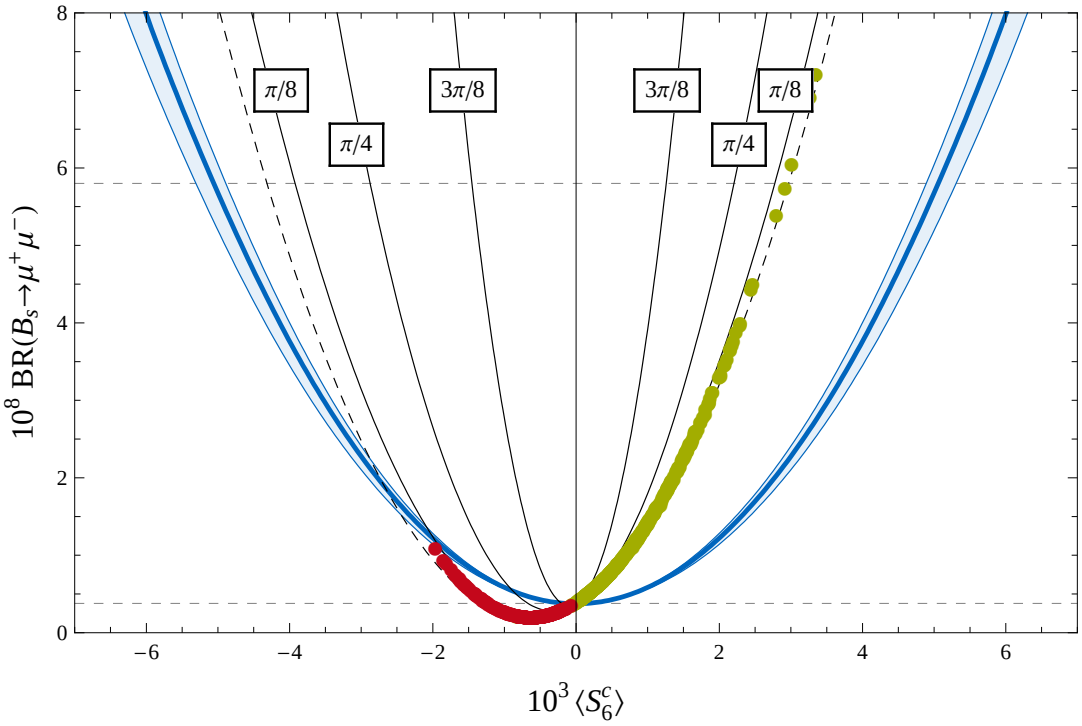

Figure 4.7: Correlation between the observable $\langle S_6^c \rangle$ and the branching ratio of $B_s \to \mu^+\mu^-$. The blue band is obtained by assuming NP contributions only to the Wilson coefficient C_S, the black curves (where error bars are omitted) by assuming $C_P = -C_S$. Different values of the phase $\mathrm{Arg}(C_S)$ are indicated. The red and green dots correspond to points in the CMSSM as described in the text. The horizontal dashed lines indicate the SM prediction for $\mathrm{BR}(B_s \to \mu^+\mu^-)$ (2.15) and the current experimental upper bound (2.16).

to a very good accuracy, a relation which could be tested by a measurement of $\mathrm{BR}(B_s \to \mu^+\mu^-)$ and S_6^c.

To illustrate this point, fig. 4.7 shows the correlation between $\mathrm{BR}(B_s \to \mu^+\mu^-)$ and $\langle S_6^c \rangle$ (as defined in Eq. (4.71)). The blue band has been obtained by assuming that NP contributions enter only through C_S, i.e. setting $C_P/C_S = 0$, and varying C_S accordingly; the error band takes into account all the sources of error as discussed in Sec. 4.4.2.

Assuming, in contrast, $C_P/C_S = -1$, as would be the case in the MSSM, one obtains the black dashed parabola. As an illustration, the predictions for parameter points in the constrained MSSM (CMSSM) with large $\tan\beta$ are indicated as red and green dots. These points have been generated by a random scan of the CMSSM

parameters in the ranges

$$m_0 \leq 1\,\text{TeV}, \qquad m_{1/2} \leq 1\,\text{TeV}, \tag{4.88}$$

$$-2m_0 \leq A_0 \leq 2m_0, \qquad 30 \leq \tan\beta \leq 50, \tag{4.89}$$

permitting both signs for the μ-term and discarding points violating existing mass bounds or being incompatible with the measurement of $\text{BR}(B \to X_s\gamma)$. The green dots correspond to $\mu > 0$, the red ones to $\mu < 0$. It can be seen that the CMSSM points lie on the curve corresponding to $C_S = -C_P$ and, in particular for a positive μ parameter, could be clearly distinguished from the scenario without pseudoscalar currents, assuming sufficient experimental accuracy.

Since the observable $\langle S_6^c \rangle$ probes the real part of $(C_S - C_S')$, the correlation gets modified if one allows a phase in C_S. More precisely, $|\langle S_6^c \rangle|$ gets reduced for a fixed value of $\text{BR}(B_s \to \mu^+\mu^-)$. This is illustrated by the black curves corresponding to $C_S = -C_P$, where both Wilson coefficients are now complex, with the respective phase $\text{Arg}(C_S)$ indicated by the labels on the curves. In such a scenario, the measurement of the correlation between $\text{BR}(B_s \to \mu^+\mu^-)$ and $\langle S_6^c \rangle$ would thus directly probe the phase of the scalar Wilson coefficient.

To summarize, while pseudoscalar operators are numerically irrelevant in the decay $B \to K^*(\to K\pi)\mu^+\mu^-$, a study of the angular distribution allows one to probe the scalar sector of a theory beyond the SM, in a way that is theoretically clean and complementary to $B_s \to \mu^+\mu^-$.

4.6 Summary

The decay $B \to K^*\mu^+\mu^-$ gives access to numerous observables that allow to test the SM and to probe for New Physics. The discussion in this chapter concentrated on the construction of a complete basis of observables having a clear relation to the quantities measured in experiment, being as theoretically clean as possible and separating CP violating from CP conserving effects. Two new observables have been presented, which are only nonzero if scalar operators are present and lepton mass effects are taken into account.

While only two of these observables, F_L and A_{FB}, have been measured to date, the LHCb experiment is expected to greatly improve the sensitivity to these observables and to constrain or measure several others (see e.g. [127]). By the end of the decade, also the planned Super B factories might contribute to the measurement of the $B \to K^*\ell^+\ell^-$ angular distribution.

It will be interesting to see whether this decay mode will be able to live up to its potential to distinguish different models of New Physics.

5 B decays with missing energy

$b \to s\nu\bar{\nu}$ transitions are interesting probes of new physics. While they share many similarities with the $b \to s\ell^+\ell^-$ transition discussed in the previous chapter, they probe only a much more limited set of interactions; in the absence of photon or gluon penguin contributions, $b \to s\nu\bar{\nu}$ decays allow to transparentely probe new physics in Z penguins.

Experimentally, these processes are naturally very challenging since the neutrinos cannot be detected but escape the detectors unmeasured, showing up only as missing energy. Two immediate consequences are that these decays can only be observed at the clean environment of an e^+e^- collider, where the kinematics of the decaying B meson are known, but not at hadron machines like LHC, and that the inclusive decay mode $B \to X_s\nu\bar{\nu}$ is even more difficult to measure. The prospects are therefore best for measuring the exclusive decays, $B \to K\nu\bar{\nu}$ and $B \to K^*\nu\bar{\nu}$, at planned Super B factories.

In theories beyond the SM, the observables accessible in these decays can be modified by new contributions to the operators governing the $b \to s\nu\bar{\nu}$ transition. However, since experiments only measure the processes $B \to K^{(*)}\not{E}$, completely different non-standard effects are possible as well: if there exist new neutral particles which couple to the $b \to s$ current and are light enough to be produced in the $B \to K^{(*)}$ decay, they can contribute to the $B \to K^{(*)}\not{E}$ signal and fake a non-standard contribution to $b \to s\nu\bar{\nu}$.

Section 5.1 will deal with inclusive and exclusive $b \to s\nu\bar{\nu}$ decays in the SM and beyond and is based on results published in [128]. Section 5.2 will discuss neutrinoless $b \to s$ transitions with missing energy as constraints on NP models.

5.1 $b \to s\nu\bar{\nu}$ decays in the Standard Model and beyond

5.1.1 Effective Hamiltonian

The effective Hamiltonian for $b \to s\nu\bar{\nu}$ transitions is generally given by

$$\mathcal{H}_{\text{eff}} = -\frac{4\,G_F}{\sqrt{2}} V_{tb}V_{ts}^* \left(C_L^\nu \mathcal{O}_L^\nu + C_R^\nu \mathcal{O}_R^\nu\right) \;+\; \text{h.c.}\,, \tag{5.1}$$

with the operators

$$\mathcal{O}_L^\nu = \frac{e^2}{16\pi^2}(\bar{s}\gamma_\mu P_L b)(\bar{\nu}\gamma^\mu(1-\gamma_5)\nu) \ , \quad \mathcal{O}_R^\nu = \frac{e^2}{16\pi^2}(\bar{s}\gamma_\mu P_R b)(\bar{\nu}\gamma^\mu(1-\gamma_5)\nu) \ . \quad (5.2)$$

In the SM, C_R^ν is negligible while

$$(C_L^\nu)^{\rm SM} = -X(x_t)/\sin^2\theta_w = -6.38 \pm 0.06 \ , \quad (5.3)$$

where $x_t = m_t^2/m_W^2$ and the function $X(x_t)$ can be found e.g. in [129] at the next-to-leading order in QCD. The error in (5.3) is dominated by the experimental uncertainty on the top quark mass [130].

The operators $\mathcal{O}_{L,R}$ have vanishing anomalous dimensions, i.e. they are renormalization scale invariant.

5.1.2 Decay modes and observables

$B \to K^*\nu\bar{\nu}$

The calculation of the $B \to K^*\nu\bar{\nu}$ amplitude proceeds very similarly to $B \to K^*\ell^+\ell^-$ discussed in chapter 4. A major simplification is given by the fact that, the neutrinos being SM gauge singlets, factorization between the leptonic and hadronic currents is exact and no non-factorizable corrections have to be taken into account.

The same $B \to K^*$ form factors as in $B \to K^*\ell^+\ell^-$ enter, although only a subset of them, since the contributions proportional to the tensor form factors are absent, due to the lack of photon penguins. However, since the problematic regions in the dilepton spectrum of $B \to K^*\ell^+\ell^-$ due to charmonium production are absent in $B \to K^*\nu\bar{\nu}$, the full kinematic range for the dineutrinos is accessible experimentally. The light-cone sume rule calculation for the form factors employed in chapter 4 and valid at low q^2 thus has to be supplemented by an exptrapolation to high q^2. In practice, this is done by employing physically motivated parametrizations [131] and fitting them to the LCSR results of [112] at low q^2.

Since the K^* decays to a kaon and a pion, the kinematical variables are the dineutrino invariant mass squared q^2, the K^* invariant mass squared k^2, the angle θ between the kaon and K^* flight directions in the K^* rest frame[1], the angle between the neutrino and the K^* and the angles between the dineutrino and dimeson decay planes. Of course, the latter two angles are unobservable and, as discussed in section 4.2.1, $k^2 = m_{K^*}^2$ should be imposed experimentally to be able to express the $B \to K\pi$ matrix elements in terms of $B \to K^*$ form factors by means of the narrow width approximation. In the end, there are two relevant kinematical variables: q^2 and θ. Of course, the dineutrino momenta are not accessible experimentally, but

[1] θ corresponds precisely to θ_{K^*} of chapter 4.

q^2 is simply related to the missing energy in the decaying B rest frame as (cf. eq. (4.16))

$$\not{E} = \frac{m_{K^*}^2 - m_B^2 - q^2}{2m_B} \ . \tag{5.4}$$

The differential decay distribution for $B \to K^*\nu\bar{\nu}$ can be obtained by integrating out the angles θ_ℓ and ϕ in eqs. (4.51)–(4.52). Multiplying by an additional factor of 3 to account for the fact that the 3 neutrino flavours cannot be distinguished experimentally, one obtains

$$\frac{d^2\Gamma}{dq^2 d\cos\theta} = \frac{3}{4}\frac{d\Gamma_T}{dq^2}\sin^2\theta + \frac{3}{2}\frac{d\Gamma_L}{dq^2}\cos^2\theta \ , \tag{5.5}$$

where Γ_L and Γ_T refer to a longitudinally and transversely polarized K^*, respectively, and can be written in terms of transversity amplitudes as

$$\frac{d\Gamma_L}{dq^2} = 3|A_0|^2 \ , \qquad \frac{d\Gamma_T}{dq^2} = 3\left(|A_\perp|^2 + |A_\parallel|^2\right) \ . \tag{5.6}$$

The transversity amplitudes can correspondingly be obtained from eqs. (4.44)–(4.46) by performing the replacements

$$C_9 - C_{10} \to 2C_L^\nu \,, \qquad C_9' - C_{10}' \to 2C_R^\nu \,, \tag{5.7}$$

$$C_9 + C_{10} \to 0 \,, \qquad C_9' + C_{10}' \to 0 \,, \tag{5.8}$$

$$C_{7,S,P}^{(\prime)} \to 0 \,, \qquad m_\mu \to 0 \,, \tag{5.9}$$

leading to

$$A_\perp(q^2) = 2N\sqrt{2}\ \lambda^{1/2}(m_B^2, m_{K^*}^2, q^2)\ (C_L^\nu + C_R^\nu)\ \frac{V(q^2)}{m_B(m_B + m_{K^*})} \ , \tag{5.10}$$

$$A_\parallel(q^2) = -2N\sqrt{2}\ \frac{m_B + m_{K^*}}{m_B}\ (C_L^\nu - C_R^\nu)\ A_1(q^2) \ , \tag{5.11}$$

$$\begin{aligned} A_0(q^2) = &-\frac{N}{m_{K^*} m_B \sqrt{q^2}}\ (C_L^\nu - C_R^\nu) \\ &\times \left[(m_B^2 - m_{K^*}^2 - q^2)(m_B + m_{K^*})A_1(q^2) - \lambda(m_B^2, m_{K^*}^2, q^2)\frac{A_2(q^2)}{m_B + m_{K^*}}\right] \ , \end{aligned} \tag{5.12}$$

where

$$N = V_{tb}V_{ts}^* \left[\frac{G_F^2\alpha^2}{3\cdot 2^{10}\pi^5 m_B} q^2 \lambda^{1/2}(m_B^2, m_{K^*}^2, q^2)\right]^{1/2} \ . \tag{5.13}$$

and the function $\lambda(a,b,c)$ has been defined in (4.50).

Instead of $d\Gamma_L/dq^2$ and $d\Gamma_T/dq^2$, one can choose a different set of independent observables accessible from the double differential decay distribution: the dineutrino mass distribution $d\Gamma/dq^2$, where

$$\frac{d\Gamma}{dq^2} = \int_{-1}^{1} d\cos\theta \, \frac{d^2\Gamma}{q^2 d\cos\theta} = \frac{d\Gamma_L}{q^2} + \frac{d\Gamma_T}{q^2} = 3m_B^2 \left(|A_\perp|^2 + |A_\parallel|^2 + |A_0|^2\right) \ , \quad (5.14)$$

and one of the K^* longitudinal and transverse polarization fractions $F_{L,T}$, defined analogously to $B \to K^*\ell^+\ell^-$ as

$$F_{L,T} = \frac{d\Gamma_{L,T}/ds_B}{d\Gamma/ds_B} \ , \quad F_L = 1 - F_T \ . \quad (5.15)$$

The advantage of this choice of observables is twofold. First, the normalization of $F_{L,T}$ on the total dineutrino spectrum strongly reduces the hadronic uncertainties associated with the form factors as well as parametric uncertainties associated with CKM elements. Second, in the absence of right-handed currents ($C_R^\nu = 0$), the dependence on the remaining Wilson coefficient C_L^ν drops out in $F_{L,T}$, making it a perfect observable to probe such right-handed currents.

One can also consider the q^2-integrated $F_{L,T}$, defined as

$$\langle F_{L,T} \rangle = \frac{\Gamma_{L,T}}{\Gamma}, \qquad \text{where } \ \Gamma_{L,T} = \int_0^{q^2_{\rm max}} dq_2 \, \frac{d\Gamma_{L,T}}{dq^2} \quad (5.16)$$

and $q^2_{\rm max} = (m_B - m_{K^*})^2$.

$B \to K\nu\bar{\nu}$

In $B \to K\nu\bar{\nu}$, no angular analysis is required and the only observable is the dineutrino invariant mass distribution. It reads

$$\frac{d\Gamma(B \to K\nu\bar{\nu})}{dq^2} = \frac{G_F^2\alpha^2}{256\pi^5 m_B^3} \, |V_{ts}^* V_{tb}|^2 \, \lambda^{3/2}(q^2, m_K^2, m_B^2) \left[f_+^K(q^2)\right]^2 |C_L^\nu + C_R^\nu|^2 \ . \quad (5.17)$$

The $B \to K$ form factor f_+^K has been calculated in [132] for the full kinematical range $0 \le q^2 \le (m_B - m_K)^2$.

While the result (5.17) is in principle valid both for charged and neutral B decays, the $B^+ \to K^+\nu\bar{\nu}$ mode receives an additional background from the process $B^+ \to \tau^+(\to K^+\bar{\nu}_\tau)\nu_\tau$ with a resonant τ that cannot be disentangled experimentally [133]. The differential decay rate for this process, assuming the narrow-width approximation for the τ, can be written as

$$\frac{d\Gamma(B^+ \to \tau^+(\to K^+\bar{\nu})\nu)}{dq^2} = \mathrm{BR}(B^+ \to \tau^+\nu) \times \mathrm{BR}(\tau^+ \to K^+\nu) \times 2\left(1 - \frac{q^2}{q^2_{\rm max}}\right) \ , \quad (5.18)$$

where now $q^2_{\text{max}} = (m_B^2 - m_\tau^2)(m_\tau^2 - m_K^2)/m_\tau^2$. Plugging in the experimentally measured branching ratios for the two subprocesses [39, 48], the branching ratio reads

$$\text{BR}(B^+ \to \tau^+(\to K^+\bar{\nu})\nu)_{\text{exp}} = (1.2 \pm 0.2) \times 10^{-6} \,, \tag{5.19}$$

which amounts to roughly one fourth of the pure $B^+ \to K^+\nu\bar{\nu}$ branching ratio. This mode will not be treated as a contribution to the $B^+ \to K^+\nu\bar{\nu}$ SM branching ratio in the following, but as an experimental background that should be subtracted. Since this background has not been taken into account in experimental studies to date, existing experimental bounds are in fact stronger by the amount given in eq. (5.19).

Within the SM, a more precise estimate of the $B \to K\nu\bar{\nu}$ branching ratio than by using eq. (5.17) can be obtained by making use of the existing measurement of the $B \to K\ell^+\ell^-$ decay, where the same form factors enter [134]. However, this approach is only valid if $B \to K\ell^+\ell^-$ is free from NP contributions, so should not be used as the value of the SM contribution in a NP model modifying also $B \to K\ell^+\ell^-$.

$B \to X_s\nu\bar{\nu}$

The inclusive decay $B \to X_s\nu\bar{\nu}$ is theoretically cleaner than the exclusive ones since no form factors are required. To zeroth order in Λ_{QCD}/m_b, the dineutrino invariant mass distribution reads

$$\begin{aligned}\frac{d\Gamma(B \to X_s\nu\bar{\nu})}{dq^2} &= \frac{\alpha^2 G_F^2}{128\pi^5 m_b}|V_{ts}^* V_{tb}|^2 \kappa(0)(|C_L^\nu|^2 + |C_R^\nu|^2) \\ &\times \sqrt{\lambda(m_b^2, m_s^2, q^2)}\left[3q^2(q^2 + m_s^2 - q^2 - 4m_s\frac{\text{Re}\,(C_L^\nu C_R^{\nu *})}{|C_L^\nu|^2 + |C_R^\nu|^2}) + \lambda(q^2, m_s^2, q^2)\right] \,,\end{aligned} \tag{5.20}$$

where $\kappa(0) = 0.83$ represents the QCD correction to the $b \to s\nu\bar{\nu}$ matrix element [110, 135, 136].

The dominant source of uncertainty in (5.20) is the b quark mass. The scheme and scale dependence of m_b has to be cancelled by higher orders in the Λ_{QCD}/m_b expansion. The best results are obtained by using the b quark mass in the 1S scheme and the $O(\Lambda^2_{\text{QCD}}/m_b^2)$ corrections [135, 137] with the HQET parameters in the 1S scheme as well [138].

5.1.3 Standard Model

The SM predictions for the differential branching ratios of all three decays and for $F_L(q^2)$ are shown in figure 5.1; the branching ratios and the integrated F_L are listed in table 5.2. Neither the inclusive nor the two exclusive $b \to s\nu\bar{\nu}$ decay modes have been observed in experiment so far; however, experimental upper bounds on the

Parameter	Value	Ref.
m_b^{1S}	(4.68 ± 0.03) GeV	[138, 139]
$m_s(2\text{ GeV})$	0.1 GeV	[39]
$m_t(m_t)$	(162.3 ± 1.2) GeV	[130]
τ_{B^+}	1.638 ps	[39]
τ_{B^0}	1.530 ps	[39]
λ	0.2255(7)	[140]
$\lvert V_{cb}\rvert$	$(4.13 \pm 0.05) \times 10^{-2}$	[141]
$\bar{\rho}$	0.154 ± 0.022	[141]
$\bar{\eta}$	0.342 ± 0.014	[141]
λ_1	(-0.27 ± 0.04) GeV^2	[138]
λ_2	(0.12 ± 0.01) GeV^2	[39]

Table 5.1: Parameters used in the numerical analysis. $\lambda_{1,2}$ are the HQET parameters needed for the evaluation of the $\Lambda_{\text{QCD}}^2/m_b^2$ corrections to $\text{BR}(B \to X_s\nu\bar{\nu})$ [135].

Observable	SM prediction	Experiment
$\text{BR}(B \to K^*\nu\bar{\nu})$	$(6.8^{+1.0}_{-1.1}) \times 10^{-6}$ [128]	$< 80 \times 10^{-6}$ [142]
$\text{BR}(B^+ \to K^+\nu\bar{\nu})$	$(4.5 \pm 0.7) \times 10^{-6}$ [128]	$< 14 \times 10^{-6}$ [143]
	$(3.64 \pm 0.47) \times 10^{-6}$ [134]	
$\text{BR}(B \to X_s\nu\bar{\nu})$	$(2.7 \pm 0.2) \times 10^{-5}$ [128]	$< 64 \times 10^{-5}$ [144]
$\langle F_L(B \to K^*\nu\bar{\nu})\rangle$	0.54 ± 0.01 [128]	–

Table 5.2: SM predictions and experimental bounds (all at the 90% C.L.) for the four $b \to s\nu\bar{\nu}$ observables. The second, more precise prediction for $\text{BR}(B^+ \to K^+\nu\bar{\nu})$ is valid if the $B \to K\ell^+\ell^-$ decay is NP free (cf. the discussion in section 5.1.2).

branching ratios have been set by the BaBar, Belle and ALEPH collaborations, and are shown in table 5.2 as well.

The estimates of the theoretical uncertainties in table 5.2 and the error bands in figure 5.1 include the uncertainties due to the form factors in the case of the exclusive decays and the uncertainties of the CKM elements as listed in table 5.1 as well as the uncertainty in the SM Wilson coefficient as given in eq. (5.3), for all decays.

For the inclusive decay, the uncertainty is dominated by the theory error of m_b^{1S}.

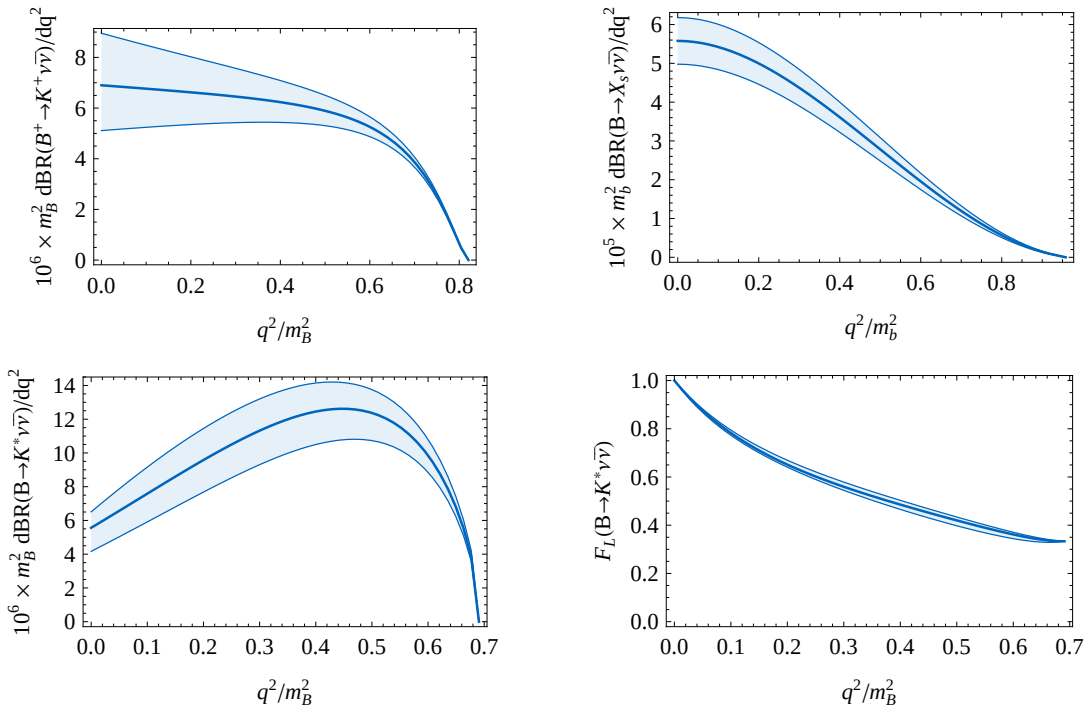

Figure 5.1: The four $b \to s\nu\bar{\nu}$ observables, three differential branching ratios and the K^* longitudinal polarization fraction in the SM. The error bands show the theoretical uncertainties, which are dominated by the form factor uncertainties in the case of exlusive decays and by the b quark mass in the inclusive decay.

For the branching ratio prediction, the HQET parameters $\lambda_{1,2}$ required for the $O(\Lambda^2_{\rm QCD}/m_b^2)$ corrections are listed in table 5.1 and the corresponding uncertainties are taken into account as well. To be conservative, an additional uncertainty of 5% was added to account for neglected higher order power corrections. For the inclusive dineutrino mass spectrum in figure 5.1, the $O(\Lambda^2_{\rm QCD}/m_b^2)$ corrections have been omitted, since they become singular at the kinematical endpoint, and the uncertainty on the dineutrino mass spectrum accordingly increased to 10%.

All individual uncertainties have been added in quadrature.

5.1.4 Beyond the Standard Model

Model-independent constraints on Wilson coefficients

The four observables accessible in the three different $b \to s\nu\bar{\nu}$ decays are dependent on the two in principle complex Wilson coefficients C_L^ν and C_R^ν. However, only two combinations of these complex quantities enter the formulae given in section 5.1.2

and are thus observable. These are [135, 145]

$$\epsilon = \frac{\sqrt{|C_L^\nu|^2 + |C_R^\nu|^2}}{|(C_L^\nu)^{\rm SM}|} \ , \qquad \eta = \frac{-{\rm Re}\,(C_L^\nu C_R^{\nu *})}{|C_L^\nu|^2 + |C_R^\nu|^2} \ , \tag{5.21}$$

such that η lies in the range $[-\frac{1}{2}, \frac{1}{2}]$. The observables discussed in section 5.1.2 can be expressed in terms of ϵ and η as follows

$$\begin{aligned}
{\rm BR}(B \to K^* \nu\bar{\nu}) &= 6.8 \times 10^{-6}\,(1 + 1.31\,\eta)\epsilon^2 \ , && (5.22)\\
{\rm BR}(B \to K \nu\bar{\nu}) &= 4.5 \times 10^{-6}\,(1 - 2\,\eta)\epsilon^2 \ , && (5.23)\\
{\rm BR}(B \to X_s \nu\bar{\nu}) &= 2.7 \times 10^{-5}\,(1 + 0.09\,\eta)\epsilon^2 \ , && (5.24)\\
\langle F_L \rangle &= 0.54\,\frac{(1 + 2\,\eta)}{(1 + 1.31\,\eta)} \ . && (5.25)
\end{aligned}$$

As ϵ and η can be calculated in any model by means of eq. (5.21), these four expressions can be considered as fundamental formulae for any phenomenological analysis of the decays in question.

The experimental bounds on the branching ratios, cf. table 5.2, can now be translated to excluded areas in the ϵ-η-plane, where the SM corresponds to $(\epsilon, \eta) = (1, 0)$. Figure 5.2 shows these excluded areas as well as the constraints on the ϵ-η-plane that would be obtained from a hypothetical measurements of the SM values of all observables with infinite precision. Finally, the figure also shows the projected sensitivity on the observables at the proposed Belle-II experiment. Preliminary results from sensitivity studies for the planned SuperB experiment indicate that an angular analysis of $B \to K^* \nu\bar{\nu}$ would be feasible and the observable $\langle F_L \rangle$ therfore accessible [147].

A special role is played by the observable $\langle F_L \rangle$: since it only depends on η, cf. eq. (5.25), it leads to a horizontal line in the ϵ-η plane. Although a similar constraint could be obtained by dividing two of the branching ratios to cancel the common factor of ϵ^2, the use of $\langle F_L \rangle$ is theoretically much cleaner since in this case, the hadronic uncertainties cancel, while they would add up when using the branching ratios.

Modified Z penguins

In many models beyond the SM, NP effects in the Wilson coefficients $C_{L,R}^\nu$ are dominated by Z penguins. This can be discussed model-independently by assuming an effective flavour violating $\bar{b}sZ$ coupling [120], which will not only modify the Wilson coefficients $C_{L,R}^\nu$, but also the Wilson coefficients $C_{9,10}^{(\prime)}$ of the semi-leptonic operators governing $b \to s\ell^+\ell^-$ transitions. Therefore, interesting correlations between these processes and the $b \to s\nu\bar{\nu}$ transitions are to be expected in this scenario.

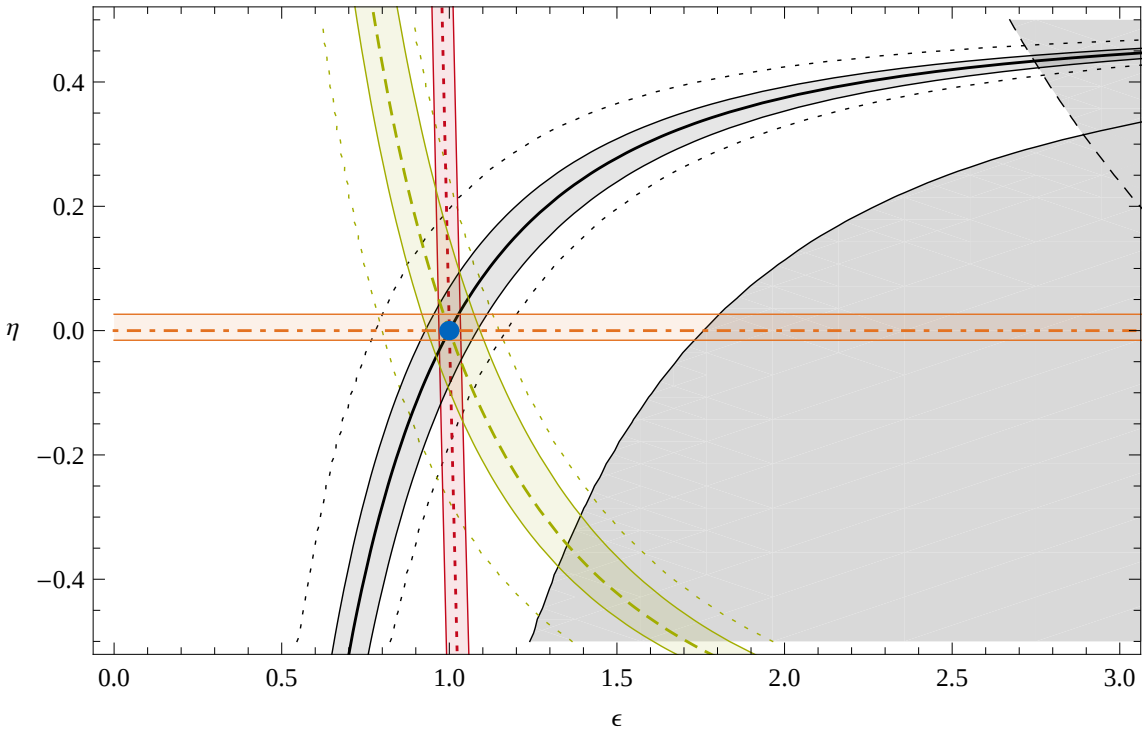

Figure 5.2: Existing experimental constraints, SM predictions and projected experimental sensitivity in the ϵ-η plane. The shaded area limited by the dashed black line is ruled out at 90% C.L. by BR($B \to K^*\nu\bar{\nu}$), the area limited by the solid black line by BR($B \to K\nu\bar{\nu}$). The green band with the dashed line represents the SM prediction for BR($B \to K^*\nu\bar{\nu}$), the black band with the solid line the one for BR($B \to K\nu\bar{\nu}$), the red band with the dotted line the one for BR($B \to X_s\nu\bar{\nu}$) and the orange band with the dot-dashed line represents the SM prediction for $\langle F_L \rangle$. The dashed lines show the expected experimental sensitivity on the $B \to K^*\nu\bar{\nu}$ and $B \to K\nu\bar{\nu}$ branching ratios at the proposed Belle-II experiment, given an integrated luminosity of 50 ab^{-1} [146]. The blue circle represents the SM point.

The flavour violating $\bar{b}sZ$ coupling can be parametrized in terms of the effective Lagrangian [120]

$$\mathcal{L}_{\text{eff}}^{\bar{b}sZ} = \frac{G_F}{\sqrt{2}} \frac{e}{\pi^2} m_Z^2 c_w s_w V_{tb}^* V_{ts} \, Z^\mu \left(Z_L \, \bar{b} \gamma_\mu P_L s + Z_R \, \bar{b} \gamma_\mu P_R s \right) \, , \tag{5.26}$$

with $s_w = \sin\theta_w$ and $c_w = \cos\theta_w$. In the SM, the right-handed coupling is negligible, while $Z_L = C_0(x_t)/s_w^2$. The function C_0 can be found e.g. in [110]. In models with CMFV, Z_L is a real function of the model parameters and Z_R is strongly suppressed, while in general NP models Z_L and Z_R can be arbitrary complex couplings.

It should be remarked that the Z penguins are generally gauge dependent. In the SM, this gauge dependence is rather weak as it enters only in non-leading terms in m_t and is cancelled through box diagrams and photon penguin diagrams. As the latter diagrams receive subdominant contributions in most extensions of the SM with respect to NP contributions to Z penguins, we expect that the gauge dependence of NP contributions to $Z_{L,R}$ is also very weak and it is a very good approximation to parametrize the NP contributions by the modifications of $Z_{L,R}$ only [148, 149].

The impact of NP effects in the $\bar{b}sZ$ couplings $Z_{L,R}$ on the Wilson coefficients (cf. (4.7), (5.2)) is

$$C_L^\nu = (C_L^\nu)^{\text{SM}} - Z_L^{\text{NP}} \, , \qquad C_R^\nu = -Z_R \, , \tag{5.27}$$

$$C_{10} = C_{10}^{\text{SM}} - Z_L^{\text{NP}} \, , \qquad C_{10}' = -Z_R \, , \tag{5.28}$$

$$C_9 = C_9^{\text{SM}} + Z_L^{\text{NP}}(1 - 4s_w^2) \, , \qquad C_9' = Z_R(1 - 4s_w^2) \, . \tag{5.29}$$

The contributions to $C_9^{(\prime)}$ are strongly suppressed by the small vector coupling of the Z to charged leptons $(1 - 4s_w^2) \approx 0.08$.

The most stringent constraint on $Z_{L,R}^{\text{NP}}$ comes from the measurement of the branching ratio of the inclusive decay $B \to X_s \ell^+ \ell^-$, which reads in the low-q^2 region, $1\,\text{GeV}^2 < q^2 < 6\,\text{GeV}^2$ [89, 90],

$$\text{BR}(B \to X_s \ell^+ \ell^-)_{\text{exp.}} = (1.60 \pm 0.51) \times 10^{-6} \, . \tag{5.30}$$

Assuming that NP contributions enter exclusively through modified Z penguins, which we will assume throughout this section, this can be translated into a bound on the flavour-changing Z couplings,

$$4.3 < |Z_L|^2 + |Z_R|^2 < 28.8 \tag{5.31}$$

at the 1σ level. An additional (currently weaker) constraint arises from the experimental upper bound on the branching ratio of $B_s \to \mu^+\mu^-$ (cf. section 2.2.2),

$$\text{BR}(B_s \to \mu^+\mu^-)_{\text{exp.}} < 4.3 \times 10^{-8} \text{ at } 95\% \text{ C.L.} \, , \tag{5.32}$$

leading to

$$|Z_L - Z_R|^2 < 194 \ , \tag{5.33}$$

again assuming that scalar or pseudoscalar operator contributions to $B_s \to \mu^+\mu^-$ are negligible.

The couplings $Z_{L,R}$ also contributes to B_s-$\bar{B}_s$ mixing via double Z penguin diagrams, which contribute to the amplitude a term

$$\frac{\langle B_s|\mathcal{H}|\bar{B}_s\rangle^{\bar{b}sZ}}{\langle B_s|\mathcal{H}|\bar{B}_s\rangle^{\rm SM}} = \frac{4\alpha s_w^2}{\pi S_0(x_t)}(Z_L^2 + xZ_LZ_R + Z_R^2) \ , \tag{5.34}$$

where the function S_0 can be found e.g. in [110] and $x \simeq -3.5$ is a hadronic parameter containing the ratio of hadronic matrix elements of the respective $\Delta B = 2$ operators [128]. The amplitude is usually parametrized as

$$\langle B_s|\mathcal{H}|\bar{B}_s\rangle = \frac{\Delta M_s}{2}\, e^{2i(\phi_{B_s}+\beta_s)} \ . \tag{5.35}$$

The mass difference has been measured to be [88]

$$(\Delta M_s)_{\rm exp.} = (17.77 \pm 0.12)\,{\rm ps}^{-1} \ , \tag{5.36}$$

however, the theory prediction is afflicted with an uncertainty of roughly 30% due to uncertainties in hadronic parameters. While the B_s mixing phase predicted by the SM is tiny, $\beta_s \approx 1°$, recent Tevatron data seem to indicate the presence of a sizable phase ϕ_{B_s} [150–154].

In principle, large complex $\bar{b}sZ$ couplings $Z_{L,R}$ could give rise to a such a phase. However, taking into account the constraint in eq. (5.31), the double penguin contribution is too small to generate a sizable phase. We visualize the constraints from $B \to X_s\ell^+\ell^-$, $B_s \to \mu^+\mu^-$ and from B_s mixing in figure 5.3 for the case $Z_R = 0$. In the general case of nonzero and complex Z_L and Z_R, the correlation is more complicated (e.g., for $Z_L = Z_R$ the constraint from $B_s \to \mu^+\mu^-$ disappears) but it turns out that it is never possible to bring the stringent constraint from $B \to X_s\ell^+\ell^-$ into agreement with a large B_s mixing phase[2].

Figure 5.4 shows the correlation between the three $b \to s\nu\bar{\nu}$ branching ratios and ${\rm BR}(B \to X_s\ell^+\ell^-)$. Assuming $Z_R = 0$ and Z_L real, which holds in CMFV models, there are clear correlations, indicated as black curves, between the neutrino modes and the charged lepton mode. In the general case of arbitrary and complex $Z_{L,R}$, the entire shaded areas are accessible. It is interesting to note, however, that in all three $b \to s\nu\bar{\nu}$ decay modes, an enhancement of the branching ratio by more than a factor of two with respect to the SM is excluded by the measurement of ${\rm BR}(B \to X_s\ell^+\ell^-)$

[2] As pointed out in [126], the experimental indication of a SM-like sign of the forward-backward asymmetry of $B \to K^*\ell^+\ell^-$ in the high-q^2 region [121, 155] puts additional constraints on $C_{10}^{\rm NP}$ (and thus on $Z_L^{\rm NP}$), further strengthening this conclusion.

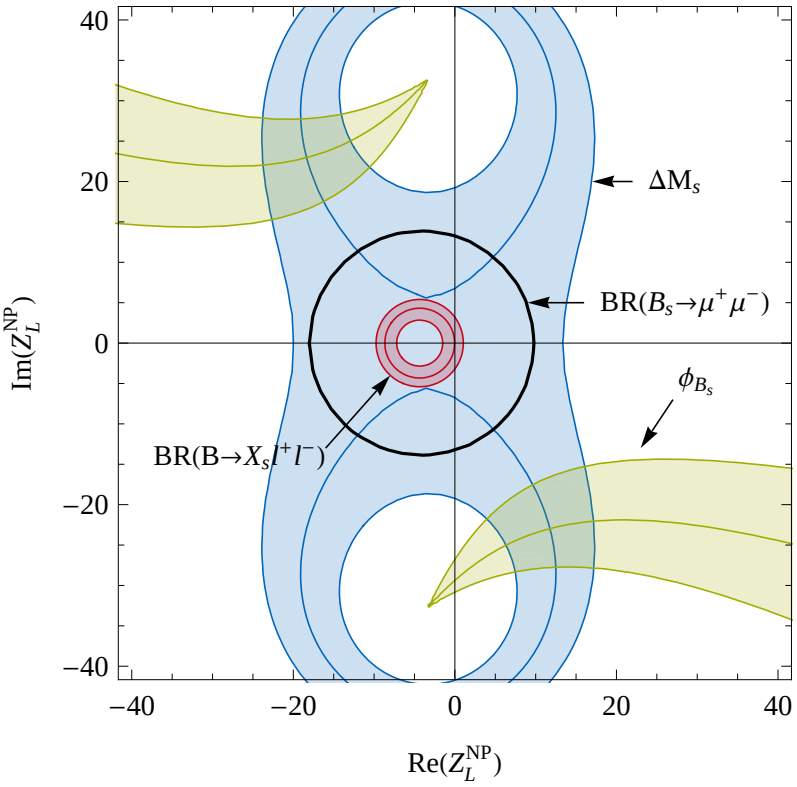

Figure 5.3: Constraints on the real and imaginary parts of $Z_L^{\rm NP}$ coming from ΔM_s (blue, assuming 30% theory uncertainty), BR($B \to X_s \ell^+ \ell^-$) (red) and BR($B_s \to \mu^+ \mu^-$) (black) assuming $Z_R = 0$. The green lines correspond to values of the B_s mixing phase $\phi_{B_s} = -11°$, $-19°$ and $-27°$, respectively [150].

in eq. (5.30). By construction, this statement is valid for all models in which NP contributions to $b \to s\nu\bar{\nu}$ and $b \to s\ell^+\ell^-$ processes enter dominantly through flavour-changing Z penguins.

Flavour violating Z' penguins

One way to circumvent this constraint is by replacing the Z boson in the above considerations by the Z' gauge boson of an additional $U(1)'$ symmetry, i.e. assuming an SM-like $\bar{b}sZ$ coupling but a flavour violating $\bar{b}sZ'$ coupling. Then, instead of eq. (5.26), one has

$$\mathcal{L}_{\rm eff}^{\bar{b}sZ'} = \frac{G_F}{\sqrt{2}} \frac{e}{\pi^2} m_{Z'}^2 c_w s_w V_{tb}^* V_{ts}\, Z'^{\mu} \left(Z'_L\, \bar{b}\gamma_\mu P_L s + Z'_R\, \bar{b}\gamma_\mu P_R s \right) \ . \tag{5.37}$$

Such couplings can arise either as effective couplings induced by loop effects of particles charged under the $U(1)'$, or even at tree level in the case of generation

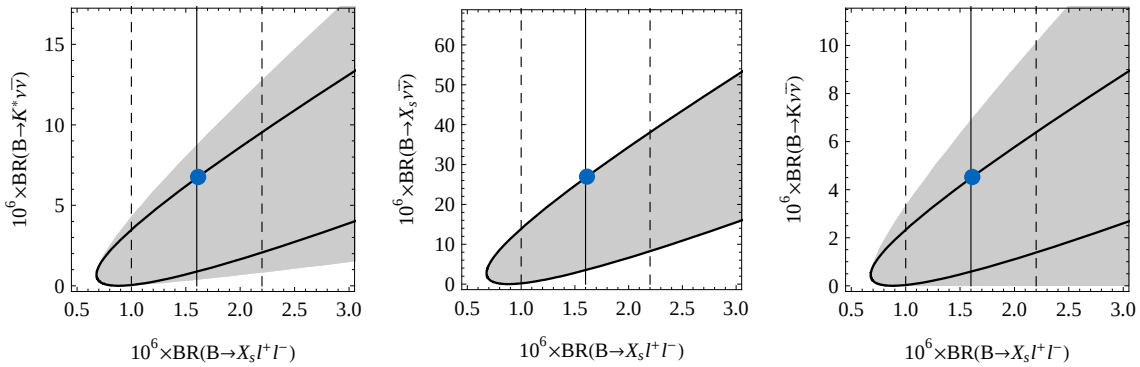

Figure 5.4: Correlations between $b \to s\nu\bar{\nu}$ branching ratios and $\mathrm{BR}(B \to X_s\ell^+\ell^-)$. The black curves correspond to $Z_R = 0$ and real Z_L; The shaded areas are accessible for arbitrary $Z_{L,R}$; The blue dots represent the SM. The solid and dashed vertical lines correspond to the experimental central value and 1σ error, respectively, of $\mathrm{BR}(B \to X_s\ell^+\ell^-)$.

non-universal $U(1)'$ charges of the quarks [156]. In this setup, the analogues to eqs. (5.27)–(5.29) read

$$C_L^\nu = (C_L^\nu)^{\mathrm{SM}} - \frac{g_V'^\nu}{2} Z_L' \,, \qquad C_R^\nu = -\frac{g_V'^\nu}{2} Z_R' \,, \tag{5.38}$$

$$C_{10} = C_{10}^{\mathrm{SM}} + \frac{g_A'^\ell}{2} Z_L' \,, \qquad C_{10}' = +\frac{g_A'^\ell}{2} Z_R' \,, \tag{5.39}$$

$$C_9 = C_9^{\mathrm{SM}} - \frac{g_V'^\ell}{2} Z_L' \,, \qquad C_9' = -\frac{g_V'^\ell}{2} Z_R' \,, \tag{5.40}$$

where the couplings $g_{V,A}'^{\nu,\ell}$ denote the vector and axial vector couplings of the Z' to neutrinos and charged leptons, respectively. These couplings are given by the $U(1)'$ charges of the respective fields and are arbitrary – apart from anomaly constraints, which can however always be fulfilled by adjusting the quark $U(1)'$ charges and/or adding new, exotic fermions.

The contribution to the B_s mixing amplitude, on the other hand, is independent of the g' couplings and is simply given by eq. (5.34) after the replacements $Z_{L,R} \to Z'_{L,R}$. Therefore, in a general Z' model, by choosing small or zero $U(1)'$ charges for the charged leptons it is possible in principle to completely suppress the NP contributions to $b \to s\ell^+\ell^-$ as well as $B_s \to \ell^+\ell^-$ decays, while it is at the same time possible to obtain a strong enhancement of $b \to s\nu\bar{\nu}$ modes and/or a sizable, potentially complex, contribution to the B_s mixing amplitude.

5.2 Neutrinoless B decays with missing energy

Experimental searches for $b \to s\nu\bar{\nu}$ decays in fact rely on the signature $b \to s\not{E}$, since the neutrinos escape the detector undetected, but the missing energy can be unambiguously assigned to a $\nu\bar{\nu}$ pair only within the SM. In models beyond the SM containing neutral particles with mass below a few GeV, these particles may be produced in $s \to d$ or $b \to s$ transitions as well, superimposing the $\nu\bar{\nu}$ decay modes in the experimental signature. Even assuming the $s \to d\nu\bar{\nu}$ and $b \to s\nu\bar{\nu}$ amplitudes to be unaffected by NP, the current experimental bounds still allow a large room for such non-standard contributions, as table 5.2 shows.

In section 5.1, it was shown that the observables accessible in inclusive and exclusive $b \to s\nu\bar{\nu}$ decays allow to overconstrain the relevant Wilson coefficients. Likewise, the complementartiy between the different modes could be exploited to tell whether a neutrinoless contribution to $b \to s\not{E}$ is present, and if so, what the nature and masses of the new particles are.

In the following section, the differential decay rates for various $b \to s$ transitions with additional, light neutral particles in the final state will be calculated. For definiteness, this exercise will be performed assuming that these particles are scalars, as is the case in several conrete models; however, also particles with different spin, like Majorana fermions (e.g. in the case of light neutralinos [157–159]) could contribute with distinct signatures.

In the numerical results, it will be assumed that the Wilson coefficients of the $b \to s\nu\bar{\nu}$ transition discussed in section 5.1 are not affected by NP, such that the upper bounds on the branching ratios into new particles are given by the current experimental bound minus the SM contribution as given in table 5.2.

5.2.1 Scalar effective interaction

The effective Lagrangian for a $b \to s\phi^n$ transition, where ϕ is a neutral scalar or pseudoscalar particle, can be written as

$$\mathcal{L}_{\text{eff}} = \sum_{A=L,R} \frac{C_A^{(n)} m_b}{n!\Lambda^n} \, (\bar{s} P_A b) \, \phi^n \,, \tag{5.41}$$

where Λ is an arbitrary parameter with mass dimension 1 and $C_{L,R}^{(n)}$ are the two Wilson coefficients governing the $b \to s$ transition with n scalars in the final state.

5.2.2 Decay modes

$B \to K\phi^n$

The decay rate for $n = 1$ reads

$$\Gamma(B \to K\phi) = \frac{1}{\Lambda^2}\left|C_L^{(1)} + C_R^{(1)}\right|^2 \left[f_0^K(m_\phi^2)\right]^2 \Phi(m_\phi^2) \ , \tag{5.42}$$

where $f_0^K(q^2)$ is the scalar $B \to K$ form factor and

$$\Phi(s) = \frac{(m_B^2 - m_K^2)^2}{64\pi m_B^3}\lambda^{1/2}(m_B^2, s, m_K^2) \ , \tag{5.43}$$

where the function λ has been defined in (4.50). For $n = 2$, the differential decay rate reads

$$\frac{d\Gamma(B \to K\phi^2)}{dq^2} = \frac{1}{32\pi^2\Lambda^4}\left|C_L^{(2)} + C_R^{(2)}\right|^2 \left[f_0^K(q^2)\right]^2 \sqrt{1 - \frac{4m_\phi^2}{q^2}}\ \Phi(q^2) \ . \tag{5.44}$$

For $n > 2$, the phase space integral cannot be solved in a closed form if $m_\phi > 0$.

Fig. 5.5 shows the predictions for the branching ratios in units of 10^{-6} in the case of one and two scalars in the final state, respectively, as functions of the scalar mass and the Wilson coefficient combination $|C_L^{(n)} + C_R^{(n)}|/\Lambda^n$. The shaded areas are excluded experimentally, assuming $B \to K\nu\bar{\nu}$ to be SM-like (cf. table 5.2).

Fig. 5.6 shows the q^2 dependence of the differential branching ratio in the case of two scalars in the final state, for different values of the scalar mass. The kinemtically allowed range for q^2 is $(2m_\phi)^2 < q^2 < (m_B - m_K)^2$.

$B \to K^*\phi^n$

The differential decay rate for the decay $B \to K^*\phi^2$, with the K^* further decaying into $K\pi$, can be written as

$$\frac{d^2\Gamma(B \to K^*(\to K\pi)\phi^2)}{dq^2 d\cos\theta} = \frac{1}{\Lambda^4}\left|C_L^{(2)} - C_R^{(2)}\right|^2 3A_0^2(q^2)\,\Phi_*(q^2)\cos^2\theta \ , \tag{5.45}$$

where

$$\Phi_*(q^2) = \frac{1}{2^{12}\pi^3 m_B^3}\sqrt{1 - \frac{4m_\phi^2}{q^2}}\lambda^{3/2}(m_B^2, m_{K^*}^2, q^2) \tag{5.46}$$

and θ is defined just as in section 5.1.

While the $B \to K^*\not{E}$ and $B \to X_s\not{E}$ modes are less contraining than $B \to K\not{E}$ at present, it is instructive to look at the dineutrino invariant mass distributions of the SM ($b \to s\nu\bar{\nu}$) contribution superimposed by a $b \to s\phi^2$ contribution. In particular,

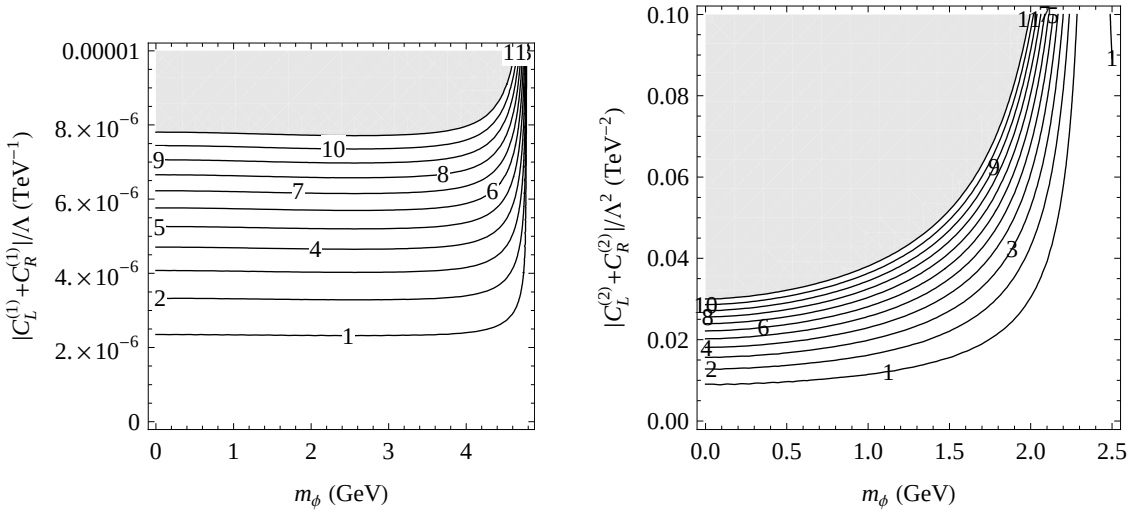

Figure 5.5: Predictions for BR($B \to K\phi$) and BR($B \to K\phi^2$) as functions of m_ϕ and the relevant combinations of Wilson coefficients, in units of 10^{-6}.

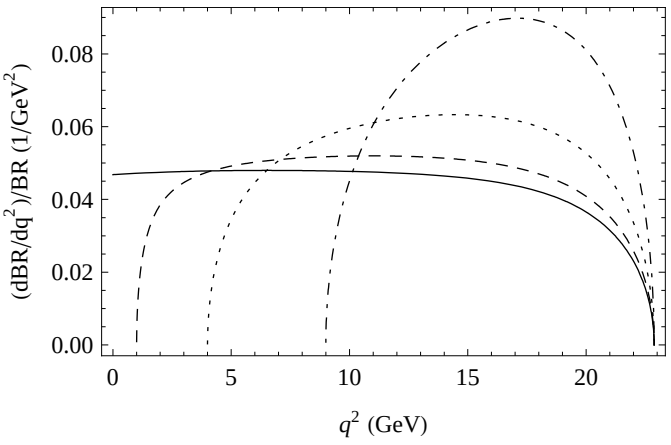

Figure 5.6: Dependence of the differential branching ratio of $B \to K\phi^2$ (normalized to the total branching ratio) on the scalar invariant mass squared q^2 for different values of the scalar mass m_ϕ: 0 (solid), 0.5 GeV (dashed), 1 GeV (dotted), 1.5 GeV (dot-dashed).

it can be seen from eq. (5.45) that the doubly differential $B \to K^* \phi^2$ decay rate is proportional to $\cos^2\theta$, since the K^* is always produced with longitudinal polarization in the $B \to K^* \phi^2$ decay, so the observable F_L, as it is extracted from the angular distribution of $B \to K^*(\to K\pi)\not{E}$ according to the formula (cf. eq. (5.5))

$$\frac{d^2\Gamma}{dq^2 d\cos\theta} \Big/ \frac{d\Gamma}{dq^2} = \frac{3}{4}(1 - F_L)\sin^2\theta + \frac{3}{2} F_L \cos^2\theta \ , \tag{5.47}$$

is modified according to

$$F_L(B \to K^* \not{E}) = \frac{d\Gamma_L(B \to K^* \nu\bar{\nu})/dq^2 + d\Gamma(B \to K^* \phi^2)/dq^2}{d\Gamma(B \to K^* \nu\bar{\nu})/dq^2 + d\Gamma(B \to K^* \phi^2)/dq^2} \ . \tag{5.48}$$

As a consequence, it is clear that eqs. (5.22)–(5.25), relating the observables to the parameters ϵ and η, are no longer valid.

$B_s \to \phi^n$

For $n > 1$, the decay mode $B_s \to \phi^n$ can be used as an additional constraint on the effective Lagrangian (5.41). At present, the decay mode $B_s \to \not{E}$ is not constrained yet, in contrast to $B_0 \to \not{E}$ [160].

The decay rate for $n = 2$ reads

$$\Gamma(B_s \to \phi^2) = \frac{1}{32\pi} \frac{m_{B_s}^3 f_{B_s}^2}{\Lambda^4} \sqrt{1 - \frac{4m_\phi^2}{m_{B_s}^2}} \left| C_L^{(2)} - C_R^{(2)} \right|^2 \ . \tag{5.49}$$

Fig. 5.7 shows the prediction for the branching ratio of $B_s \to \phi^2$ in units of 10^{-4}, as function of the scalar mass and the Wilson coefficient combination $|C_L^{(2)} - C_R^{(2)}|/\Lambda^2$.

5.2.3 Models

Warped top condensation

In [161], the warped top condensation model (WTCM) was proposed where EWSB is triggered by top condensation mediated by Kaluza-Klein gluons. In [162], it was shown that this model contains a radion ϕ which can be naturally light and might contribute to $b \to s\phi$ decays.

The effective Lagrangian for the coupling of the radion ϕ to down-type quarks is [163]

$$\mathcal{L}_{\text{eff}} = \frac{\phi}{\Lambda_\phi} \sqrt{m_{d_i} m_{d_j}} \ (a_{ij} \bar{d}_i d_j + \text{h.c.}) \ . \tag{5.50}$$

Comparing this to (5.41), the Wilson coefficients $C_{L,R}^{(1)}$ can be expressed in terms of the radion couplings as

$$\frac{C_R^{(1)}}{\Lambda} = \frac{a_{23}}{\Lambda_\phi} \frac{m_s}{m_b} \ , \qquad \frac{C_L^{(1)}}{\Lambda} = \frac{a_{32}^*}{\Lambda_\phi} \frac{m_s}{m_b} \ . \tag{5.51}$$

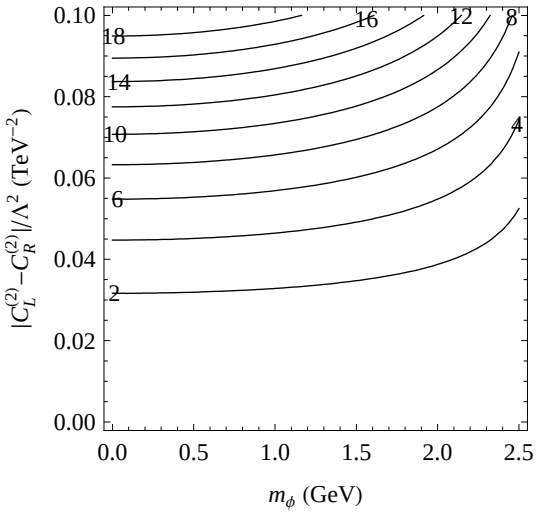

Figure 5.7: Prediction for BR($B_s \to \phi^2$) as function of m_ϕ and the relevant combination of Wilson coefficients, in units of 10^{-4}.

Comparing to the present experimental bound $|C_L^{(1)} + C_R^{(1)}|/\Lambda \lesssim 8 \times 10^{-6}$ for $m_\phi \lesssim 4\,\text{GeV}$ in fig. 5.5, this can be translated to

$$|a_{23} + a_{32}^*| \lesssim 0.06 \left(\frac{\Lambda_\phi}{10^3\,\text{TeV}}\right) , \tag{5.52}$$

so the current bound on BR($B \to K\not{E}$) is already in the ballpark of the WTCM prediction for the typical range of parameters $\Lambda_\phi \sim 10^3\,\text{TeV}$, $a_{ij} \sim 0.05$ [162] and represents an important constraint on the WTCM.

Light scalar dark matter

In [164, 165], a light neutral scalar ϕ was discussed as a candidate for the dark matter of the universe. The scalar ϕ couples to the SM Higgs via a renormalizable coupling $\mathcal{L} \supset -\lambda v \phi^2 h$. The $b \to s$ current can in turn couple to the Higgs through a Higgs penguin (see e.g. [166]). The resulting effective Lagrangian for the coupling of the scalars to down-type quarks is [164]

$$\mathcal{L}_{\text{eff}} = \frac{m_b}{2} C_{\text{DM}} (\bar{s} P_R b + \text{h.c.})\, \phi^2 , \tag{5.53}$$

where

$$C_{\text{DM}} = -\frac{\lambda}{m_h^2} \frac{3g^2}{32\pi^2} \frac{m_t^2}{m_W^2} V_{ts}^* V_{tb} \approx 6.3 \times 10^{-3} \left(\frac{\lambda}{m_h^2}\right) . \tag{5.54}$$

Comparing (5.53) with (5.41), the Wilson coefficients $C_{L,R}^{(2)}$ can be expressed in

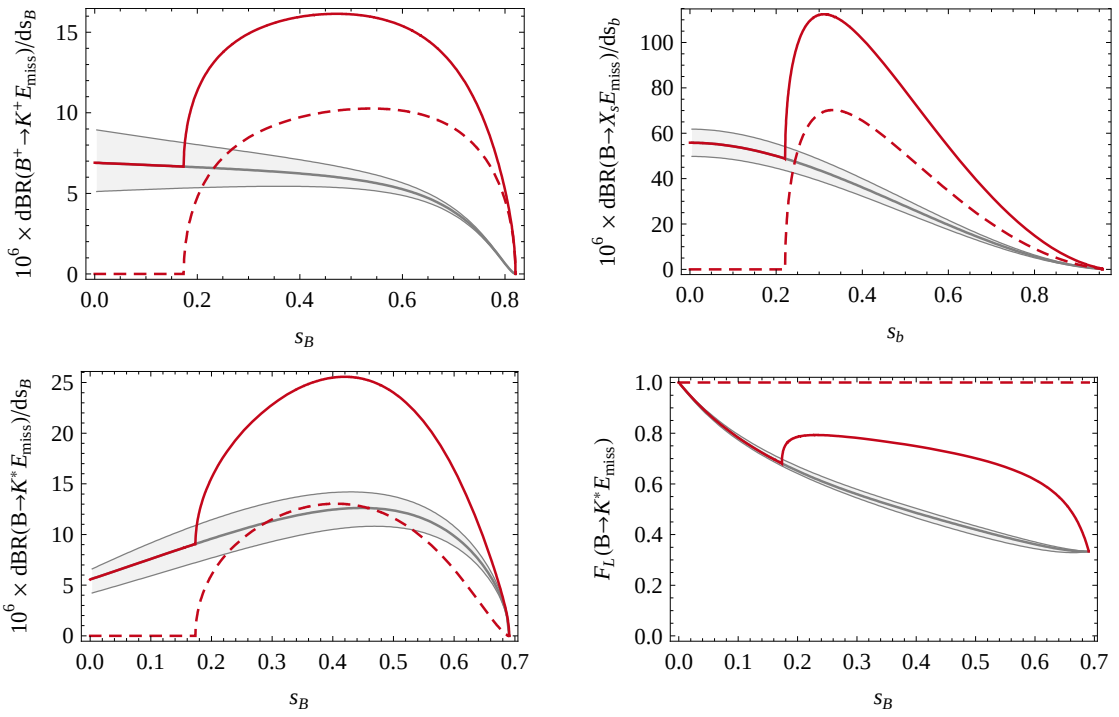

Figure 5.8: Dependence of the four observables on the normalized neutrino invariant mass squared in a scenario in which SM-like $b \to s\nu\bar{\nu}$ processes overlap with $b \to s\phi^2$ decays. The parameters chosen are $m_\phi = 1.1$ GeV, $C_L^{(2)} = 0$ and $C_R^{(2)}/\Lambda^2 = 2.8 \times 10^{-8}$ GeV^{-2}. The grey curves show the pure $b \to s\nu\bar{\nu}$ (i.e. SM) contribution with theoretical uncertainties, the red dashed curves the pure $b \to s\phi^2$ contribution and the red solid curves the resulting combination.

terms of the scalar coupling as

$$\frac{C_R^{(2)}}{\Lambda^2} = C_{\mathrm{DM}} \ , \tag{5.55}$$

while $C_L^{(2)}$ is strongly suppressed by the small ratio m_s/m_b.

The upper bound on $\mathrm{BR}(B \to K\phi^2)$ illustrated in figure 5.7 can then be translated into a bound

$$|\lambda| \times \left[\frac{120\,\mathrm{GeV}}{m_h}\right]^2 < 0.09\ (0.23) \text{ for } m_\phi = 1\ (2)\,\mathrm{GeV} \ . \tag{5.56}$$

To illustrate the modification of the observables for a viable parameter point of this model, figure 5.8 shows the differential branching ratios of all three decays as well as $F_L(q^2)$ for a scenario in which $m_\phi = 1.1$ GeV, $C_L^S = 0$ and $C_R^S = 2.8 \times 10^{-8}$ GeV^{-2}

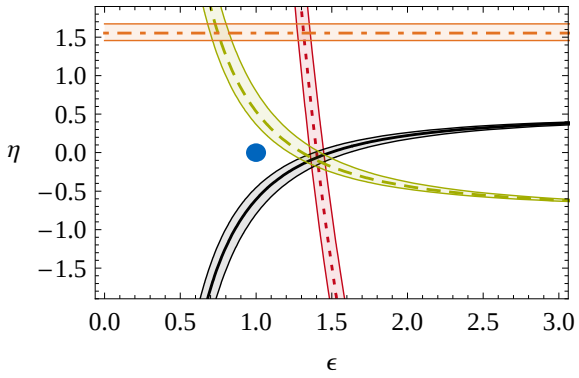

Figure 5.9: Constraints on the ϵ-η-plane obtained by applying eqs. (5.22)–(5.25) in a scenario in which SM-like $b \to s\nu\bar{\nu}$ processes overlap with $b \to s\phi^2$ decays. The parameters are chosen as in figure 5.8.

have been chosen such that all the branching ratios are well below their experimental upper bounds in table 5.2.

Figure 5.9 shows the constraints on the ϵ-η-plane which would result by naively applying eqs. (5.22)–(5.25) anyway, with the parameter values chosen as above. As a result, the bands corresponding to the different observables do not meet at a single point any longer. One observes that, while this splitting is quite small for the three branching ratios, the observable $\langle F_L \rangle$ displays unambiguously the invalidity of eqs. (5.22)–(5.25). While, according to its definition in section 5.1.4, η is restricted to the interval $[-\frac{1}{2}, \frac{1}{2}]$, its feigned value in this scenario, obtained by naively applying eq. (5.25), can be bigger than $\frac{1}{2}$.

Summary and Outlook

In the introduction, I stressed that the Standard Model of particle physics is plagued by a naturalness problem, the *gauge hierarchy problem*, and confronts us with a *flavour puzzle*. While supersymmetry is one of the most attractive solutions to the former, it aggravates the latter, since the new potential sources of flavour and CP violation introduced in the MSSM can lead to effects in flavour observables which are incompatible with the experimental data. On the other hand, the framework of supersymmetry adds new aspects to the flavour puzzle, like the presence of two Higgs doublets, the possibility of grand unification or the explanation of Yukawa hierarchies by means of flavour symmetries. In any case, a detailed study of precision observables in the flavour sector like rare decays or electric and magnetic dipole moments is mandatory as a complement to the high-energy searches at LHC.

In the first part of this thesis, I discussed several aspects of the flavour puzzle within the MSSM. After a brief review of the MSSM in chapter 1, chapter 2 dealt with the unification of Yukawa couplings in SUSY GUTs, demonstrating that the hypothesis of precision Yukawa unification is strongly dependent on the soft SUSY breaking parameters, and that FCNC constraints are crucial to assess its phenomenological viability. In particular,

- In the MSSM with non-universal Higgs mass boundary conditions (NUHM), exact t-b-τ Yukawa unification at the GUT scale is disfavoured by the combined constraints of $B \to X_s\gamma$, $B \to X_s\ell^+\ell^-$ and $B \to \tau\nu$ unless the sfermion masses are decoupled well above 1 TeV.

- In the NUHM, exact b-τ Yukawa unification is still phenomenologically viable in view of the above constraints, but only in a narrow region of MSSM parameter space, implying that this hypothesis is easily falsifiable at the LHC.

- t-b-τ Yukawa unification can be reconciled with the FCNC constraints if the universality among trilinear couplings of up- and down-type sfermions is relaxed. The emerging scenario interstingly does not require a decoupling of the SUSY spectrum, but in fact requires part of the spectrum, most notably the stop and gluino, to be very light.

In chapter 3, I discussed other aspects of the flavour puzzle within the MSSM. Section 3.1 addressed the SUSY CP problem in the MSSM with MFV, noting that the MFV principle does not guarantee the absence of new sources of CP violation beyond the CKM phase. It was found that

- Making the hypothesis that the MSSM is CP conserving in the limit of flavour blindness, and CP is only violated by the terms breaking the flavour blindness, the CP problem of the MFV MSSM can be ameliorated.

- The above assumption is not RG invariant. If it is imposed at low energies, all the complex coefficients in the MFV expansion of soft terms are allowed to have $O(1)$ phases, implying viable but observable predictions for EDMs.

- If the assumption is instead imposed at the GUT scale, RG effects lead to an enhancement of the EDMs. In particular, the μ term acquires an effective phase. As a consequence, not all MFV coefficients are allowed to have $O(1)$ phases.

Section 3.2 was devoted to the question whether the quark and lepton masses are indeed dominantly generated by tree-level Yukawa couplings or whether loop-induced non-holomorphic couplings can strongly modify this picture. This is particular relevant in the region where $\tan\beta$ is very large, i.e. $\gtrsim 50$. In short:

- The scale where one of the Yukawa couplings becomes non-perturbative, depending on their values at low energies, was calculated.

- The actual values of the Yukawa couplings needed to reproduce the known quark and lepton masses, taking into account the loop-induced and potentially large threshold corrections, were calculated for two different setups: First, a low-energy scan of the MSSM with flavour blind soft terms. Second, a scan of the MSSM with general gauge mediation of SUSY breaking and a low mediation scale of 100 TeV.

- In both scenarios, it was found that the most important constraints are $(g-2)_\mu$, disfavouring negative μM_2 and thus positive threshold corrections to the tau lepton mass, and $B \to \tau\nu$, disfavouring a light Higgs spectrum at large $\tan\beta$.

- In the low energy scan, viable points were found up to $\tan\beta = 200$, implying however a non-perturbativity scale as low as 10 TeV.

- In the GGM setup, no points with $\tan\beta = 150$ or larger were found, since Yukawa couplings would become non-perturbative below the mediation scale.

- A vanishing b term at the mediation scale was found to be incompatible with the very large $\tan\beta$ regime within GGM.

In the second part of the thesis, I discussed in detail two related processes which are interesting probes of new physics: the exclusive $B \to K^*\mu^+\mu^-$ decay and inclusive as well as exclusive $b \to s\nu\bar{\nu}$ decays. $B \to K^*\mu^+\mu^-$, which was discussed in chapter 4, is interesting because its angular decay distribution gives access to a

large number of observables which are sensitive to new physics. The main results were:

- All the CP averaged observables and CP asymmetries have been defined in a systematic manner.
- The SM predictions for all the observables have been presented and compared to observables previously proposed in the literature as well as to existing experimental results.
- In the presence of scalar operators, a new transversity amplitude and two new observables, S_6^c and A_6^c are present. Combined with $B_s \to \mu^+\mu^-$, they in principle allow to determine the sign of the scalar Wilson coefficient.

From a theoretical point of view, $b \to s\nu\bar{\nu}$ processes are quite similar to $b \to s\ell^+\ell^-$, but much cleaner since only a smaller number of operators contributes and since electromagnetic corrections are absent, the neutrinos being SM singlets. Experimentally however, they are of course much more challenging since the neutrinos escape the detector unmeasured. In section 5.1, the processes $B \to K\nu\bar{\nu}$, $B \to K^*\nu\bar{\nu}$ and $B \to X_s\nu\bar{\nu}$ have been studied in the SM and beyond. To summarize:

- In addition to the three branching ratios, a fourth observable is given by the K^* longitudinal polarization fraction F_L in $B \to K^*\nu\bar{\nu}$, which is theoretically clean and probes the presence of right-handed currents.
- The SM predictions for all observables have been presented and confronted with the experimental upper bounds. None of the decays has been observed yet, but the exclusive ones are in reach of the planned Super B factories.
- In any model beyond the SM, the $b \to s\nu\bar{\nu}$ observables can be expressed in terms of only two real parameters ϵ and η. Experimentally, a measurement can thus be represented as a constraint on the ϵ-η plane.

Since the two neutrinos escape the detector unmeasured, the experimental signature of $b \to s\nu\bar{\nu}$ decays is actually $b \to s\not{E}$. This signature could be "polluted" by $b \to s$ transitions with new light SM-singlet particles in the final state. In section 5.2, I presented some results for $b \to s$ transitions with one or two scalars ϕ in the final state and discussed models where such processes are predicted. I found that

- $B \to K\phi$ is a relevant constraint on the warped top condensation model.
- If the $b \to s\nu\bar{\nu}$ observables are polluted by contributions from $b \to s\phi^2$, their expressions in terms of ϵ and η are no longer valid. As a consequence, individual constraints do not meet in a single point any longer.

- $B_s \to \phi^2$ could be an interesting constraint on the $b \to s\phi^2$ Wilson coefficients once invisible B_s decays have been constrained experimentally.

The coming decade will be a busy and exciting period for particle physics. The unprecedented collision energy at the LHC will probe the mechanism of electroweak symmetry breaking and might help shed light on the gauge hierarchy problem. If nature is indeed supersymmetric at its fundamental level and supersymmetry stabilizes the large hierarchy beween the weak and the Planck scales, the LHC experiments looking for events with large transverse momentum, ATLAS and CMS, should find evidence for superpartners. Revolutionary as such a discovery would be, the plethora of free parameters introduced by the breaking of SUSY calls for high-precision flavour physics experiments to distinguish between different SUSY models. Even before direct evidence for SUSY particles is established, flavour observables are crucial tools to constrain or even discard models of new physics on the basis of the precise existing experimental data.

The results presented in chapters 2 and 3 can contribute to this effort. The different approaches to explain the SUSY flavour puzzle lead to distinct patterns for observables in the flavour sector. These patterns allow already today to put strong constraints on the parameter space of these models. This is thanks to experimental results from the B factory experiments BaBar and Belle, the Tevatron experiments CDF and D0, and numerous other high-precision searches for new physics. In the future, experiments like LHCb, planned Super B factories in Japan and in Italy as well as ongoing or planned searches for electric dipole moments, anomalous magnetic moments, lepton flavour violation or dark matter will continue to put these models under scrutiny.

Also the $B \to K^*\ell^+\ell^-$ decay discussed in detail in chapter 4 will be studied experimentally within the next decade, most notably at the LHCb experiment. If the Super B factories are realized, also the $b \to s\nu\bar{\nu}$ decays studied in chapter 5 will be accessible. The high statistics required for these decays make it unlikely that they will show the first signs of deviation from the SM, but the large number of observables with different sensitivity to NP might turn out to be powerful tools to discriminate different models of NP and shed light on their flavour sector. In that case, the results of chapters 4 and 5 would contribute to another step towards answering the flavour puzzle.

Appendix

A Notation

Unfortunately, no universally agreed upon convention for the notation of MSSM parameters exists. Among the most widely used sets of conventions are the ones used by Rosiek in his MSSM Feynman rules [16] and the ones of the SUSY Les Houches accord (SLHA) 2 [167]. In this thesis, I worked with a compromise between the two, avoiding some peculiarities: the fact that the down-type Yukawa couplings in Rosiek's conventions are negative and the fact that the trilinear couplings are transposed before performing the biunitary transformations of eq. (1.31) when going from the weak basis to the Super CKM basis in the SLHA conventions.

The following dictionary translates the different notations into each other.

This work	SLHA 2 [167]	Rosiek [16]	MV [26]
Y_U	$\hat{Y}_U$	Y_u	$(\mathbf{Y}_u)^T$
$Y_{D,E}$	$\hat{Y}_{D,E}$	$-Y_{d,l}$	$-(\mathbf{Y}_{d,e})^T$
T_U	$(\hat{T}_U)^T$	$-A_u$	$(\mathbf{h}_u)^T$
$T_{D,E}$	$(\hat{T}_{D,E})^T$	$A_{d,l}$	$-(\mathbf{h}_{d,e})^T$
b	m_3^2	$-m_{12}^2$	B
$m_{H_{u,d}}^2$	$m_{H_{2,1}}^2$	$m_{H_{2,1}}^2$	$m_{H_{u,d}}^2$
$m_{Q,L}^2$	$\hat{m}_{\tilde{Q},\tilde{L}}^2$	$m_{Q,L}^2$	$\mathbf{m}_{Q,L}^2$
$m_{U,D,E}^2$	$\hat{m}_{\tilde{u},\tilde{d},\tilde{e}}^2$	$(m_{U,D,E}^2)^T$	$\mathbf{m}_{u,d,e}^2$

This dictionary can be used both for translations between parameters in the SCKM basis and in a weak eigenstate basis (with the exception of the SLHA 2 column, which is only valid in the SCKM basis due to the peculiar convention mentioned above). The transformation between the SCKM and weak bases was discussed in section 1.3.3.

As a final note, the convention for the two-dimensional ϵ tensor appearing in chapter 1 is $\epsilon^{12} = -\epsilon^{21} = -\epsilon_{12} = \epsilon_{21} = +1$, which agrees with Rosiek [16], but differs by an overall sign from SLHA 2 [167].

B MSSM RG evolution

This appendix collects some approximate expressions for the RG equations of MSSM parameters and approximate solutions to them. It is by no means exhaustive; the complete set of two-loop RGEs can be found in [26]. The dictionary between the notation of this thesis and that reference was given in appendix A.

B.1 Off-diagonal squark mass matrix elements

Many models predict the pattern of off-diagonal elements of the squark mass matrices at the GUT scale while for the calculation of physical observables, their values at low energies are relevant. Crucial questions in this respect are whether these off-diagonal elements are strongly reduced or enhanced in the running, whether they mix with each other and whether they are generated if they vanish at the initial scale. Let us address these points, disregarding for simplicity off-diagonalities in the trilinear couplings, i.e. LR and RL mass insertions, as well as the slepton sector.

A close inspection of the relevant RG equations (RGEs) [26] shows that for m_U^2 and m_D^2, i.e. the RR MIs, all mixing terms are suppressed by 1st or 2nd generation Yukawa couplings and can therefore be safely neglected. In fact, neglecting 1st and 2nd generation Yukawa couplings, the RGEs for the off-diagonal elements of $m_{U,D}^2$ read at the one-loop level

$$16\pi^2 \frac{d}{dt}(m_U^2)_{ij} \overset{i\neq j}{=} 2\left(y_t^2\right)(m_U^2)_{ij}(\delta_{i3}+\delta_{j3}) + 4(T_U^\dagger T_U)_{ji}\,, \tag{B.1}$$

$$16\pi^2 \frac{d}{dt}(m_D^2)_{ij} \overset{i\neq j}{=} 2\left(y_b^2\right)(m_D^2)_{ij}(\delta_{i3}+\delta_{j3}) + 4(T_D^\dagger T_D)_{ji}\,, \tag{B.2}$$

where $t = \log(\mu/\mu_0)$. As can be easily seen, $(m_{U,D}^2)_{12}$ are RG invariant in this approximation; we have checked that this holds numerically to an excellent approximation even if light generation Yukawas and two-loop effects are taken into account.

Concerning the remaining entries, we find that their values at low energies are well approximated by

$$\left(m_U^2\right)_{13} \simeq 0.87\left(m_U^2\right)_{13}^0\,, \qquad \left(m_U^2\right)_{23} \simeq 0.82\left(m_U^2\right)_{23}^0\,, \tag{B.3}$$

$$\left(m_D^2\right)_{13} \simeq (1-0.10\,\tilde{t}^2-0.05\,\tilde{t}^4)\left(m_D^2\right)_{13}^0\,, \tag{B.4}$$

$$\left(m_D^2\right)_{23} \simeq (1 - 0.10\,\tilde{t}^2 - 0.05\,\tilde{t}^4)\left(m_D^2\right)^0_{23}\,, \tag{B.5}$$

where $\tilde{t} = \tan\beta/50$ and quantities with superscript 0 on the right-hand side denote the values at the GUT scale, while those on the left-hand side are meant to be evaluated at the weak scale.

To summarize, the off-diagonal squark mass matrix elements in the RR sector are reduced by at most 15%, they do not mix among each other or with LL MIs, and they are not generated by the running once they vanish at the GUT scale.

The situation in the LL sector is different; there, also mixing takes place, and the elements can be generated by RG effects even if they vanish at the GUT scale. Of course, both these effects are suppressed by combinations of CKM elements, since they would be absent if the CKM matrix were diagonal. The RG equation for the off-diagonal elements of m_Q^2 reads

$$\begin{aligned} 16\pi^2 \frac{d}{dt}(m_Q^2)_{ij} \overset{i\neq j}{=}\; & 2\,(y_{d,i}\,y_{d,j})\,(m_D^2)_{ij} + \left(y_b^2\right)(m_Q^2)_{ij}(\delta_{i3}+\delta_{j3}) \\ & + y_t^2 (m_Q^2)_{ik}\lambda_{kj} + y_t^2 (m_Q^2)_{kj}\lambda_{ik} + y_t^2 2m_{H_u}^2\lambda_{ij} \\ & + 2y_t^2 (m_U^2)_{33}\lambda_{ij} + 2(T_U T_U^\dagger)_{ji} + 2(T_D T_D^\dagger)_{ji}\,, \end{aligned} \tag{B.6}$$

where $\lambda_{ij} = V_{ti}^* V_{tj}$ and light generation Yukawas have again been neglected , except in the first term, which in the case of $(ij) = (23)$ is only suppressed by y_s/y_b, but unsuppressed by CKM angles and can therefore be comparable in size to the remaining terms.

Consequently one finds that, numerically, the low-energy values of the $(m_Q^2)_{ij}$ are well approximated by the following formulae,

$$\begin{aligned} \left(m_Q^2\right)_{13} \simeq\; & (0.91 - 0.05\,\tilde{t}^2)\left(m_Q^2\right)^0_{13} - \Delta m_{13}^2 \\ & - 0.09\left[\lambda_{12}\left(m_Q^2\right)^0_{23} + \lambda_{23}\left(m_Q^2\right)^0_{12}\right], \end{aligned} \tag{B.7}$$

$$\begin{aligned} \left(m_Q^2\right)_{23} \simeq\; & (0.91 - 0.05\,\tilde{t}^2)\left(m_Q^2\right)^0_{23} - \Delta m_{23}^2 \\ & - 0.09\left[\lambda_{21}\left(m_Q^2\right)^0_{13} + \lambda_{13}\left(m_Q^2\right)^0_{21} + 0.02\tilde{t}^2\left(m_D^2\right)^0_{23}\right], \end{aligned} \tag{B.8}$$

$$\left(m_Q^2\right)_{12} \simeq \left(m_Q^2\right)^0_{12} - \Delta m_{12}^2 - 0.09\left[\lambda_{13}\left(m_Q^2\right)^0_{32} + \lambda_{32}\left(m_Q^2\right)^0_{13}\right], \tag{B.9}$$

where

$$\Delta m_{ij}^2 = \lambda_{ij}\left(0.33\,m_0^2 + 0.89\,M_{1/2}^2 + 0.03\,A_0^2 - 0.14\,M_{1/2}A_0\right), \tag{B.10}$$

assuming CMSSM-like boundary conditions for the gaugino masses, trilinear couplings and the diagonal elements of sfermion mass matrices.

As in the RR sector, the Yukawa-induced reduction of the elements, cf. the first terms in (B.6) and (B.7)–(B.9), is only sizable in the $(13, 23)$ sectors. The terms in

square brackets describe the mixing among the LL elements, while Δm^2_{ij} describes the CKM-induced generation of LL MIs, which takes place even in a completely flavour blind situation at the GUT scale, such as in the CMSSM.

To summarize, the off-diagonal squark mass matrix elements in the LL sector mix among each other and they can be generated even if vanishing at the GUT scale; however, these effects are suppressed by combinations of CKM elements. Mixing of RR elements into LL elements only takes place in the 23-sector and is suppressed by a factor $y_s y_b / y_t^2$.

B.2 The μ and b terms

The one-loop RGE for the μ term reads

$$\frac{d}{dt}\mu = \frac{1}{16\pi^2}\beta_\mu^{(1)} \ . \tag{B.11}$$

Neglecting CKM mixing and first and second generation Yukawa couplings, the beta function reads

$$\beta_\mu^{(1)} = \mu\left(3y_t^2 + 3y_b^2 + y_\tau^2 - 3g_2^2 - \frac{3}{5}g_1^2\right) . \tag{B.12}$$

The proportionality of the beta function to μ signals that μ is protected by the non-renormalization theorem. The fact that the term in brackets is real reflects the fact that the phase of μ is RG invariant.

The RGE for b simplifies by writing $b = B\mu$. Then, one obtains, in the same approximation as above,

$$\frac{dB}{dt} = \frac{1}{8\pi^2}\left(3y_t^2 A_t + 3y_b^2 A_b + y_\tau^2 A_\tau + 3g_2^2\, M_2 + \frac{3}{5}g_1^2\, M_1\right) \ . \tag{B.13}$$

B.3 Trilinear couplings

Writing the trilinear coupling matrices as

$$(T_{U,D,E})_{ij} = (A_{U,D,E})_{ij}(Y_{U,D,E})_{ij} \ , \tag{B.14}$$

the RGEs for the diagonal elements of $A_{U,D,E}$, can be written to one-loop order as

$$\frac{d}{dt}A_i = \frac{1}{16\pi^2}\beta_{A_i}^{(1)} \ . \tag{B.15}$$

Neglecting Yukawa couplings of the two light generations, the one-loop β-functions are

$$\beta_{A_t}^{(1)} = 2A_b y_b^2 + 12A_t y_t^2 + \frac{26}{15}g_1^2 M_1 + 6g_2^2 M_2 + \frac{32}{3}g_3^2 M_3 \ , \tag{B.16}$$

$$\beta^{(1)}_{A_u} = 6A_t y_t^2 + \frac{26}{15} g_1^2 M_2 + 6 g_2^2 M_2 + \frac{32}{3} g_3^2 M_3 \ , \tag{B.17}$$

$$\beta^{(1)}_{A_b} = 12 A_b y_b^2 + 2 A_t y_t^2 + 2 A_\tau y_\tau 2 + \frac{14}{15} g_1^2 M_1 + 6 g_2^2 M_2 + \frac{32}{3} g_3^2 M_3 \ , \tag{B.18}$$

$$\beta^{(1)}_{A_d} = 6 A_b y_b 2 + 2 A_\tau y_\tau 2 + \frac{14}{15} g_1^2 M_1 + 6 g_2^2 M_2 + \frac{32}{3} g_3^2 M_3 \ , \tag{B.19}$$

$$\beta^{(1)}_{A_\tau} = 6 A_b y_b 2 + 8 A_\tau y_\tau 2 + \frac{18}{5} g_1^2 M_1 + 6 g_2^2 M_2 \ , \tag{B.20}$$

$$\beta^{(1)}_{A_e} = 6 A_b y_b^2 + 2 A_\tau y_\tau^2 + \frac{18}{5} g_1^2 M_1 + 6 g_2^2 M_2 \ . \tag{B.21}$$

Acknowledgements

This thesis summarizes results and insights obtained during three years of research conducted at the Institute for Theoretical Elementary Particle Physics (T31) at the Physics Department of the Technische Universität München (TUM) in Munich. It is a pleasure to thank the numerous people who contributed and are contributing to make this place such a fruitful environment for research and who helped and supported me in my work.

First and foremost, I express my deepest gratitude to my advisor Prof. Andrzej J. Buras. His impressive understanding of and approach to physics where extremely helpful to find my way into research. I appreciate that he enabled me to travel to numerous conferences, workshops and schools and always valued his advice.

The results presented in this thesis are the fruits of several collaborations that lead to seven publications [34, 53, 79, 80, 101, 112, 128]. I am indebted to my collaborators Wolfang Altmannshofer, Andrzej Buras, Diego Guadagnoli, Paride Paradisi, Stuart Raby, Michael Wick, Patricia Ball, Stefania Gori and Aoife Bharucha and wish to thank them for the pleasant collaboration and for what I learned from each of them. I also thank Michael Wick for a careful reading of the manuscript.

I thank all the current and former members of T31, who made these three years such an exciting and enjoyable time: Andi J., Andi W., Andrzej, Anton, Björn, Cecilia, Christoph, Diego, Felix, Gino, Katrin, Maria Valentina, Michael, Michaela, Monika, Paride, Sebastian, Selma, Stefan, Stefania, Thorsten, Tillmann, Woife and Yasutaka. Special thanks go to Michaela and Stefania for being nice and uncomplicated officemates.

I want to thank the Cluster of Excellence "Origin and Structure of the Universe" for funding my dissertation research.

Finally, I wholeheartedly thank my family, in particular my parents and my wife Katrin, for their unconditional and indispensable support.

Bibliography

[1] S. R. Coleman and J. Mandula, "All possible symmetries of the S matrix," *Phys. Rev.* **159** (1967) 1251–1256.

[2] S. Dimopoulos, S. Raby, and F. Wilczek, "Supersymmetry and the Scale of Unification," *Phys. Rev.* **D24** (1981) 1681–1683.

[3] S. P. Martin, "A Supersymmetry Primer," `arXiv:hep-ph/9709356`.

[4] Y. Shirman, "TASI 2008 Lectures: Introduction to Supersymmetry and Supersymmetry Breaking," `arXiv:0907.0039 [hep-ph]`.

[5] I. J. R. Aitchison, "Supersymmetry and the MSSM: An Elementary introduction," `arXiv:hep-ph/0505105`.

[6] M. Drees, R. Godbole, and P. Roy, "Theory and phenomenology of sparticles: An account of four-dimensional N=1 supersymmetry in high energy physics,". Hackensack, USA: World Scientific (2004) 555 p.

[7] P. Binetruy, "Supersymmetry: Theory, experiment and cosmology,". Oxford, UK: Oxford Univ. Pr. (2006) 520 p.

[8] D. J. H. Chung *et al.*, "The soft supersymmetry-breaking Lagrangian: Theory and applications," *Phys. Rept.* **407** (2005) 1–203, `arXiv:hep-ph/0312378`.

[9] A. J. Buras, P. Gambino, M. Gorbahn, S. Jäger, and L. Silvestrini, "Universal unitarity triangle and physics beyond the standard model," *Phys. Lett.* **B500** (2001) 161–167, `arXiv:hep-ph/0007085`.

[10] G. D'Ambrosio, G. F. Giudice, G. Isidori, and A. Strumia, "Minimal flavour violation: An effective field theory approach," *Nucl. Phys.* **B645** (2002) 155–187, `arXiv:hep-ph/0207036`.

[11] G. Colangelo, E. Nikolidakis, and C. Smith, "Supersymmetric models with minimal flavour violation and their running," *Eur. Phys. J.* **C59** (2009) 75–98, `arXiv:0807.0801 [hep-ph]`.

[12] T. Feldmann and T. Mannel, "Large Top Mass and Non-Linear Representation of Flavour Symmetry," *Phys. Rev. Lett.* **100** (2008) 171601, `arXiv:0801.1802 [hep-ph]`.

[13] A. L. Kagan, G. Perez, T. Volansky, and J. Zupan, "General Minimal Flavor Violation," *Phys. Rev.* **D80** (2009) 076002, arXiv:0903.1794 [hep-ph].

[14] A. J. Buras, M. V. Carlucci, S. Gori, and G. Isidori, "Higgs-mediated FCNCs: Natural Flavour Conservation vs. Minimal Flavour Violation," arXiv:1005.5310 [hep-ph].

[15] T. Feldmann, M. Jung, and T. Mannel, "Sequential Flavour Symmetry Breaking," *Phys. Rev.* **D80** (2009) 033003, arXiv:0906.1523 [hep-ph].

[16] J. Rosiek, "Complete set of Feynman rules for the the minimal supersymmetric extension of the standard model," *Phys. Rev.* **D41** (1990) 3464, hep-ph/9511250. (Erratum). 2009 update available at http://www.fuw.edu.pl/ rosiek/physics/prd41.html.

[17] D. M. Straub, "Flavour Violation Challenging a Predictive SO(10) SUSY GUT," Diplomarbeit, Technische Universität München, 2007.

[18] D. M. Pierce, J. A. Bagger, K. T. Matchev, and R.-j. Zhang, "Precision corrections in the minimal supersymmetric standard model," *Nucl. Phys.* **B491** (1997) 3–67, arXiv:hep-ph/9606211.

[19] L. J. Hall, V. A. Kostelecky, and S. Raby, "New Flavor Violations in Supergravity Models," *Nucl. Phys.* **B267** (1986) 415.

[20] H. Baer, J. Ferrandis, K. Melnikov, and X. Tata, "Relating bottom quark mass in DR-bar and MS-bar regularization schemes," *Phys. Rev.* **D66** (2002) 074007, arXiv:hep-ph/0207126.

[21] K. G. Chetyrkin, J. H. Kuhn, and M. Steinhauser, "RunDec: A Mathematica package for running and decoupling of the strong coupling and quark masses," *Comput. Phys. Commun.* **133** (2000) 43–65, arXiv:hep-ph/0004189.

[22] L. J. Hall, R. Rattazzi, and U. Sarid, "The Top quark mass in supersymmetric SO(10) unification," *Phys. Rev.* **D50** (1994) 7048–7065, arXiv:hep-ph/9306309.

[23] M. E. Machacek and M. T. Vaughn, "Two Loop Renormalization Group Equations in a General Quantum Field Theory. 2. Yukawa Couplings," *Nucl. Phys.* **B236** (1984) 221.

[24] M. E. Machacek and M. T. Vaughn, "Two Loop Renormalization Group Equations in a General Quantum Field Theory. 1. Wave Function Renormalization," *Nucl. Phys.* **B222** (1983) 83.

[25] M. E. Machacek and M. T. Vaughn, "Two Loop Renormalization Group Equations in a General Quantum Field Theory. 3. Scalar Quartic Couplings," *Nucl. Phys.* **B249** (1985) 70.

[26] S. P. Martin and M. T. Vaughn, "Two loop renormalization group equations for soft supersymmetry breaking couplings," *Phys.Rev.* **D50** (1994) 2282, `arXiv:hep-ph/9311340 [hep-ph]`.

[27] G. Giudice and R. Rattazzi, "Theories with gauge mediated supersymmetry breaking," *Phys.Rept.* **322** (1999) 419–499, `arXiv:hep-ph/9801271 [hep-ph]`.

[28] P. Meade, N. Seiberg, and D. Shih, "General Gauge Mediation," *Prog. Theor. Phys. Suppl.* **177** (2009) 143–158, `arXiv:0801.3278 [hep-ph]`.

[29] M. Buican, P. Meade, N. Seiberg, and D. Shih, "Exploring General Gauge Mediation," *JHEP* **03** (2009) 016, `arXiv:0812.3668 [hep-ph]`.

[30] G. R. Dvali, G. F. Giudice, and A. Pomarol, "The μ-Problem in Theories with Gauge-Mediated Supersymmetry Breaking," *Nucl. Phys.* **B478** (1996) 31–45, `arXiv:hep-ph/9603238`.

[31] Z. Komargodski and N. Seiberg, "μ and General Gauge Mediation," *JHEP* **03** (2009) 072, `arXiv:0812.3900 [hep-ph]`.

[32] S. Dimopoulos and G. F. Giudice, "Multi-messenger theories of gauge-mediated supersymmetry breaking," *Phys. Lett.* **B393** (1997) 72–78, `arXiv:hep-ph/9609344`.

[33] C. Froggatt and H. B. Nielsen, "Hierarchy of Quark Masses, Cabibbo Angles and CP Violation," *Nucl.Phys.* **B147** (1979) 277.

[34] W. Altmannshofer, A. J. Buras, S. Gori, P. Paradisi, and D. M. Straub, "Anatomy and Phenomenology of FCNC and CPV Effects in SUSY Theories," *Nucl. Phys.* **B830** (2010) 17–94, `arXiv:0909.1333 [hep-ph]`.

[35] V. Lucas and S. Raby, "Nucleon decay in a realistic SO(10) SUSY GUT," *Phys. Rev.* **D55** (1997) 6986–7009, `arXiv:hep-ph/9610293`.

[36] T. Goto and T. Nihei, "Effect of RRRR dimension five operator on the proton decay in the minimal SU(5) SUGRA GUT model," *Phys. Rev.* **D59** (1999) 115009, `arXiv:hep-ph/9808255`.

[37] R. Dermíšek, A. Mafi, and S. Raby, "SUSY GUTs under siege: Proton decay," *Phys. Rev.* **D63** (2001) 035001, `arXiv:hep-ph/0007213`.

[38] **ALEPH** Collaboration, S. Schael *et al.*, "Search for neutral MSSM Higgs bosons at LEP," *Eur. Phys. J.* **C47** (2006) 547–587, arXiv:hep-ex/0602042.

[39] **Particle Data Group** Collaboration, C. Amsler *et al.*, "Review of particle physics," *Phys. Lett.* **B667** (2008) 1. And 2009 partial update for the 2010 edition.

[40] C. Balazs and R. Dermíšek, "Yukawa coupling unification and non-universal gaugino mediation of supersymmetry breaking," *JHEP* **06** (2003) 024, arXiv:hep-ph/0303161.

[41] I. Gogoladze, R. Khalid, and Q. Shafi, "Yukawa Unification and Neutralino Dark Matter in $SU(4)_c \times SU(2)_L \times SU(2)_R$," *Phys. Rev.* **D79** (2009) 115004, arXiv:0903.5204 [hep-ph].

[42] M. Olechowski and S. Pokorski, "Electroweak symmetry breaking with nonuniversal scalar soft terms and large tan beta solutions," *Phys.Lett.* **B344** (1995) 201–210, arXiv:hep-ph/9407404 [hep-ph].

[43] T. Blazek, R. Dermíšek, and S. Raby, "Predictions for Higgs and SUSY spectra from SO(10) Yukawa unification with $\mu > 0$," *Phys. Rev. Lett.* **88** (2002) 111804, arXiv:hep-ph/0107097.

[44] T. Blazek, R. Dermíšek, and S. Raby, "Yukawa unification in SO(10)," *Phys. Rev.* **D65** (2002) 115004, arXiv:hep-ph/0201081.

[45] R. Dermíšek, M. Harada, and S. Raby, "SO(10) SUSY GUT for Fermion Masses: Lepton Flavor and CP Violation," *Phys. Rev.* **D74** (2006) 035011, arXiv:hep-ph/0606055.

[46] P. Gambino, U. Haisch, and M. Misiak, "Determining the sign of the $b \to s\gamma$ amplitude," *Phys. Rev. Lett.* **94** (2005) 061803, arXiv:hep-ph/0410155.

[47] M. Albrecht, W. Altmannshofer, A. J. Buras, D. Guadagnoli, and D. M. Straub, "Challenging SO(10) SUSY GUTs with family symmetries through FCNC processes," *JHEP* **10** (2007) 055, arXiv:0707.3954 [hep-ph].

[48] **Heavy Flavor Averaging Group** Collaboration, E. Barberio *et al.*, "Averages of $b-$hadron and $c-$hadron Properties at the End of 2007," arXiv:0808.1297 [hep-ex]. And online updates at http://www.slac.stanford.edu/xorg/hfag/.

[49] M. Misiak *et al.*, "The first estimate of $\mathcal{B}(\bar{B} \to X_s\gamma)$ at $\mathcal{O}(\alpha_s^2)$," *Phys. Rev. Lett.* **98** (2007) 022002, arXiv:hep-ph/0609232.

[50] W. Altmannshofer, "$\Delta F = 1$ and $\Delta F = 2$ Effective Hamiltonians in the MSSM: A Comprehensive Leading Order Analysis," Diplomarbeit, Technische Universität München, 2007.

[51] M. Wick, "Automated Evaluation of Feynman Amplitudes: Application to $\Delta F = 1$ and $\Delta F = 2$ Hamiltonians in the general MSSM," Diplomarbeit, Technische Universität München, 2007.

[52] M. Wick and W. Altmannshofer, "A Reconsideration of the $b \to s\gamma$ Decay in the Minimal Flavor Violating MSSM," *AIP Conf. Proc.* **1078** (2009) 348–353, `arXiv:0810.2874 [hep-ph]`.

[53] W. Altmannshofer and D. M. Straub, "Viability of MSSM scenarios at very large $\tan\beta$," `arXiv:1004.1993 [hep-ph]`.

[54] A. J. Buras *et al.*, "The Impact of a 4th Generation on Mixing and CP Violation in the Charm System," `arXiv:1004.4565 [hep-ph]`.

[55] **CDF** Collaboration, T. Aaltonen *et al.*, "Search for $B_s^0 \to \mu^+\mu^-$ and $B_d^0 \to \mu^+\mu^-$ decays with 2 fb^{-1} of $p\bar{p}$ collisions," *Phys. Rev. Lett.* **100** (2008) 101802, `arXiv:0712.1708 [hep-ex]`.

[56] **CDF** Collaboration, "Search for $B_s \to \mu^+\mu^-$ and $B_d \to \mu^+\mu^-$ Decays in 3.7 fb^{-1} of $p\bar{p}$ Collisions with CDF II," *CDF Public Note* 9892. http://www-cdf.fnal.gov/physics/new/bottom/090813.blessed-Bsd2mumu//welcome.html.

[57] **D0** Collaboration, V. Abazov *et al.*, "Search for the rare decay $B_s^0 \to \mu^+\mu^-$," `arXiv:1006.3469 [hep-ex]`.

[58] S. R. Choudhury and N. Gaur, "Dileptonic decay of B_s meson in SUSY models with large $\tan\beta$," *Phys. Lett.* **B451** (1999) 86–92, `arXiv:hep-ph/9810307`.

[59] K. S. Babu and C. F. Kolda, "Higgs mediated $B^0 \to \mu^+\mu^-$ in minimal supersymmetry," *Phys. Rev. Lett.* **84** (2000) 228–231, `arXiv:hep-ph/9909476`.

[60] W.-S. Hou, "Enhanced charged Higgs boson effects in $B\tau\bar{\nu}$, $\mu\bar{\nu}$ and $b \to \tau\bar{\nu} + X$," *Phys.Rev.* **D48** (1993) 2342–2344.

[61] A. Akeroyd and S. Recksiegel, "The Effect of $H^\pm$ on $B^\pm \to \tau^\pm\nu_\tau$ and $B^\pm \to \mu^\pm\nu_\mu$," *J.Phys.G* **G29** (2003) 2311–2317, `arXiv:hep-ph/0306037 [hep-ph]`.

[62] G. Isidori and P. Paradisi, "Hints of large $\tan\beta$ in flavour physics," *Phys.Lett.* **B639** (2006) 499–507, arXiv:hep-ph/0605012 [hep-ph].

[63] A. J. Buras, P. H. Chankowski, J. Rosiek, and L. Slawianowska, "$\Delta M_{d,s}, B^0 d, s \to \mu^+\mu^-$ and $B \to X_s\gamma$ in supersymmetry at large $\tan\beta$," *Nucl. Phys.* **B659** (2003) 3, arXiv:hep-ph/0210145.

[64] V. Tisserand, "CKM fits as of winter 2009 and sensitivity to New Physics," arXiv:0905.1572 [hep-ph].

[65] **UTfit** Collaboration, M. Bona *et al.*, "An improved Standard Model prediction Of BR($B \to \tau\nu$) and its implications for New Physics," *Phys. Lett.* **B687** (2010) 61–69, arXiv:0908.3470 [hep-ph].

[66] J. Prades, "Standard Model Prediction of the Muon Anomalous Magnetic Moment," arXiv:0909.2546 [hep-ph].

[67] **Muon G-2** Collaboration, G. W. Bennett *et al.*, "Final report of the muon E821 anomalous magnetic moment measurement at BNL," *Phys. Rev.* **D73** (2006) 072003, arXiv:hep-ex/0602035.

[68] B. L. Roberts, "Status of the Fermilab Muon $(g-2)$ Experiment," arXiv:1001.2898 [hep-ex].

[69] T. Moroi, "The Muon Anomalous Magnetic Dipole Moment in the Minimal Supersymmetric Standard Model," *Phys. Rev.* **D53** (1996) 6565–6575, arXiv:hep-ph/9512396.

[70] S. Marchetti, S. Mertens, U. Nierste, and D. Stockinger, "$\tan\beta$-enhanced supersymmetric corrections to the anomalous magnetic moment of the muon," *Phys. Rev.* **D79** (2009) 013010, arXiv:0808.1530 [hep-ph].

[71] K. Tobe and J. D. Wells, "Revisiting top-bottom-tau Yukawa unification in supersymmetric grand unified theories," *Nucl. Phys.* **B663** (2003) 123–140, arXiv:hep-ph/0301015.

[72] D. Auto *et al.*, "Yukawa coupling unification in supersymmetric models," *JHEP* **06** (2003) 023, arXiv:hep-ph/0302155.

[73] H. Baer, S. Kraml, S. Sekmen, and H. Summy, "Prospects for Yukawa Unified SO(10) SUSY GUTs at the CERN LHC," *JHEP* **10** (2008) 079, arXiv:0809.0710 [hep-ph].

[74] S. Antusch and M. Spinrath, "Quark and lepton masses at the GUT scale including SUSY threshold corrections," *Phys. Rev.* **D78** (2008) 075020, arXiv:0804.0717 [hep-ph].

[75] S. Antusch and M. Spinrath, "New GUT predictions for quark and lepton mass ratios confronted with phenomenology," *Phys. Rev.* **D79** (2009) 095004, arXiv:0902.4644 [hep-ph].

[76] H. Baer, S. Kraml, S. Sekmen, and H. Summy, "Dark matter allowed scenarios for Yukawa-unified SO(10) SUSY GUTs," *JHEP* **03** (2008) 056, arXiv:0801.1831 [hep-ph].

[77] H. Baer, M. Haider, S. Kraml, S. Sekmen, and H. Summy, "Cosmological consequences of Yukawa-unified SUSY with mixed axion/axino cold and warm dark matter," *JCAP* **0902** (2009) 002, arXiv:0812.2693 [hep-ph].

[78] R. Dermíšek and S. Raby, "Bi-large neutrino mixing and CP violation in an SO(10) SUSY GUT for fermion masses," *Phys. Lett.* **B622** (2005) 327–338, arXiv:hep-ph/0507045.

[79] W. Altmannshofer, D. Guadagnoli, S. Raby, and D. M. Straub, "SUSY GUTs with Yukawa unification: A Go/no-go study using FCNC processes," *Phys. Lett.* **B668** (2008) 385–391, arXiv:0801.4363 [hep-ph].

[80] D. Guadagnoli, S. Raby, and D. M. Straub, "Viable and testable SUSY GUTs with Yukawa unification: the case of split trilinears," *JHEP* **10** (2009) 059, arXiv:0907.4709 [hep-ph].

[81] S. Heinemeyer, W. Hollik, and G. Weiglein, "FeynHiggs: a program for the calculation of the masses of the neutral CP-even Higgs bosons in the MSSM," *Comput. Phys. Commun.* **124** (2000) 76–89, arXiv:hep-ph/9812320.

[82] S. Heinemeyer, W. Hollik, and G. Weiglein, "The Masses of the neutral CP - even Higgs bosons in the MSSM: Accurate analysis at the two loop level," *Eur. Phys. J.* **C9** (1999) 343–366, arXiv:hep-ph/9812472.

[83] G. Degrassi, S. Heinemeyer, W. Hollik, P. Slavich, and G. Weiglein, "Towards high-precision predictions for the MSSM Higgs sector," *Eur. Phys. J.* **C28** (2003) 133–143, arXiv:hep-ph/0212020.

[84] M. Frank *et al.*, "The Higgs boson masses and mixings of the complex MSSM in the Feynman-diagrammatic approach," *JHEP* **02** (2007) 047, arXiv:hep-ph/0611326.

[85] J. Hisano, T. Moroi, K. Tobe, and M. Yamaguchi, "Lepton-Flavor Violation via Right-Handed Neutrino Yukawa Couplings in Supersymmetric Standard Model," *Phys. Rev.* **D53** (1996) 2442–2459, arXiv:hep-ph/9510309.

[86] S. Antusch, J. Kersten, M. Lindner, and M. Ratz, "Neutrino mass matrix running for non-degenerate see-saw scales," *Phys. Lett.* **B538** (2002) 87–95, arXiv:hep-ph/0203233.

[87] S. T. Petcov, S. Profumo, Y. Takanishi, and C. E. Yaguna, "Charged lepton flavor violating decays: Leading logarithmic approximation versus full RG results," *Nucl. Phys.* **B676** (2004) 453–480, arXiv:hep-ph/0306195.

[88] **CDF** Collaboration, A. Abulencia *et al.*, "Observation of B_s^0-$\bar{B}_s^0$ oscillations," *Phys. Rev. Lett.* **97** (2006) 242003, arXiv:hep-ex/0609040.

[89] **BABAR** Collaboration, B. Aubert *et al.*, "Measurement of the $B \to X_s \ell^+ \ell^-$ branching fraction with a sum over exclusive modes," *Phys. Rev. Lett.* **93** (2004) 081802, arXiv:hep-ex/0404006.

[90] **Belle** Collaboration, M. Iwasaki *et al.*, "Improved measurement of the electroweak penguin process $B \to X_s l^+ l^-$," *Phys. Rev.* **D72** (2005) 092005, arXiv:hep-ex/0503044.

[91] See the CERNlib website: cernlib.web.cern.ch/cernlib/.

[92] S. M. Barr and S. Raby, "Minimal SO(10) unification," *Phys. Rev. Lett.* **79** (1997) 4748–4751, arXiv:hep-ph/9705366.

[93] K. S. Babu, J. C. Pati, and F. Wilczek, "Fermion masses, neutrino oscillations, and proton decay in the light of SuperKamiokande," *Nucl. Phys.* **B566** (2000) 33–91, arXiv:hep-ph/9812538.

[94] C. H. Albright and S. M. Barr, "Construction of a minimal Higgs SO(10) SUSY GUT model," *Phys. Rev.* **D62** (2000) 093008, arXiv:hep-ph/0003251.

[95] J. A. Bagger, J. L. Feng, N. Polonsky, and R.-J. Zhang, "Superheavy supersymmetry from scalar mass A-parameter fixed points," *Phys. Lett.* **B473** (2000) 264–271, arXiv:hep-ph/9911255.

[96] M. Pospelov and A. Ritz, "Electric dipole moments as probes of new physics," *Annals Phys.* **318** (2005) 119–169, arXiv:hep-ph/0504231.

[97] M. E. Pospelov and I. B. Khriplovich, "Electric dipole moment of the W boson and the electron in the Kobayashi-Maskawa model," *Sov. J. Nucl. Phys.* **53** (1991) 638–640.

[98] C. A. Baker *et al.*, "An improved experimental limit on the electric dipole moment of the neutron," *Phys. Rev. Lett.* **97** (2006) 131801, arXiv:hep-ex/0602020.

[99] W. Griffith, M. Swallows, T. Loftus, M. Romalis, B. Heckel, *et al.*, "Improved Limit on the Permanent Electric Dipole Moment of Hg-199," *Phys.Rev.Lett.* **102** (2009) 101601.

[100] B. C. Regan, E. D. Commins, C. J. Schmidt, and D. DeMille, "New limit on the electron electric dipole moment," *Phys. Rev. Lett.* **88** (2002) 071805.

[101] P. Paradisi and D. M. Straub, "The SUSY CP Problem and the MFV Principle," *Phys. Lett.* **B684** (2010) 147–153, `arXiv:0906.4551 [hep-ph]`.

[102] D. M. Straub, "MFV and the SUSY CP Problem," *AIP Conf. Proc.* **1200** (2010) 904–907, `arXiv:0909.3296 [hep-ph]`.

[103] P. Paradisi, M. Ratz, R. Schieren, and C. Simonetto, "Running minimal flavor violation," *Phys.Lett.* **B668** (2008) 202–209, `arXiv:arXiv:0805.3989 [hep-ph]`.

[104] M. Dine, Y. Nir, and Y. Shirman, "Variations on minimal gauge mediated supersymmetry breaking," *Phys. Rev.* **D55** (1997) 1501–1508, `arXiv:hep-ph/9607397`.

[105] R. Rattazzi and U. Sarid, "Large $\tan\beta$ in gauge-mediated SUSY-breaking models," *Nucl. Phys.* **B501** (1997) 297–331, `arXiv:hep-ph/9612464`.

[106] B. A. Dobrescu and P. J. Fox, "Uplifted supersymmetric Higgs region," `arXiv:1001.3147 [hep-ph]`.

[107] P. Ferreira, I. Jack, and D. Jones, "The Three loop SSM beta functions," *Phys.Lett.* **B387** (1996) 80–86, `arXiv:hep-ph/9605440 [hep-ph]`.

[108] A. Brignole, G. Degrassi, P. Slavich, and F. Zwirner, "On the two-loop sbottom corrections to the neutral Higgs boson masses in the MSSM," *Nucl. Phys.* **B643** (2002) 79–92, `arXiv:hep-ph/0206101`.

[109] S. Abel, M. J. Dolan, J. Jaeckel, and V. V. Khoze, "Phenomenology of Pure General Gauge Mediation," *JHEP* **12** (2009) 001, `arXiv:0910.2674 [hep-ph]`.

[110] G. Buchalla, A. J. Buras, and M. E. Lautenbacher, "Weak decays beyond leading logarithms," *Rev. Mod. Phys.* **68** (1996) 1125–1144, `arXiv:hep-ph/9512380`.

[111] A. Bharucha, T. Feldmann, and M. Wick, "Theoretical and Phenomenological Constraints on Form Factors for Radiative and Semi-Leptonic B-Meson Decays," `arXiv:1004.3249 [hep-ph]`.

[112] W. Altmannshofer *et al.*, "Symmetries and Asymmetries of $B \to K^* \mu^+ \mu^-$ Decays in the Standard Model and Beyond," *JHEP* **01** (2009) 019, arXiv:0811.1214 [hep-ph].

[113] M. Beneke, T. Feldmann, and D. Seidel, "Systematic approach to exclusive $B \to V l^+ l^-$, $V\gamma$ decays," *Nucl. Phys.* **B612** (2001) 25–58, arXiv:hep-ph/0106067.

[114] M. Beneke, T. Feldmann, and D. Seidel, "Exclusive radiative and electroweak $b \to d$ and $b \to s$ penguin decays at NLO," *Eur. Phys. J.* **C41** (2005) 173–188, arXiv:hep-ph/0412400.

[115] U. Egede, T. Hurth, J. Matias, M. Ramon, and W. Reece, "New observables in the decay mode $\bar{B} \to \bar{K}^{*0} l^+ l^-$," *JHEP* **11** (2008) 032, arXiv:0807.2589 [hep-ph].

[116] F. Krüger, L. M. Sehgal, N. Sinha, and R. Sinha, "Angular distribution and CP asymmetries in the decays $\bar{B} \to K^- \pi^+ e^- e^+$ and $\bar{B} \to \pi^- pi^+ e^- e^+$," *Phys. Rev.* **D61** (2000) 114028, arXiv:hep-ph/9907386.

[117] C. S. Kim, Y. G. Kim, C.-D. Lu, and T. Morozumi, "Azimuthal angle distribution in $B \to K^*(\to K\pi) l^+ l^-$ at low invariant $m_{l^+ l^-}$ region," *Phys. Rev.* **D62** (2000) 034013, arXiv:hep-ph/0001151.

[118] A. Faessler, T. Gutsche, M. A. Ivanov, J. G. Korner, and V. E. Lyubovitskij, "The Exclusive rare decays $B \to K(K*)\bar{\ell}\ell$ and $B_c \to D(D*)\bar{\ell}\ell$ in a relativistic quark model," *Eur. Phys. J. direct* **C4** (2002) 18, arXiv:hep-ph/0205287.

[119] F. Krüger and J. Matias, "Probing new physics via the transverse amplitudes of $B^0 \to K^{*0}(\to K^- \pi^+) l^+ l^-$ at large recoil," *Phys. Rev.* **D71** (2005) 094009, arXiv:hep-ph/0502060.

[120] G. Buchalla, G. Hiller, and G. Isidori, "Phenomenology of nonstandard Z couplings in exclusive semileptonic $b \to s$ transitions," *Phys. Rev.* **D63** (2000) 014015, arXiv:hep-ph/0006136.

[121] **BABAR** Collaboration, B. Aubert *et al.*, "Angular Distributions in the Decays $B \to K^* \ell^+ \ell^-$," *Phys. Rev.* **D79** (2009) 031102, arXiv:0804.4412 [hep-ex].

[122] **Belle** Collaboration, J.-T. Wei *et al.*, "Measurement of the Differential Branching Fraction and Forward-Backword Asymmetry for $B \to K^{(*)} l^+ l^-$," *Phys. Rev. Lett.* **103** (2009) 171801, arXiv:0904.0770 [hep-ex].

[123] **CDF** Collaboration, "Measurement of Forward-Backward Asymmetry in $B \to K^{(*)}\mu^+\mu^-$ and First Observation of $B_s^0 \to \phi\mu^+\mu^-$," *CDF Public Note* 10047. http://www-cdf.fnal.gov/physics/new/bottom/091112.blessed-b2smumu_afb/index.html.

[124] **BABAR** Collaboration, B. Aubert *et al.*, "A measurement of the total width, the electronic width, and the mass of the $\Upsilon(10580)$ resonance," *Phys. Rev.* **D72** (2005) 032005, arXiv:hep-ex/0405025.

[125] E. Lunghi and J. Matias, "Huge right-handed current effects in $B \to K^*(K\pi)l^+l^-$ in supersymmetry," *JHEP* **04** (2007) 058, arXiv:hep-ph/0612166.

[126] C. Bobeth, G. Hiller, and G. Piranishvili, "CP Asymmetries in bar $B \to \bar{K}^*(\to \bar{K}\pi)\bar{\ell}\ell$ and Untagged $\bar{B}_s$, $B_s \to \phi(\to K^+K^-)\bar{\ell}\ell$ Decays at NLO," *JHEP* **07** (2008) 106, arXiv:0805.2525 [hep-ph].

[127] A. Bharucha and W. Reece, "Constraining new physics with $B \to K^*\mu^+\mu^-$ in the early LHC era," arXiv:1002.4310 [hep-ph].

[128] W. Altmannshofer, A. J. Buras, D. M. Straub, and M. Wick, "New strategies for New Physics search in $B \to K^*\nu\bar{\nu}$, $B \to K\nu\bar{\nu}$ and $B \to X_s\nu\bar{\nu}$ decays," *JHEP* **04** (2009) 022, arXiv:0902.0160 [hep-ph].

[129] G. Buchalla and A. J. Buras, "The rare decays $K \to \pi\nu\bar{\nu}$, $B \to X\nu\bar{\nu}$ and $B \to \ell^+\ell^-$: An update," *Nucl. Phys.* **B548** (1999) 309–327, arXiv:hep-ph/9901288.

[130] Tevatron Electroweak Working Group, "Combination of CDF and D0 Results on the Mass of the Top Quark," arXiv:0808.1089 [hep-ex].

[131] P. Ball and R. Zwicky, "$B_{d,s} \to \rho, \omega, K^*, \phi$ decay form-factors from light-cone sum rules revisited," *Phys.Rev.* **D71** (2005) 014029, arXiv:hep-ph/0412079 [hep-ph].

[132] P. Ball and R. Zwicky, "New results on $B \to \pi, K, \eta$ decay formfactors from light-cone sum rules," *Phys. Rev.* **D71** (2005) 014015, arXiv:hep-ph/0406232.

[133] J. F. Kamenik and C. Smith, "Tree-level contributions to the rare decays $B^+ \to \pi^+\nu\bar{\nu}$, $B^+ \to K^+\nu\bar{\nu}$, and $B^+ \to K^{*+}\nu\bar{\nu}$ in the Standard Model," *Phys.Lett.* **B680** (2009) 471–475, arXiv:arXiv:0908.1174 [hep-ph].

[134] M. Bartsch, M. Beylich, G. Buchalla, and D. N. Gao, "Precision Flavour Physics with $B \to K\nu\bar{\nu}$ and $B \to Kl^+l^-$," *JHEP* **11** (2009) 011, arXiv:0909.1512 [hep-ph].

[135] Y. Grossman, Z. Ligeti, and E. Nardi, "First limit on inclusive $B \to X_s \nu\bar{\nu}$ decay and constraints on new physics," *Nucl. Phys.* **B465** (1996) 369–398, arXiv:hep-ph/9510378.

[136] C. Bobeth, A. J. Buras, F. Krüger, and J. Urban, "QCD corrections to $\bar{B} \to X_{d,s}\nu\bar{\nu}$, $\bar{B}_{d,s} \to \ell^+\ell^-$, $K \to \pi\nu\bar{\nu}$ and $K_L \to \mu^+\mu^-$ in the MSSM," *Nucl. Phys.* **B630** (2002) 87–131, arXiv:hep-ph/0112305.

[137] A. F. Falk, M. E. Luke, and M. J. Savage, "Hadron spectra for semileptonic heavy quark decay," *Phys. Rev.* **D53** (1996) 2491–2505, arXiv:hep-ph/9507284.

[138] C. W. Bauer, Z. Ligeti, M. Luke, A. V. Manohar, and M. Trott, "Global analysis of inclusive B decays," *Phys. Rev.* **D70** (2004) 094017, arXiv:hep-ph/0408002.

[139] A. Hoang, "Bottom quark mass from Upsilon mesons: Charm mass effects," arXiv:hep-ph/0008102 [hep-ph].

[140] **FlaviaNet Working Group on Kaon Decays** Collaboration, M. Antonelli *et al.*, "Precision tests of the Standard Model with leptonic and semileptonic kaon decays," arXiv:arXiv:0801.1817 [hep-ph].

[141] **UTfit Collaboration** Collaboration, M. Bona *et al.*, "The Unitarity Triangle Fit in the Standard Model and Hadronic Parameters from Lattice QCD: A Reappraisal after the Measurements of Δm_s and $BR(B \to \tau\nu_\tau)$," *JHEP* **0610** (2006) 081, arXiv:hep-ph/0606167 [hep-ph]. And web updates at http://www.utfit.org.

[142] **BABAR** Collaboration, B. Aubert *et al.*, "Search for $B \to K^*\nu\bar{\nu}$ decays," *Phys. Rev.* **D78** (2008) 072007, arXiv:0808.1338 [hep-ex].

[143] **BELLE** Collaboration, K. F. Chen *et al.*, "Search for $B \to h^{(*)}\nu\bar{\nu}$ Decays at Belle," *Phys. Rev. Lett.* **99** (2007) 221802, arXiv:0707.0138 [hep-ex].

[144] **ALEPH** Collaboration, R. Barate *et al.*, "Measurements of BR($b \to \tau^-\bar{\nu}_\tau X$) and BR($b \to \tau^-\bar{\nu}_\tau D^{*\pm} X$) and upper limits on BR($B^- \to \tau^-\bar{\nu}_\tau$) and BR($b \to s\nu\bar{\nu}$)," *Eur. Phys. J.* **C19** (2001) 213–227, arXiv:hep-ex/0010022.

[145] D. Melikhov, N. Nikitin, and S. Simula, "Right-handed currents in rare exclusive $B \to (K, K^*)\nu\bar{\nu}$ decays," *Phys.Lett.* **B428** (1998) 171–178, arXiv:hep-ph/9803269 [hep-ph].

[146] T. Aushev *et al.*, "Physics at Super B Factory," arXiv:1002.5012 [hep-ex].

[147] F. Renga, E. Manoni, and A. Pérez, "Recoil Analysis and $B \to K^* \nu\bar{\nu}$ at SuperB." Talk given by F. Renga at the SuperB Physics workshop in Warwick, UK on April 16, 2009.

[148] A. J. Buras and L. Silvestrini, "Upper bounds on $K \to \pi\nu\bar{\nu}$ and $K_L \to \pi^0 e^+ e^-$ from ϵ'/ϵ and $K_L \to \mu^+\mu^-$," *Nucl. Phys.* **B546** (1999) 299–314, arXiv:hep-ph/9811471.

[149] A. J. Buras, G. Colangelo, G. Isidori, A. Romanino, and L. Silvestrini, "Connections between ϵ'/ϵ and rare kaon decays in supersymmetry," *Nucl. Phys.* **B566** (2000) 3–32, arXiv:hep-ph/9908371.

[150] **UTfit** Collaboration, M. Bona *et al.*, "First Evidence of New Physics in $b \leftrightarrow s$ Transitions," arXiv:0803.0659 [hep-ph]. updated values obtained from www.utfit.org.

[151] A. J. Lenz, "Search for new physics in B_s-mixing," arXiv:0808.1944 [hep-ph].

[152] **CDF** Collaboration, G. Brooijmans, "Mixing and CP Violation at the Tevatron," arXiv:0808.0726 [hep-ex].

[153] A. Lenz and U. Nierste, "Theoretical update of $B_s - \bar{B}_s$ mixing," *JHEP* **06** (2007) 072, arXiv:hep-ph/0612167.

[154] P. Ball and R. Fleischer, "Probing new physics through B mixing: Status, benchmarks and prospects," *Eur. Phys. J.* **C48** (2006) 413–426, arXiv:hep-ph/0604249.

[155] **Belle** Collaboration, A. Ishikawa *et al.*, "Measurement of forward-backward asymmetry and Wilson coefficients in $B \to K^* l^+ l^-$," *Phys. Rev. Lett.* **96** (2006) 251801, arXiv:hep-ex/0603018.

[156] P. Langacker and M. Plümacher, "Flavor changing effects in theories with a heavy Z' boson with family non-universal couplings," *Phys. Rev.* **D62** (2000) 013006, arXiv:hep-ph/0001204.

[157] R. Adhikari and B. Mukhopadhyaya, "Light neutralinos in B decays," *Phys. Rev.* **D52** (1995) 3125–3127, arXiv:hep-ph/9411347.

[158] H. K. Dreiner *et al.*, "Mass Bounds on a Very Light Neutralino," arXiv:0901.3485 [hep-ph].

[159] H. K. Dreiner *et al.*, "Rare meson decays into very light neutralinos," arXiv:0905.2051 [hep-ph].

[160] **BABAR** Collaboration, B. Aubert *et al.*, "Search for B^0 decays to invisible final states and to $\nu\bar{\nu}\gamma$," *Phys. Rev. Lett.* **93** (2004) 091802, arXiv:hep-ex/0405071.

[161] Y. Bai, M. Carena, and E. Ponton, "The Planck Scale from Top Condensation," *Phys.Rev.* **D81** (2010) 065004, arXiv:arXiv:0809.1658 [hep-ph].

[162] H. Davoudiasl and E. Ponton, "B-Decay Signatures of Warped Top-Condensation," arXiv:0903.3410 [hep-ph].

[163] A. Azatov, M. Toharia, and L. Zhu, "Radion Mediated Flavor Changing Neutral Currents," arXiv:0812.2489 [hep-ph].

[164] C. Bird, P. Jackson, R. V. Kowalewski, and M. Pospelov, "Search for dark matter in $b \to s$ transitions with missing energy," *Phys. Rev. Lett.* **93** (2004) 201803, arXiv:hep-ph/0401195.

[165] D. McKeen, "WIMPless Dark Matter and Meson Decays with Missing Energy," *Phys. Rev.* **D79** (2009) 114001, arXiv:0903.4982 [hep-ph].

[166] A. Dedes, "The Higgs penguin and its applications: An Overview," *Mod. Phys. Lett.* **A18** (2003) 2627–2644, arXiv:hep-ph/0309233.

[167] B. Allanach, C. Balazs, G. Belanger, M. Bernhardt, F. Boudjema, *et al.*, "SUSY Les Houches Accord 2," *Comput.Phys.Commun.* **180** (2009) 8–25, arXiv:arXiv:0801.0045 [hep-ph].